Northumbria Research Link

Control of Brushless Doubly-Fed Reluctance Machines under Normal and Faulty Operating Conditions

MOHAMMED SAADI HASAN

PhD

2014

Control of Brushless Doubly-Fed Reluctance Machines under Normal and Faulty Operating Conditions

MOHAMMED SAADI   HASAN

A thesis submitted in partial fulfilment of the requirements of the

University of Northumbria at Newcastle

For the degree of

Doctor of Philosophy

Research undertaken in the

Faculty of Engineering and Environment

May 2014

Abstract

The brushless doubly fed reluctance machine (BDFRM) is an attractive alternative technology to traditional slip-ring doubly fed induction machine (DFIM) for slip-power recovery applications with limited variable speed ranges such as wind turbines or pump-alike drives. Owing to its favourable operational characteristics, the BDFRM has been receiving increasing attention by the research and industrial communities, foremost because of its brushless design and high reliability (these being the main DFIM limitations) as well as cost advantages of using a partially rated power electronics converter.

A comprehensive, largely or small scale lab model machine parameter independent control development and comparative performance analysis of this emerging machine topology have been done both by computer simulations and experimentally on a dSPACE platform using the parameters of a small-scale laboratory prototype obtained by off-line testing. A Maximum Torque Per Inverter Ampere (MTPIA) strategy and scalar control method with voltage boost, which is rather suited to drive and generator systems under consideration where fast dynamic response is not required, have been implemented and efficiency of the machine (e.g. copper losses) investigated in both motoring and generating modes. Such kind of work has not been reported in the literature available on the subject.

A large-scale BDFRG for grid-connected wind turbines with maximum power point tracking (MPPT) has also been examined by simulation studies under the same scalar control conditions referenced above. Comparisons with high-performance control algorithms as primary flux (field) oriented control (FOC) have been made and associated trade-offs considered for typical

wind profiles. A vector control (VC) scheme, similar to the FOC approach, has also been demonstrated on both the machine side converter (MSC) and grid side converter (GSC) in the BDFRM(motoring and generating)modes.

The BDFRG low-voltage fault-ride through capability has also been researched and a dedicated FOC scheme developed to allow the generator to stay on-line and provide the necessary reactive power support for the network voltage recovery under the faulty operating conditions. The BDFRG has been shown to be able to safely ride through the fault without the crowbar circuitry this being difficult to achieve with a comparable DFIG. This desirable BDFRG property can be attributed to the relatively large leakage reactance's and consequently lower fault current levels compared to the equivalent DFIG.

Acknowledgement:

Declaration

I declare that the work contained in this thesis has not been submitted for any other award and that it is all my own work. I also confirm that this work fully acknowledges options, ideas and contributions from the work of others.

Name: Mohammed Saadi Hasan

Signature:

Date: 28/5/2014

Contents

List of Figures

List of Tables

Glossary of Abbreviations and Symbols

Machine parameter and variables

v_{pd}, v_{pq} primary direct and quadrature voltage components [V];

v_{sd}, v_{sq} secondary direct and quadrature voltage components [V];

i_{pd}, i_{pq} primary direct and quadrature current components [A];

i_{sd}, i_{sq} secondary direct and quadrature current components [A];

$\lambda_{pd}, \lambda_{pq}$ primary direct and quadrature flux components [Wb];

$\lambda_{sd}, \lambda_{sq}$ secondary direct and quadrature flux components [Wb];

ω angular velocity of reference frame [rad/sec];

ω_{rm} mechanical angular velocity of the shaft [rad/sec];

ω_r electrical angular velocity of the rotor [rad/sec];

$\omega_{p, s}$ primary and secondary winding frequencies [rad/sec];

P_r number of rotor poles (or the sum of the windings pole pairs);

L_p, L_s, L_{ps} primary, secondary and mutual 3-phase inductances of the windings [H];

R_p, R_s primary and secondary windings resistances [Ω];

T_e, T_L electromagnetic and load torque [Nm].

$P_{p.cu}$ Primary Copper Losses

$P_{s.cu}$ Secondary Copper Losses

P_w Wind Power

Machines

BDFRM	Brushless Doubly Fed Reluctance Machine
IM	Induction Machine
CIM	Cascade Induction Machine
DERIM	Doubly Excited Reluctance Induction Machine
PE	Power Electronics
PWMSWI	Pulse Width Modulated Sine Wave Inverter
SVPWMI	Space Vector Pulse Width Modulated Inverter
MPPT	Maximum Power Point Tracking
MTPIA	Maximum Torque per Inverter Ampere
WECS	Wind Energy Conversion System
PLL	Phase Lock Loop
MSC	Machine Side Control
GSC	Grid Side Control
SC	Scalar Control
VC	Vector Control
FOC	Field Oriented Control
LVRT	Low Voltage Ride Through
VRT	Voltage Ride Through

Chapter 1 **Introduction**

1.1   Introduction

Renewable energy is crucial to minimise the detrimental effects of global warming, which is one of the main reasons for the latest changes in Earth's climate. Furthermore, the traditional fossil-fuel sources, like coal and oil, are expected to dry up in the near future. On the other hand, nuclear power, as the major non-fossil energy source, is difficult to control and produces harmful waste to humans and nature alike. Incidents in nuclear reactors in Chernobyl (1986) and Fukushima (2011) have provoked the latest negative reaction toward the production of nuclear energy, which has prompted States such as Germany to declare that it will close its remaining nuclear power plants in the near future [1-3]. The above-mentioned disadvantages of classical power sources clearly indicate the importance of development reliable clean energy sources as an alternative solution.

Wind is certainly one of the most important natural non-exhaustible sources of green energy. For this reason, scientists and researchers have started an intensive work on design and control of different wind turbines generator technologies for higher electrical energy production. For instance, the construction of the world's biggest offshore wind farm at Thanet, South East Coast of England testifies the maturity of the idea and its success [4]. However, Wind Energy Conversion Systems (WECS) have to overcome wind fluctuations in order to ensure quality fixed voltage and frequency supply to the end users[5]. This fundamental issue has occupied significant attention by both industrial and research communities and various power control

strategies have been proposed for this purpose [6, 7]. In addition to considering these aspects and other challenges affecting the smoothness of generator normal operation [8], which are certainly of most practical importance for efficient energy production, in response to the grid codes requirements which have been recently introduced worldwide, researchers have also been looking at establishing procedures to effectively deal with implications of incidental faults and allow the wind generators to stay on-line under the faulty conditions (e.g. low-voltage fault ride through) and provide the necessary reactive power support for speedy voltage recovery in variable speed WECS.

Conventional induction machines with cage or wound rotors are by far the most popular in the market because of their structural simplicity, low cost (especially a cage option), high efficiency and, foremost, the possibility for direct-on-line operation [9]. The latter advantage has made a brushless cage type indispensable and still widely used in fixed speed wind power applications (e.g. 'Danish' concept). Moreover, the promising self-cascaded induction machines have also been investigated[10], the Brushless Doubly Fed Reluctance Machine (BDFRM) in particular [11] due to its attractive design and performance properties to be elaborated more in the following paragraphs.

1.2   Research Motivation

Brushless Doubly Fed Machines (BDFM's) have been considered as a potential alternative to the existing solutions in applications with limited variable speed ranges (such as wind turbines and large pump-alike drives)[12]. The main reasons for this interest by the academic and industrial communities in the BDFM are its appealing features, which are in many respects similar to the traditional slip ring Doubly Fed Induction Generator (DFIG), such as competitive

performance at low cost afforded by the use of partially-rated power electronics(relative to the machine rating). Unlike the DFIG, however, the BDFM has a brushless structure, which should bring further benefits in terms of higher reliability and maintenance-free operation and hence operation and maintenance cost reductions. The cost savings can be particularly high in offshore wind turbine installations where the BDFM use instead of DFIG would be preferable from this point of view.

The BDFM comes in two distinct types: with a special 'nested' cage rotor, known as the brushless doubly fed induction machine (BDFIM) or with a cage-less reluctance rotor, which can be similar (although not the most optimal) to modern synchronous reluctance machines[13]. The latter BDFM form is called the Brushless Doubly fed Reluctance Machine (BDFRM) and it will be the focus of research in this thesis. The rationale for considering this type is behind its simpler dynamic modelling, lower machine parameter dependence and thus easier control compared to its BDFIM counterpart[14]. All these BDFRM merits can be largely attributed by the absence of the rotor windings, unlike the BDFIM.

Another potential advantage of the BDFRM over DFIG to be investigated in this project is the low-voltage fault ride through performance, which should be superior to DFIG's due to the higher leakage inductances and therefore lower fault current levels. It should be noted that the main issue with the DFIG relative to a comparably rated synchronous permanent magnet generator is its inferior Fault Ride Through (FRT) capability requiring a larger inverter rating and therefore trading off the main DFIG cost advantage in this sense. For this reason, the DFIG role on the wind power market has recently been continuously taken over by multi-pole synchronous machines (foremost permanent magnet but also classical wound rotor designs) despite the higher cost of permanent magnets and/or a fully rated inverter with increasing sizes

of large-scale generators[15]. It is expected that this compromise with an inverter-rating requirement under normal and faulty operating conditions minimised by using the BDFRM.

1.3 Proposed Research

1.3.1 Aims

The purpose of this project is to investigate, develop and compare scalar and vector control strategies for the BDFRM under healthy (considering both motoring and generating modes) and/or faulty (e.g. investigating fault-ride-through capabilities of the machine in generating regime) operating conditions. The target variable speed applications to be considered are large pump-alike drives and grid-connected wind turbines. The developed control algorithms will be first examined by computer simulation followed by experimental verification on the existing test rig based on a small-scale BDFRM prototype in the power laboratory. The controllable DC machine with a commercial 4-quadrant drive operating as a dynamic dynamometer, serves to emulate typical industrial loads (e.g. squared torque-speed characteristics typical with centrifugal pump devices) or wind turbine operation (e.g. aerodynamic torque/power profiles).

1.3.2 Objectives

- Carry out a comprehensive literature review on the subject(s).

- Investigate scalar and vector control techniques as well as the corresponding power electronic converter topologies for considered variable speed applications and choose suitable designs for performance-cost implementation trade-offs as the main selection criteria.

- Run computer simulations in Matlab/Simulink for preliminary performance comparisons of a large-scale BDFRG wind turbine under normal and faulty operating conditions. Repeat the above for motoring, pump-alike applications looking at normal operating conditions only.

- Experimentally verify the simulation results for BDFRG on the existing laboratory test rig(s) available in-house for both target applications. Investigate the suitability of simple scalar control for the above systems (given their modest dynamic response) and compare the respective results using vector control.

- Draw appropriate conclusions from the comparative studies and propose the most promising technological solutions for the future industrial applications specifically addressing issues associated with achievable performance vs. cost.

1.4   Original Contributions

The following original contributions to knowledge on the subject have been made from the results of this project (similar work, in either of the terms itemised below, has not been reported in the refereed literature to date):

- A comprehensive, largely machine parameter independent, control development and comparative performance analysis of scalar and vector control methods for the emerging machine technology, the BDFRM(G), in large-scale WECS with maximum power point tracking (MPPT) for high-efficiency operation.

- Simulation and experimental studies of scalar control with secondary voltage boost using the Maximum Torque per Inverter Ampere Strategy and parameters of a small BDFRM

prototype in the power laboratory; derivation of control conditions for copper loss optimisation and efficiency improvement of the BDFRM with scalar control in both motoring and generating modes.

- The investigation of LVRT capabilities of the BDFRM and comparisons with DFIG for symmetrical and/or asymmetrical faults; the development of the respective field-oriented control approach (including dedicated converter configuration) and preliminary performance analysis of the entire system using computer simulations.

1.5   Thesis Outline

Chapter 2 presents critical reviews of the key papers published on BDFRM with particular attention on the control related work and performance analysis. Aspects related to the machine construction, main properties (e.g. advantages and limitations), fundamental principles of operation and dynamic modelling, as well as space-vector steady-state equations have been considered.

Chapter 3 is concerned with the experimental work using dSPACE development platform for rapid control prototyping. The results for the BDFRM in motoring and generating operating modes under variable speed and/or loading conditions with scalar control real-time implementation of the MTPIA strategy have been presented and discussed.

Chapter 4 outlines a new simulation study approach for a custom-designed large-scale BDFRG for wind turbines with MPPT.

Chapter 5 describes in detail a vector control (VC) algorithm for bi-directional power converter (e.g. machine-side and grid-side bridges) followed by extensive simulation studies.

Chapter 6 addresses issues related to low-voltage fault ride through performance and development of a dedicated control scheme. This kind of work is novel and has not been published for this particular machine.

Appendix A explains the methodologies and sequential step of the real-time implementation (RTI) in the laboratory environment. Additional steps were introduced to demonstrate compatibility amongst the simulation studies and hardware interface for the BDFRM test rig.

1.6   Problem formulation

The most important obstacles facing the work that there is no specific algorithm to deal with BDFRM as an emerging machine respected to scalar control, but merely hypotheses accept the right and wrong on one hand, on the other hand, at simulation work, characterized by parochialism, so the use literature review of the experiences of others are important to start from the last point they stopped and developed to achieve the goal. Traditional scalar control methods based *V/f* gained same success with induction machines, that is bounce another motive to test its efficiency with this emerging machine.

The second group of problem is the amount of difficulty in dealing with the machine, though the test rigs stand and adapted to work with dutiful software. The success of the real time implementation built on the ability to engage the simulation model as the software signal with machine through dSPACE as a hardware side.

The required software programme has ability to convert the voltage vector (simulation side) to the suitable time vector (SVPWM-dSPACE test rigs) and both respected to the same amount of change.

The success of the scalar control should give all BDFRM properties that's lead to further investigation to enhance efficiency of the scale model based MTPIA to find the optimal *V/f* ratio to keep machines in less copper losses (target).

The future target to use emerging large scale BDFRG in wind power application impose new investigation about the capability and limitation of scalar control algorithm as a backup method control based WECS.

In order to deal with low voltage ride through capability based FOC control strategy the manipulating with theoretical equation and the simulation model based VC due the similarity between the two theories in behaviour, is quite necessary to develop the simulation software skills in normal condition and gain deep understanding to the currents behaviours before get outlined concerning (target) faulty module LVRT.

Chapter 2 **BDFRM Fundamentals**

2.1   Introduction

The BDFRM has an unconventional torque producing mechanism because of its unique design which eliminates the need for slip rings and brushes [16-18]. This unquestionable advantage over traditional DFIM also allows the BDFRM to retain the other DFIM merits, including the use of a partially-rated inverter with immediately obvious cost benefits. The latter is especially pronounced in variable speed drive and generator systems with limited speed ranges (such as wind turbines, centrifugal pumps, compressors, fans, blowers, etc.) where further reductions in size and cost of power electronics are feasible. These merits have undoubtedly motivated recent research activities and interests in this machine [19].

The BDFRM has two standard stator windings but with different pole numbers unlike a conventional machine; the primary (power) winding is grid connected and the secondary (control) winding is converter fed [20, 21]. A salient pole cage-less rotor [22], shown in Fig.2.1, having half of the total number of the stator poles [14, 23], makes it possible for the stator windings to couple magnetically through the rotor core. The presence of the variable reluctance rotor position dependent path essentially modulates the stator *mmf* waveforms of each winding in both spatial and temporal terms, resulting in the corresponding flux harmonic side-bands to link with the fundamental *mmf* of the complementary winding. Such a modulation process is the necessary condition for electro-mechanical energy conversion to occur in the machine [24].

One of the interesting properties of the BDFRM (and the DFIM) is the operational mode flexibility[25, 26]. It can operate as a conventional induction machine by shorting the secondary terminals which might be an important preventive measure in case of inverter failure when sustained operation would be possible. The same operating mode can also be used for the machine starting avoiding so the inverter overloading. A second feature is that when the secondary winding is fed to a variable DC voltage, the machine behaves like a classical wound rotor synchronous turbo-machine with a controllable field winding [27].
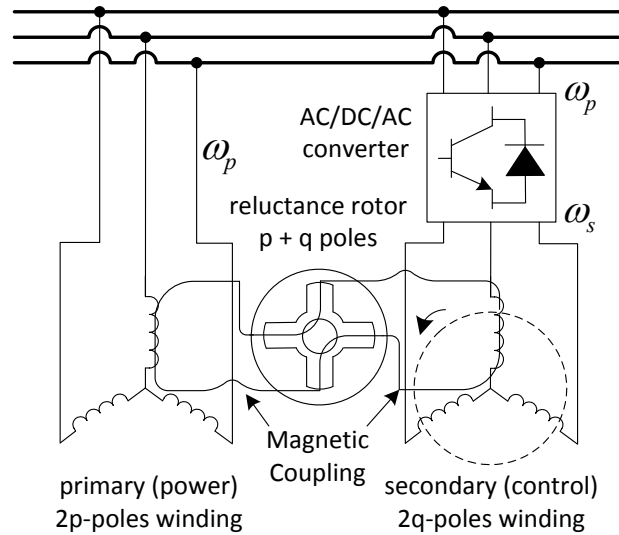
Figure 2.1: BDFRM configuration.
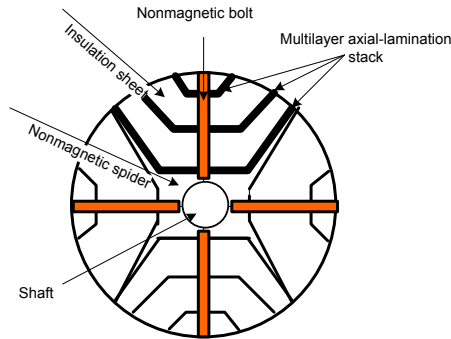
Figure 2.2: A cross-section of the modern radially-laminated reluctance rotor.

On the other hand, high-saliency-ratio cage-less rotors such as the one in Fig. 2.2, arenot only more economical to build but, more importantly, promise overall performance improvement (e.g. higher efficiency, superior torque per ampere etc.) and simpler control as compared to the 'nested' cage rotor cousin, the Brushless Doubly Fed Induction Machine (BDFIM) [20, 23, 28]. Owing to their brushless structure and consequent higher reliability as well as maintenance-free operation, both the BDFRM and BDFIM are generally preferred to any other brush type member of the family of slip power recovery machines including the traditional DFIM[29] and the classical Cascaded Induction Machine (CIM) [10].

2.2   Dynamic Model and Space-Vector Equations

The development of control algorithms and computer simulation programmes for the BDFRM requires an in-depth understanding of its main operating principles and aspects of dynamic modelling[30, 31]. The space-vector voltage and flux linkage equations for the machine in arbitrary rotating reference frames assuming *motoring* convention and using standard notation can be written as follows [32]:

$$\mathbf{u}_p = R_p \mathbf{i}_p + \frac{\partial \lambda_p}{\partial t} + j\omega \lambda_p \tag{2.1}$$

$$\mathbf{u}_s = R_s \mathbf{i}_s + \frac{\partial \lambda_s}{\partial t} + j(\omega_r - \omega)\lambda_s \tag{2.2}$$

$$\begin{cases} \lambda_p = L_p \mathbf{i}_p + L_{ps} \mathbf{i}_{sp}{}^* \\ \lambda_s = L_s \mathbf{i}_s + L_{ps} \mathbf{i}_{ps}{}^* \end{cases} \tag{2.3}$$

where ∂ indicates a partial derivative,the subscript 'p' and 's' denote the primary and secondary winding respectively, '*' represents a complex conjugate, and $\mathbf{i}_{sp}$ and $\mathbf{i}_{ps}$are the 'coupled' current

vectors from the secondary to the primary side (effectively, magnetising currents), and vice-versa, producing the mutual flux components of the two windings. The definitions of the 3-phase self and mutual inductances can be found in [32].

Note that the primary quantities above are in ω frame, and the secondary counterparts are in $\omega_r - \omega$ rotating frame. It is also important to stress that $\boldsymbol{i}_{sp} = \boldsymbol{i}_s$ as secondary to primary magnetizing currents vectors and $\boldsymbol{i}_{ps} = \boldsymbol{i}_p$ primary to secondary vectors current in their respective frames as shown graphically in Fig. 2.3 below.
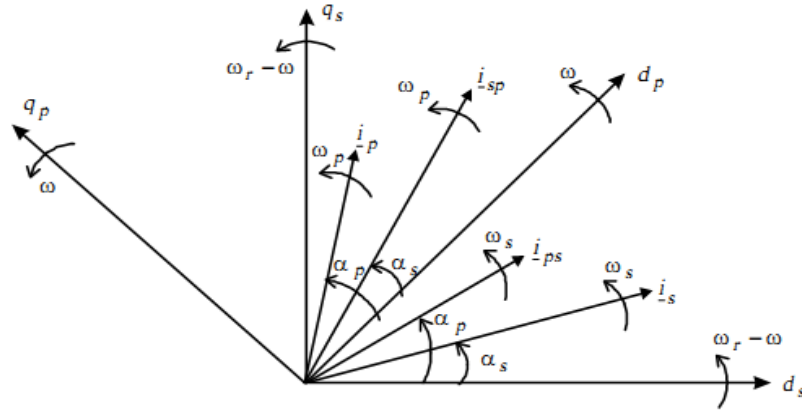
Figure 2.3: Angular positions of the characteristic space vectors in respective reference frames.

The fundamental angular velocity and corresponding position relationships for the machine torque production are:

$$\omega_r = \omega_{rm} p_r = \omega_p + \omega_s \tag{2.4}$$

$$\omega_{rm} = \frac{\omega_p + \omega_s}{p_r} = \frac{(1\text{-}s).\omega_p}{p+q} = (1\text{-}s).\omega_{syn} \leftrightarrow n_{rm} = 60\frac{f_p + f_s}{p_r} \tag{2.5}$$

$$\begin{cases} \omega_{rm} = \frac{d\theta_{rm}(t)}{dt} \leftrightarrow \theta_{rm}(t) = \int_{t0}^{t} \omega_{rm} dt + \theta_{rm}(t0) \\ \omega_{p,s} = \frac{d\theta_{p,s}(t)}{dt} \leftrightarrow \theta_{p,s}(t) = \int_{t0}^{t} \omega_{p,s} dt + \theta_{p,s}(t0) \end{cases} \tag{2.6}$$

$$\theta_r(t) = \theta_{rm}(t)\, p_r = \theta_p(t) + \theta_s(t) \tag{2.7}$$

12

Where the generalized slip is s= - ω_s/ω_p, and $\omega_{syn} = \omega_p/p_r$ is the synchronous speed (for $\omega_s=0$) as with a *$2p_r$*-pole wound rotor synchronous turbo machine. If $\omega_s>0$ then the machine operates in super synchronous speed mode, else, i.e. for $\omega_s<0$ (e.g. the opposite phase sequence of the secondary winding to the primary one) when it is in sub-synchronous mode.

Given (2.4), the above generic model can now be presented in the 'natural' reference frames i.e. ω_p for the primary winding and $\omega_r - \omega_p = \omega_s$ for the secondary winding:

$$\mathbf{u}_p = R_p\mathbf{i}_p + \frac{\partial\lambda_p}{\partial t} + j\omega_p\lambda_p \tag{2.8}$$

$$\mathbf{u}_s = R_s\mathbf{i}_s + \frac{\partial\lambda_s}{\partial t} + j\omega_s\lambda_s \tag{2.9}$$

$$\lambda_p = \underbrace{L_p i_{pd} + L_{ps}i_{sd}}_{\lambda_{pd}} + j\underbrace{(L_p i_{pq} - L_{ps}i_{sq})}_{\lambda_{pq}} \tag{2.10}$$

$$\lambda_s = \underbrace{\sigma L_s i_{sd} + \lambda_{ps_d}}_{\lambda_{sd}} + j\underbrace{(\sigma L_s i_{sq} + \lambda_{ps_q})}_{\lambda_{sq}} = \sigma L_s \mathbf{i}_s + \underbrace{\frac{L_{ps}}{L_p}\lambda_p^*}_{\lambda_{ps}} \tag{2.11}$$

where $\sigma = 1 - L_{ps}^2/(L_p L_s)$ is the leakage factor, and λ_{ps} is the primary flux linking the secondary winding (i.e. the mutual flux).

2.3   Reference Frame Transformations

In order to simplify the analysis, simulation studies and control development of any 3-phase synchronous machine in time domain, a conventional *d-q* theory has been used for the BDFRM [33]. The MMF space distribution (i.e. the current space vector) in a stationary *d-q* frame assuming the phase sequence as in Fig.2.4 can be written as follows [34]:

$$\mathbf{i}_s = \frac{2}{3}\left(i_a + e^{j2\pi/3} \cdot i_b + e^{-j2\pi/3} \cdot i_c\right) = i_{ds} + ji_{qs} \qquad (2.12)$$

$$I_a = i_a(j0)$$
$$I_b = i_b(j120)$$
$$I_c = i_c(j240)$$
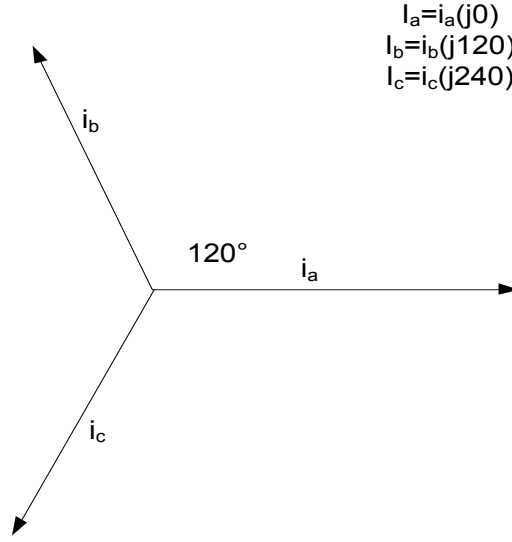
Figure 2.4: ABC phase sequence of a generic 3-phase winding.

Using (2.13), it is also possible to express the *d-q* current components in terms of the 3-phase currents as:

$$\begin{bmatrix} i_{ds} \\ i_{qs} \end{bmatrix} = \begin{bmatrix} \frac{2}{3} & -\frac{1}{3} & -\frac{1}{3} \\ 0 & \frac{1}{\sqrt{3}} & -\frac{1}{\sqrt{3}} \end{bmatrix} \begin{bmatrix} i_a \\ i_b \\ i_c \end{bmatrix} \qquad (2.13)$$

or the other way around by applying a reverse transformation:

$$\begin{bmatrix} i_a \\ i_b \\ i_c \end{bmatrix} = \begin{bmatrix} 1 & 0 \\ -\frac{1}{2} & \frac{\sqrt{3}}{2} \\ -\frac{1}{2} & -\frac{\sqrt{3}}{2} \end{bmatrix} \begin{bmatrix} i_{ds} \\ i_{qs} \end{bmatrix} \qquad (2.14)$$

A conversion from stationary to rotating reference frame (and vice-versa) in Fig.2.5 can be done using the following well-known relationships:
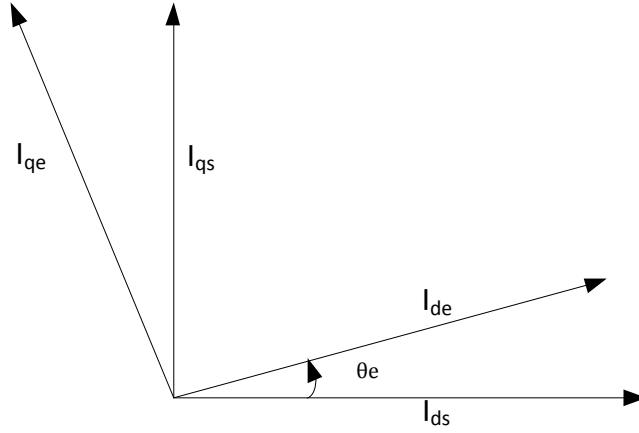
Figure 2.5 : Angular displacement of rotating ('e') and stationary ('s') d-q frames.

$$\begin{bmatrix} i_{de} \\ i_{qe} \end{bmatrix} = \begin{bmatrix} \cos\theta_e & \sin\theta_e \\ -\sin\theta_e & \cos\theta_e \end{bmatrix} \begin{bmatrix} i_{ds} \\ i_{qs} \end{bmatrix} \qquad (2.15)$$

$$\begin{bmatrix} i_{ds} \\ i_{qs} \end{bmatrix} = \begin{bmatrix} \cos\theta_e & -\sin\theta_e \\ \sin\theta_e & \cos\theta_e \end{bmatrix} \begin{bmatrix} i_{de} \\ i_{qe} \end{bmatrix} \qquad (2.16)$$

where θ_e represents the angular position of the rotating frame with respect to the stationary counterpart as indicated in the above figure.

2.4 BDFRM *d-q* Model

The BDFRM space-vector *d-q* model (2.1)-(2.3) in *motoring* mode in arbitrary reference frames (e.g. ω for the primary winding and $\omega_r - \omega$ for the secondary winding) can be further developed by using standard notation into the respective *dq* components as follows:

$$\begin{cases} v_{pd} = R_p i_{pd} + \dfrac{d}{dt}\lambda_{pd} - \omega\lambda_{pq} \\[2mm] v_{pq} = R_p i_{pq} + \dfrac{d}{dt}\lambda_{pq} + \omega\lambda_{pd} \\[2mm] v_{sd} = R_s i_{sd} + \dfrac{d}{dt}\lambda_{sd} - (\omega_r - \omega)\lambda_{sq} \\[2mm] v_{sq} = R_s i_{sq} + \dfrac{d}{dt}\lambda_{sq} + (\omega_r - \omega)\lambda_{sd} \end{cases} \tag{2.17}$$

Or in an equivalent form suitable for numerical integration in computer simulation studies as:

$$\begin{cases} \dfrac{d}{dt}\lambda_{pd} = v_{pd} - R_p i_{pd} + \omega\lambda_{pq} \\[2mm] \dfrac{d}{dt}\lambda_{pq} = v_{pq} - R_p i_{pq} - \omega\lambda_{pd} \\[2mm] \dfrac{d}{dt}\lambda_{sd} = v_{sd} - R_s i_{sd} + \left(\omega_r - \omega\right)\lambda_{sq} \\[2mm] \dfrac{d}{dt}\lambda_{sq} = v_{sq} - R_s i_{sq} - \left(\omega_r - \omega\right)\lambda_{sd} \end{cases} \tag{2.18}$$

Where the respective flux-current relationshipsare:

$$\begin{cases} \lambda_{pd} = L_p i_{pd} + L_{ps} i_{sd} \\[2mm] \lambda_{pq} = L_p i_{pq} - L_{ps} i_{sq} \\[2mm] \lambda_{sd} = L_s i_{sd} + L_{ps} i_{pq} \\[2mm] \lambda_{sq} = L_s i_{sq} - L_{ps} i_{pq} \end{cases} \tag{2.19}$$

In a matrix form, the above set of equations can be represented as *Y=AX*, where:

$$A = \begin{bmatrix} L_p & 0 & L_{ps} & 0 \\ 0 & L_p & 0 & -L_{ps} \\ L_{ps} & 0 & L_s & 0 \\ 0 & -L_{ps} & 0 & L_s \end{bmatrix}, X = \begin{bmatrix} i_{pd} \\ i_{pq} \\ i_{sd} \\ i_{sq} \end{bmatrix}, Y = \begin{bmatrix} \lambda_{pd} \\ \lambda_{pq} \\ \lambda_{sd} \\ \lambda_{sq} \end{bmatrix} \tag{2.20}$$

or in a developed form, (2.19) then becomes:

$$\begin{bmatrix} \lambda_{pd} \\ \lambda_{pq} \\ \lambda_{sd} \\ \lambda_{sq} \end{bmatrix} = \begin{bmatrix} L_p & 0 & L_{ps} & 0 \\ 0 & L_p & 0 & -L_{ps} \\ L_{ps} & 0 & L_s & 0 \\ 0 & -L_{ps} & 0 & L_s \end{bmatrix} \begin{bmatrix} i_{pd} \\ i_{pq} \\ i_{sd} \\ i_{sq} \end{bmatrix} \tag{2.21}$$

The corresponding current vector in matrix form can be derived as:

$$X = A^T Y \tag{2.22}$$

or:

$$
\begin{bmatrix} i_{pd} \\ i_{pq} \\ i_{sd} \\ i_{sq} \end{bmatrix} =
\begin{bmatrix}
-\dfrac{Ls}{-Lp*Ls+Lps^2} & 0 & \dfrac{Lps}{-Lp*Ls+Lps^2} & 0 \\[2ex]
0 & -\dfrac{Ls}{-Lp*Ls+Lps^2} & 0 & -\dfrac{Lps}{-Lp*Ls+Lps^2} \\[2ex]
\dfrac{Lps}{-Lp*Ls+Lps^2} & 0 & -\dfrac{Lp}{-Lp*Ls+Lps^2} & 0 \\[2ex]
0 & -\dfrac{Lps}{-Lp*Ls+Lps^2} & 0 & -\dfrac{Lp}{-Lp*Ls+Lps^2}
\end{bmatrix}
\begin{bmatrix} \lambda_{pd} \\ \lambda_{pq} \\ \lambda_{sd} \\ \lambda_{sq} \end{bmatrix} \tag{2.23}
$$

There are equivalent expressions for electro-magnetic torque of the machine, the most important one for control purposes being of the form:

$$T_e = \frac{3P_r L_m}{2L_p} \left(\lambda_{pd} i_{sq} + \lambda_{pq} i_{sd} \right) \tag{2.24}$$

Where, λ_{pd} and λ_{pq} are the flux d-q components of the grid-connected (primary) winding. However the secondary d-q currents are controllable by the inverter.

The mechanical differential equation for a single lumped inertia load (J) used for simulations is as follows [31]:

$$\frac{d\omega_{rm}}{dt} = \frac{1}{J} \left(T_e - T_L \right) \tag{2.25}$$

$$\omega_{rm} = \frac{1}{J} \int \left(T_e - T_L \right) dt \tag{2.26}$$

In this case, referring to the machine parameters listed in Table 2.1 and using (2.5), the synchronous speed of the BDFRM is 750 rpm. One distinctive characteristic of this machine is its ability to rotate above, below and at synchronous-speed [23, 25, 35] in either motoring of

generating operating mode. The allowed speed limits are directly dictated by the inverter rating being speed range.

Fig. 2.6 below shows a functional block diagram of the BDFRM dynamic model equations referenced above indicating particular input and output quantities. A similar (but more detailed) block diagram can obviously be designed in Simulink for simulation studies.
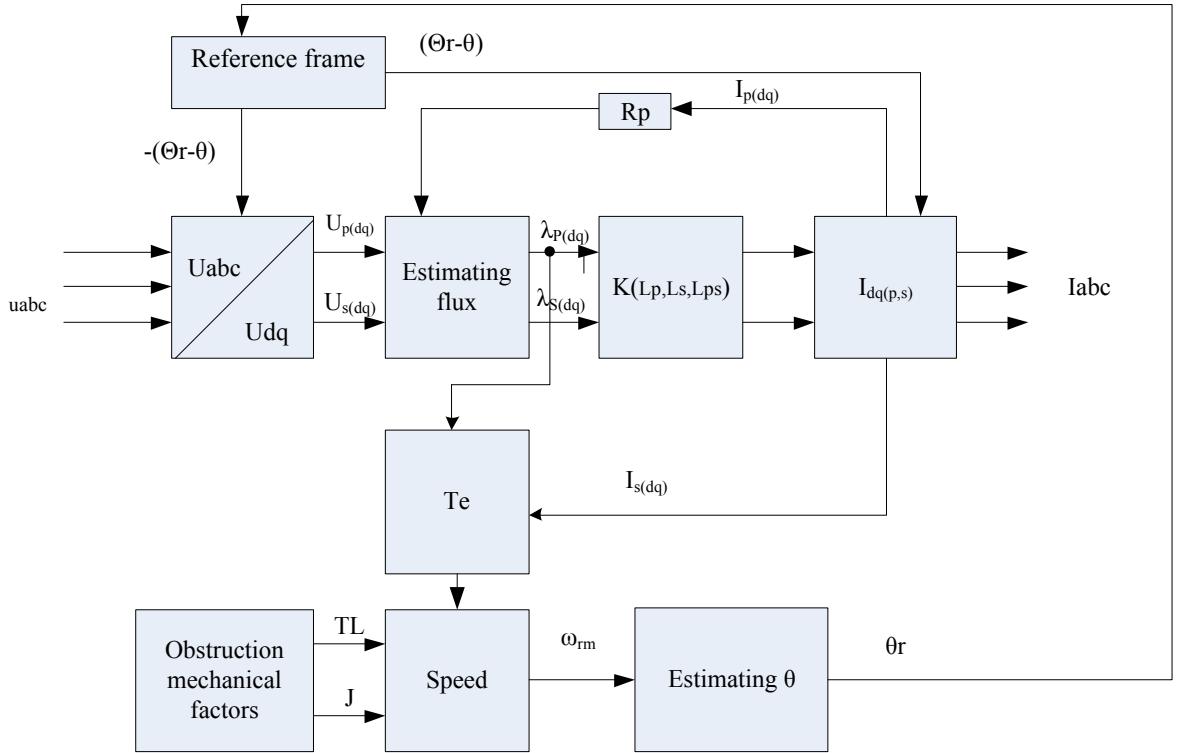
Figure 2.6: A simplified block diagram of the BDFRM dynamic model.

Preliminary simulation results for the machine direct on-line starting with the shorted secondary terminals are shown in Fig. 2.7. Such an induction machine starting procedure is one possible way to prevent the inverter overloading (if partially-rated) during start-up [16, 23]. Using the construction design information of BDFRM together with parameter data allows testing the capability of the machine under various operating conditions.

Table 2.1: Off-line testing parameters at normal temperature of the 1.5 KW BDFRM prototype

Labels	Parameters	Definition
f_p	50	Grid Frequency [Hz]
V_p	380	Primary voltage (rms) [V]
P_r	4	Rotor Poles
J	0.1	Rotor inertia [kgm^2]
R_p	11.1	Primary winding resistance [Ω]
R_s	13.5	Secondary winding resistance [Ω]
L_p	0.41	Primary winding inductance [H]
L_s	0.57	Secondary winding inductance [H]
$L_{ps}=L_m$	0.32	Mutual inductance [H]
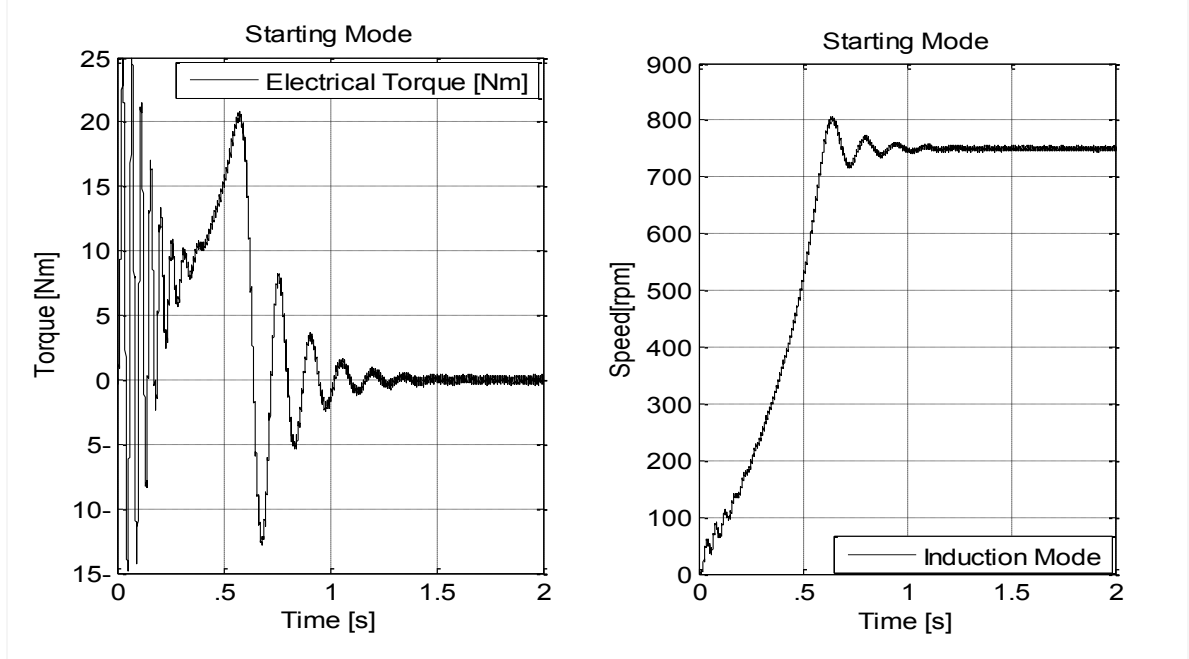
Figure 2.7: Speed and electromagnetic torque starting transients.

2.5 Power Flow

The fundamental mechanical power relationships for the machine indicating the contributions of each individual winding are [23].

$$P_m = T_e \omega_{rm} = T_e \frac{\omega_p}{P_r} + T_e \frac{\omega_s}{P_r} = P_p + P_s \tag{2.27}$$

$$P_s = T_e \frac{\omega_s}{P_r} = P_p \frac{\omega_s}{\omega_p} = -sP_p \tag{2.28}$$

The power flow on the primary and secondary side of the machine assuming motoring convention as default are given in visual form in Fig. 2.8 and summarised in Table 2.2 for both operating modes of the machine (e.g. motoring and generating) in super-synchronous and sub-synchronous speed regions.
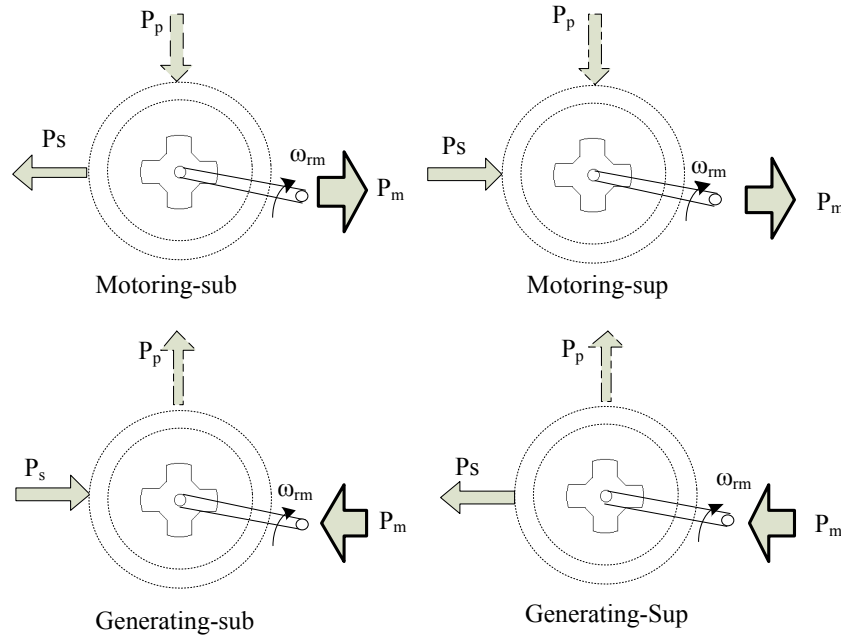
Figure 2.8: Visualizing the BDFRM power flow for typical operating modes and speed regions.

20

Table 2.2 : Power flows in case of positive and negative slip recovery modes

Speed Mode	Motor $T_e > 0$	Generator $T_e < 0$
Sub-synchronous ($\omega_s < 0$)	$P_p > 0$ & $P_s < 0$	$P_p < 0$ & $P_s > 0$
Super-synchronous ($\omega_s > 0$)	$P_p > 0$ & $P_s > 0$	$P_p < 0$ & $P_s < 0$

Chapter 3 **Scalar Control of BDFRM**

3.1   **Introduction**

In order to adequately respond to the growing demands for clean energy, it is crucial to maintain the existing and develop new environmentally friendly technologies focusing on solar but foremost wind resources as the most prominent[36]. In keeping with this world-wide trend, many wind farms have been commissioned the tendency being to build large units for off-shore applications offering the best wind power quality and thus the highest energy production required to reduce the pay-back periods of capital investments [3, 37]. As mentioned previously, the Brushless Doubly Fed Reluctance Generator BDFRG may be an attractive candidate for variable speed wind turbines with maximum power point tracking (MPPT) as it not only has the potential to provide the efficient wind energy conversion but can significantly reduce the high running costs of DFIGs by its brushless design, improved reliability and maintenance-free operation.

Conventional control methods, commonly applied to other more traditional AC machines including DFIG, have also been developed for the BDFRM/G. The scope of control related research on this particular machine has been largely based around the following topics: scalar control [25, 38], primary voltage-oriented (vector) control (VC) [39], primary-flux (field) oriented control (FOC) [40], direct torque and flux control (DTC) [41], torque and reactive

power control (TQC) [42, 43], direct power control (DPC) [44], sliding mode power control (SMPC) [45] and even non-linear multiple-input-multiple-output (MIMO) control theory [46]. Some of these control methods (such as DTC, SMPC and MIMO theory) are model-based, sensitive to parameter variations and not robust from this point of view. In addition, SMPC and MIMO [47] have not been experimentally validated to be of any practical use. The recently proposed TQC and DPC concepts [24] are viable, parameter-independent and robust, but they feature variable switching rates and higher sub-harmonic content as usual limitations of hysteresis type of control. Furthermore, fast transient responses, typical for 'bang-bang' control, are not really of immediate interest to the target BDFRM applications (e.g. wind turbines and pump-alike drives) where steady-state, rather than dynamic, performance is of primary concern.

On the other hand, VC and FOC share all the advantages of TQC and DPC but offer superior control quality by having fixed control (and inverter switching) rates with space-vector or sinusoidal PWM converters. This is foremost the case with FOC as inherently decoupled control of real power (or torque) and reactive power is possible unlike the VC where feed-forward decoupling schemes are generally required to achieve the FOC performance. However, the down side of FOC is that it has to deal with flux estimation related issues (e.g. saturation problems associated with transducers DC offsets effects on the voltage integration accuracy). Nevertheless, these two approaches, and VC in particular (e.g. cross-coupling effects referenced above are getting less pronounced with increasing machine sizes as winding resistance values then become smaller, and virtually negligible in a MW range) have been widely-adopted control solutions in a variety of drive and generator industrial applications including large-scale DFIG wind turbines.

Despite its simplicity, versatility, ease of implementation and amenability to sensorless operation, scalar control (SC) [23, 48] has been largely ignored in comparison with the aforementioned control approaches and there is very little work reported in the BDFRG literature. The method has been well established on the market for general purpose drive applications (e.g. pumps, compressors, fans, blowers etc.) of conventional cage induction motors and commercial drives of this kind are readily available. However, this appears not to be the case for generator systems, including wind turbines, even based on conventional DFIGs. The most likely reason for this lack of interest is its general inability for any sort of performance optimisation (such as efficiency or power factor control for instance), which is obviously very important for grid-connected wind turbines. It is mainly for this reason that VC or FOC have been an exclusive choice of preference in these and similar applications no matter that high dynamic performance offered by these controllers are not necessary. If it wasn't for the lack of performance optimisation, SC would be an attractive alternative option as, in its nature; it is tailored for dynamically least demanding applications and as such is ideally suited to wind turbines.

The conceptual differences in the operating principle between the BDFRG and DFIG [34, 35] will be shown to be beneficial for the SC application in the former case offering some performance advantages that can't be matched with traditional DFIGs. The higher leakage inductances and larger time constants of the BDFRG compared to DFIG [49] help in reducing transient stability problems commonly associated with SC of other AC machines. In addition, performance optimisation, similar to that achievable with vector controllers, turns out to be possible to some extent with BDFRG. These and similar issues will be addressed in this chapter.

24

Such kind of studies has not been published to date and represents one of the key contributions of this thesis.

The SC concept for the BDFRG has been introduced in [14]by analogy to that used for DFIGs [49] and some rather preliminary 'proof-of-concept' simulation results under ideal operating conditions and without taking into account any practical effects have been presented. The original SC design has been subsequently improved in [50] and a qualitative comparative analysis with VC and DTC made but without any quantitative supporting studies, either simulation or experimental, to validate the claimed enhancement of the updated scheme. The fact is that, to the best of the author knowledge, no detailed simulation studies or experimental verification of SC for the BDFRG have been documented in the peer-reviewed literature on the subject. This thesis will fill this gap by presenting an extensive set of experimental results and a comprehensive analysis of this sensorless control method using dynamic model of the BDFRG as a starting point for the algorithm development. Voltage boost at lower secondary frequencies, typical for practical speed ranges of the machine, shall be deemed necessary for enhanced dynamic and steady-state performance as well as to improve stability and convergence of the proposed scheme [51].

3.2   Open-Loop Scalar Control Theory

A characteristic of any open-loop controller is that it does not use feedback to determine if its output has achieved the desired reference input. This means that the system does not observe the output of the controlled process and that its performance entirely relies on the model quality and accuracy of the estimated parameters obtained by off-line testing.

SC is the simplest low-cost control algorithm for general purpose (e.g. low to medium performance) AC drives and especially those based on six-step, or more recently, space-vector or sinewave PWM inverter-fed induction motors [52]. Amongst different SC schemes where, as the name implies, only a single variable is effectively controlled (usually air-gap flux), constant voltage per hertz (*V/f*) with voltage boost at low frequencies (to compensate for comparable stator impedance voltage drops at low supply voltages) is certainly the most popular and widely-used method in industry. An open-loop scheme (i.e. without speed feedback) can be used in applications which do not require fast transient response and accurate speed control (e.g. fans, centrifugal pumps, compressors and similar devices). Additionally, the open-loop SC, essentially implies some sort of torque control which, in its simplest form, doesn't need any sensor or knowledge of the machine parameters.

The calculations of the desired supply voltage and applied frequency values to the secondary winding for SC purposes are based on the fundamental angular velocity relationship for the BDFRM (2.4) which is repeated in here for convenience but in an equivalent 'control' form as follows:

$$\omega_s = p_r \omega_{rm} - \omega_p \Leftrightarrow f_s = p_r \frac{n_{rm}}{60} - f_p \tag{3.1}$$

where $\omega_s = 2\pi f_s$ is the secondary angular frequency [rad/sec], f_s is the secondary frequency in [Hz], p_r is the number of rotor poles, and $\omega_p = 2\pi f_p$ is the primary (line) angular frequency with $f_p = 50$ Hz (or 60 Hz in USA). Note that if the generic slip is defined as: $s = -\omega_s / \omega_p$, then (3.1) can be rewritten in the form $\omega_{rm} = (1-s).\omega_p$ which is the same expression as that used for the rotor angular velocity of conventional induction machines. This indicates that ω_s actually plays the role of the slip frequency, the secondary BDFRM winding acting as the controllable

rotor winding and the primary as the grid-connected stator counterpart of the classical slip-ring doubly-fed induction machine (DFIM). Establishing this functional analogy which, it is interesting, exists despite the conceptually different operating principles of the two machines from the same slip power recovery family, is important because of potential *V/f* control similarities[53]. In order to implement the SC algorithm in Simulink[®], let us assume that the 3-phase sinusoidal voltages (U_c) of the windings can be expressed in generic form as follows [54]:

$$U_c = \begin{cases} v_a = V_m \cos(2\pi f.t) \\ v_b = V_m \cos\left(2\pi f.t - \frac{2\pi}{3}\right) \\ v_c = V_m \cos\left(2\pi f.t + \frac{2\pi}{3}\right) \end{cases} \tag{3.2}$$

Note that (3.2) is obviously more representative in the primary winding case by its direct grid connection and nearly sinusoidal, balanced 3-phase voltages of constant amplitude V_m at line frequency, $f = f_p$. However, the instantaneous voltages to be applied to the secondary terminals are obviously variable (so is the corresponding frequency, $f = f_s$) and should be generated through a controllable PWM inverter as indicated in Fig.3.1. Excluding the superimposed high-order switching harmonics in a kHz range, surely the desired fundamental voltages should also be closely sinusoidal depending on the IGBT converter quality and the numerical integration accuracy (e.g. system sampling rates) of simulation studies or the control (switching) rates adopted for real-time implementation.
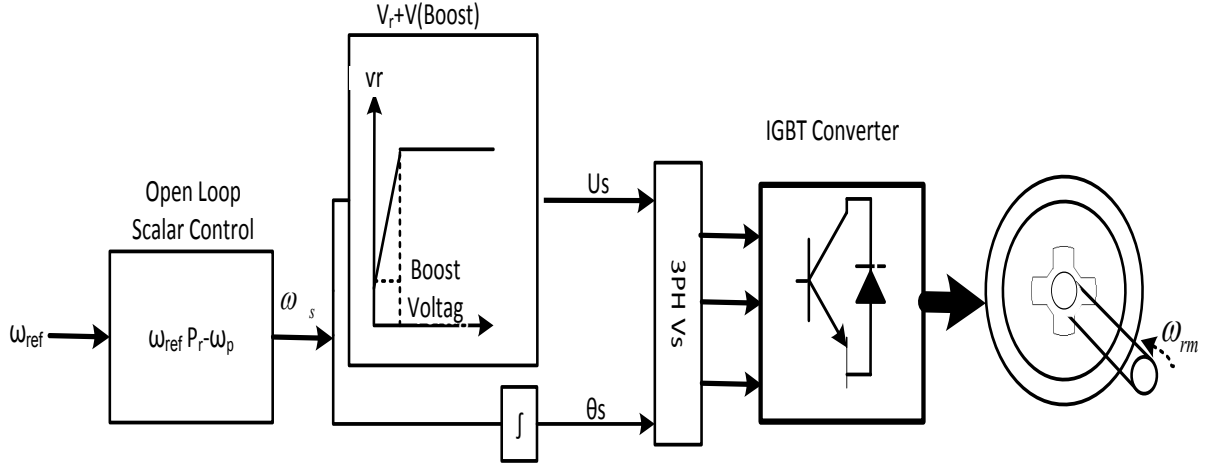
Figure 3.1: Open-loop *V/f* controller for the BDFRM.

The open-loop (i.e. without speed feedback) SC method for the BDFRM in Fig. 3.1 is in many respects of similar design to that applied to conventional cage induction machine (IM) [14]. Note however that whiles this approach would allow load-dependent speed control accuracy with the IM (e.g. determined by the resultant slip), it should provide precise speed control of BDFRM or DFIM given their synchronous operating nature, where the speed is locked at the frequencies applied to the windings according to (3.1). So, with the fixed frequency offset introduced by the primary winding, the rotor speed should be determined by the adjustable secondary frequency. In other words, for a desired speed above, at or below the synchronous speed (when $\omega_s = 0$ i.e. DC-fed secondary), the required ω_s can be found using (3.1) as also shown in Fig. 3.1. Providing the algorithm convergence and machine operating stability are preserved, quality speed control can be achieved, and more importantly, in a sensorless manner which is an important reliability advantage for wind turbines.

The secondary voltage magnitude is directly dependent on the desired reference speed i.e. secondary frequency by the *V/f* control nature. The fact that the BDFRM speed (and therefore

secondary frequency) range is limited (usually 1.5 to 2) to be able to achieve cost advantages of using a partially-rated inverter, when coupled with relatively low dynamic requirements in the target applications, means that sudden speed variations are not possible which is more than beneficial from a SC perspective. This helps minimise instability, typical for open loop SC of other machines. An additional contributing factor for maintaining the SC transient stability is the higher leakage reactance compared to DFIG as mentioned earlier.

In order to come up with an appropriate *V/f* ratio for SC of the BDFRM, one should evaluate the steady-state form of the secondary voltage equation in mutual flux-oriented reference frame for convenience of analysis [55]:

$$\underline{U}_s = R_s \underline{i}_s + j\omega_s \underline{\lambda}_s = R_s \underline{i}_s + j\omega_s (\sigma L_s \underline{i}_s + \lambda_{ps}) \qquad (3.3)$$

where λ_{ps} is the primary flux linking the secondary winding (i.e. mutual flux) and σ is the leakage factor defined as with induction machines. For instance, if Maximum Torque Per Inverter Ampere (MTPIA) is desired performance optimization (to minimise the secondary current levels for a given torque and hence reduce copper and inverter switching losses on the secondary side, with immediate efficiency implications), then $i_{sd} = 0$ so that (3.3) becomes:

$$\underline{U}_s = j(R_s i_{sq} + \omega_s \lambda_{ps}) - \sigma\omega_s L_s i_{sq} \qquad (3.4)$$

Neglecting the secondary impedance voltage drop, which can be proven to be a valid assumption for frequencies other than in a very narrow margin around zero (i.e. near synchronous speed), the above expression can be simplified to:

$$\underline{U}_s \approx j\omega_s \lambda_{ps} = j\omega_s \frac{L_{ps}}{L_p} \lambda_p \approx j\omega_s \frac{L_{ps}}{L_p} \frac{U_p}{\omega_p} \qquad (3.5)$$

where λ_p is the primary flux linkage magnitude. The previous expression can be further manipulated to give for the desired *V/f* under the MTPIA conditions:

$$\frac{U_s}{\omega_s} \approx \frac{L_{ps}}{L_p}\frac{U_p}{\omega_p} \Longrightarrow \frac{U_s}{f_s} = \frac{V}{f} = \frac{L_{ps}}{L_p}\frac{U_p}{f_p} \tag{3.6}$$

So, by keeping (3.6) satisfied, $\lambda_{ps}{\approx}const$ and the MTPIA control objective should be largely met. It will be shown in the following sections that this is not quite the case with small machines having proportionally higher resistances (as the BDFRM prototype used for simulation and experimental studies in this thesis), but may give expected optimal results on a large-scale level where both the primary and secondary resistances can be ignored in most situations when the approximations made would be more than justified by very little errors.

3.2.1 Boost Voltage for Performance Enhancement

While many features of BDFRM design (e.g. large leakage reactances and slower transient responses) and applications (e.g. dynamically least demanding such as wind turbines or pump-alike drives) would suggest SC use, one known downside is that the machine is required to operate at relatively low secondary frequencies as dictated by the limited variable speed ranges around synchronous speed (n_{syn}). Using (3.1), it can be easily shown that for a desired speed ratio $a = n_{max}/n_{min}$ (i.e. the speed range $[n_{min},n_{max}]$ where $n_{max} = n_{syn} + \Delta n$ and $n_{min} = n_{syn} - \Delta n$), the respective secondary frequency limit (Hz) is given by:

$$f_{\text{s-max}} = \frac{a\text{-}1}{a+1}{\cdot}f_p \tag{3.7}$$

For instance, if $a = 2$, which is typical for wind power applications (e.g. 500 rev/min to 1000 rev/min for a 4-pole BDFRM rotor), the maximum secondary frequency at $f_p = 50$ Hz should be

$f_{s\text{-}max} = f_p/3 \approx 16.7$ Hzwith a positive (e.g. for super-synchronous speeds) or negative (e.g. at sub-synchronous speeds) phase sequence of the secondary windings. In case of $a = 1.5$ (e.g. 600 rev/min to 900 rev/min i.e. 150 rev/min around $n_{syn} = 750$ rev/min), which can also be encountered in wind turbines, this frequency limit gets even lower $f_{s\text{-}max} = 12.5$ Hz.

Given the above preliminary considerations, the low frequency operation appears to be a general problem with all SC methods no matter which type of machine is to be controlled, a classical inverter-fed cage induction machine (IM) being by far the most popular example. A traditional approach for control performance improvement of IMs at low speeds is including appropriate voltage boost to effectively compensate for the neglected voltage drops on the stator side as their values are getting comparable to back-emf and terminal voltage levels with decreasing supply frequencies [56]. A similar concept will be applied to the BDFRM to address the low secondary frequency issues down to synchronous speed.

The starting point in this development is the machine torque expression (2.24) which can be written in a primary flux oriented form (e.g. $\lambda_{pq} = 0$) as:

$$T_e = \frac{3p_r L_{ps}}{2L_p}\lambda_p i_{sq} = \frac{3p_r}{2}\lambda_{ps} i_{sq} \qquad (3.8)$$

Substituting for the torque-producing secondary current component (e.g. i_{sq}) from (3.8) in a real part of (3.4), the latter becomes:

$$\underline{U}_s = j(R_s i_{sq} + \omega_s \lambda_{ps}) - \frac{2\sigma L_s}{3\lambda_{ps}}\frac{\omega_s T_e}{\underbrace{p_r}_{P_s}} \approx j(R_s i_{sq} + \omega_s \lambda_{ps}) \qquad (3.9)$$

The secondary power (P_s) term in (3.9) appears to have little influence on the voltage magnitude in a considered ω_s range, so the errors made by making the above approximation can be justified by the consequent control simplifications in most cases. Therefore, under this assumption, the *V/f* control law can be formulated as:

$$U_s = \underbrace{R_s i_{sq}}_{\text{Boost}} + \underbrace{2\pi\lambda_{ps}}_{\frac{V}{f}\text{ratio}} \cdot (\pm f_s) \tag{3.10}$$

The voltage boost offset is usually set to about 10% for effectual rated voltage amplitude or so to account for the unknown resistive effects in (3.10). For given machine specifications and knowledge of R_s obtained by off-line testing at normal temperature, this value can be more accurately estimated under full-load conditions (e.g. for rated i_{sq}). The existence of voltage boost is an extremely important stability measure during ride through, and especially for sustained operation at, the synchronous speed (when $f_s = 0$) as otherwise there would be not enough voltage to drive the current in the secondary winding and produce the necessary synchronising torque to reach the synchronous speed. The underlying phenomenon here is very similar to starting of a classical synchronous machine with damper windings upon feeding a DC voltage in the rotor circuit to excite the machine when near the synchronous speed and pull it into the synchronism with the grid.

In the BDFRM case, the polarity of the boost voltage should be of the ω_s sign (so that it is co-acting and not opposing the main secondary voltage) which can be achieved using a readily available 'sgn' function in the SC scheme as illustrated in Fig 3.2 (i.e. the boost sign will be '+' for super-synchronous operation and '-' in sub-synchronous speed mode) or graphically in Fig. 3.3. The implementation of this scenario ensures sustained stability of the

machine/controller combination in practice as will be demonstrated by the laboratory measurements presented in the remainder of this chapter. Unless stated otherwise, these test results have been generated by executing the SC algorithm in Fig. 3.2 at fixed 5 kHz space-vector PWM rate (i.e. the inverter switching frequency) and $V/f \approx 0.8$ this ratio being calculated using (3.6) for the BDFRM parameters in Table 2.1.
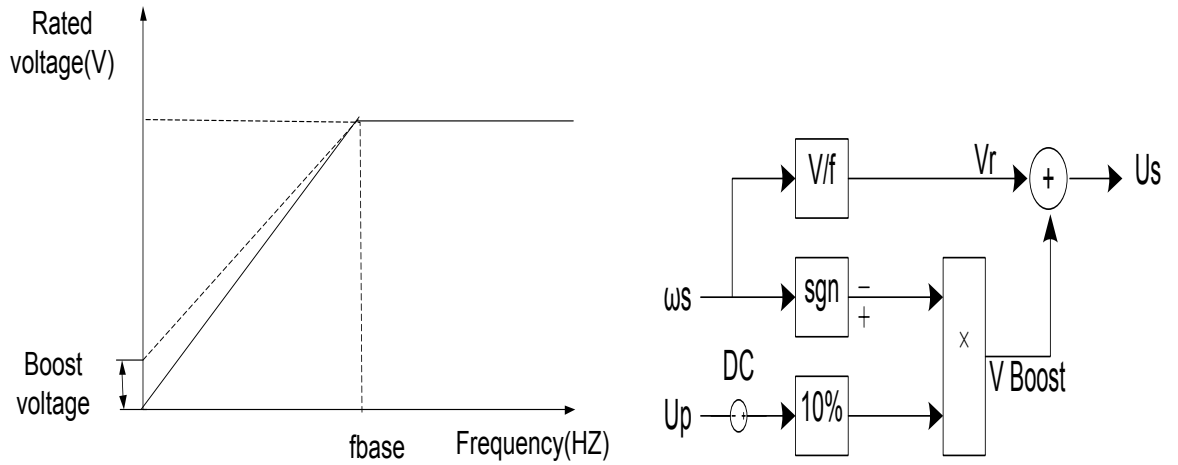
Figure 3.2: Principle of V/f control with the boost voltage included.
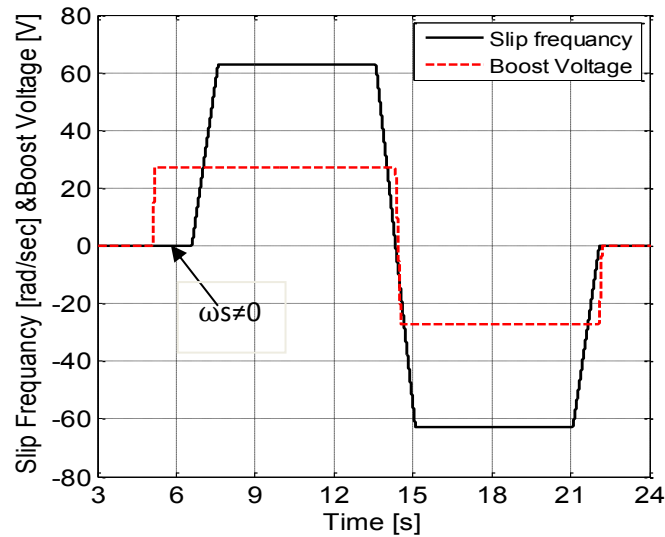
Figure 3.3: Secondary angular frequency and voltage boost in a limited speed range.

3.3 Real Time Implementation (RTI) of Open-Loop Scalar Control

In order to assess the viability of any control simulation programme, it is necessary to port it onto a physical system to verify its validity. For the project being undertaken as part of this thesis, the BDFRM test rig (see the Appendix-A, Fig. A.1, for details) is based on Simulink compatible dSPACE development platform for rapid control prototyping [57]. RTI is a Simulink toolbox which provides the required processing blocks to configure simulation models for practical use. The Control Desk of dSPACE allows the user to monitor the real-time operation by using virtual instruments. The first procedural step consists in building a working control model in Simulink and configuring appropriately the I/O connections of the connector panel via the RTI toolbox. The real-time workshop (RTW) compiles the C-code for the dSPACE board using RTI. Once the execution code has been generated, the dedicated dSPACE hardware can perform a real-time experiment which can be controlled from a PC through the Control Desk. The latter can also be used to: monitor the simulation progress, change the parameters online, capture data (in a format compatible with Matlab) etc.

3.3.1 Variable Speed Operation of BDFRM /G at Fixed Load

The SC response in open-loop mode has been tested for the machine operated as a motor (BDFRM) in a narrow speed range (600-900 rev/min) around synchronous speed (750 rev/min) at fixed load. The desired loading conditions have been emulated by a 4-quadrant DC machine drive (refer to Appendix for specifications). The BDFRM was started with the shorted secondary windings as a wound rotor induction machine to a steady sub-synchronous speed of 730 rev/min corresponding to 9 Nm load torque, as shown in Fig. 3.4. The secondary terminals

were shorted through the inverter legs directly (e.g. by applying '111' or '000' switching pattern to the power devices) due to its high rating but in reality if a partially rated converter is being used (as is normally the case), then an external contactor would be required to by-pass the inverter during start-up (and hence avoid its overloading).

The control is enabled at nearly 6s time instant with a speed reference set to 750 rev/min (i.e. $f_s = 0$) when a DC boost voltage is applied to the secondary winding according to (3.10) to force the BDFRM effectively behave as a conventional wound field $2p_r$-pole synchronous turbo-machine. It can be seen in Fig. 3.4 that the BDFRM speed after a short transient can successfully attain the desired synchronous speed (6-7.5 s). The speed commands have been sequentially changed to 900 rev/min and then 600 rev/min to show variable speed operation of the machine. A transient speed drop (monitored by an incremental encoder) just after 15s comes from the electro-magnetic torque variation associated with the sudden change of polarity in the boost voltage, and the very low inertia of the test machine. This disturbance would not be present with large machines having high inertia constant. Although dynamic performance is not imperative with SC, such speed excursions can be minimised by an alternative voltage boost strategy to be elaborated later in this chapter.
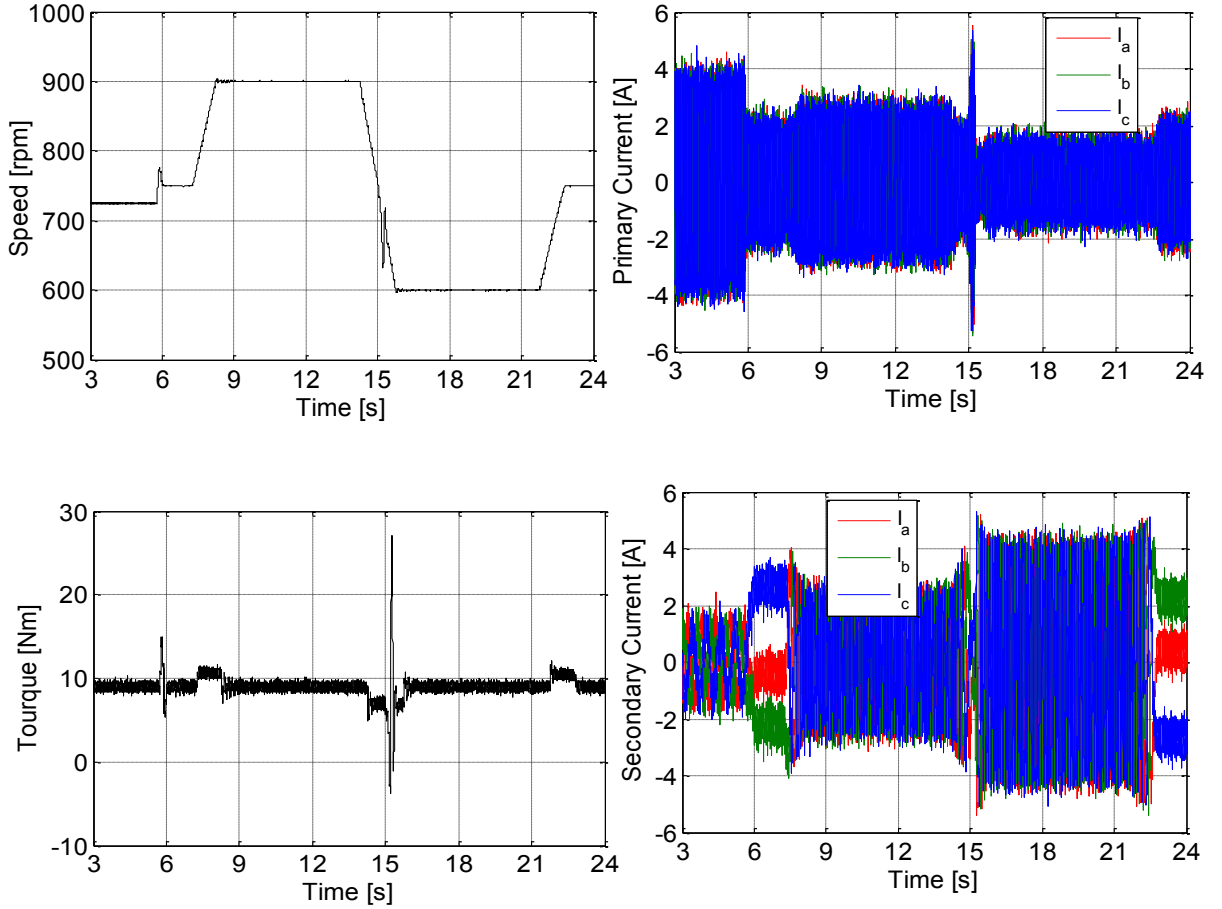
Figure 3.4: BDFRM performance with open-loop SC at 9 Nm load.

Similar results have been produced for synchronous and super-synchronous speed modes only (Fig. 3.5). Again, immediately following the start-up period, the BDFRM initially operates as an induction machine (i.e. with the shorted secondary) and then switches to synchronous machine operation upon the control activation just before 6s. The super-synchronous mode should be more efficient as the electrical power taken by both the windings is entirely converted to mechanical (and vice-versa in generating regime). This is not the case in sub-synchronous mode when part of the primary power is being regenerated back to the supply (or dumped in the dc link resistor in case of a diode bridge rectifier being used as on our test rig) through the secondary winding producing losses on its way.
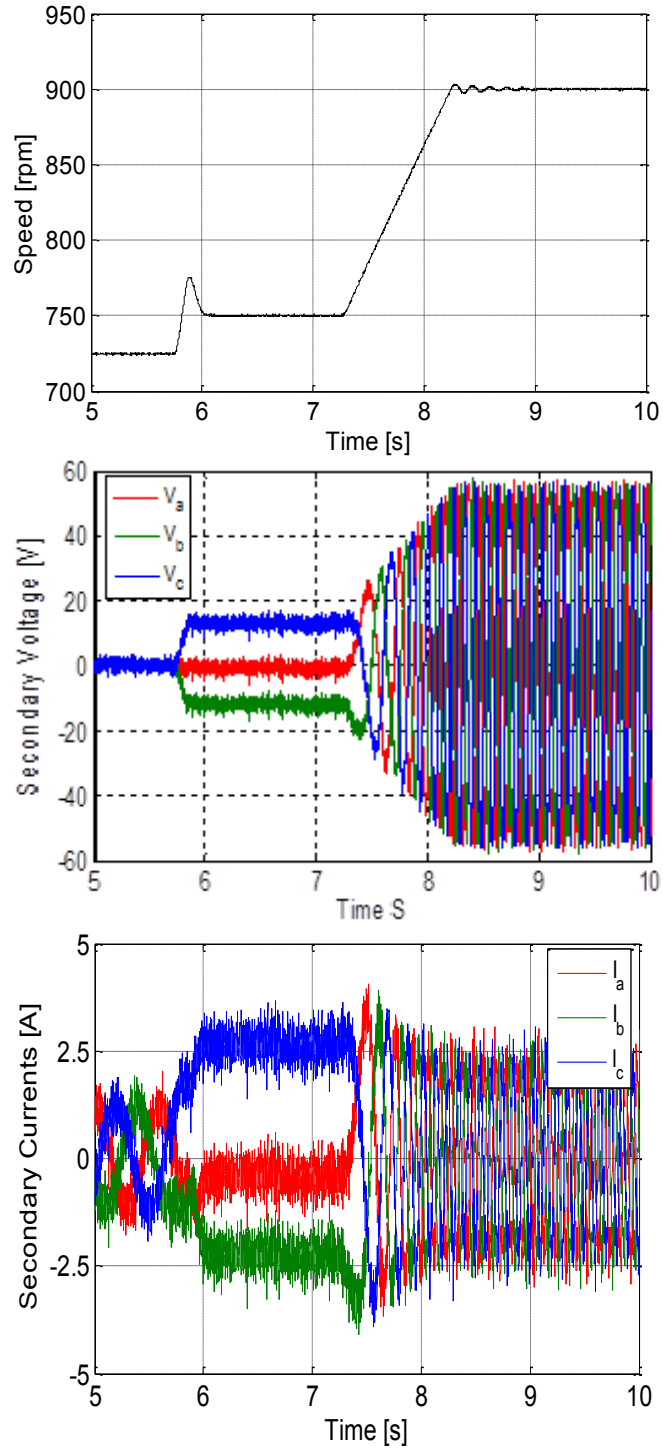
Figure 3.5: The BDFRM operating modes: induction (prior to 6s), synchronous (6-7.3s) and super-synchronous (from about 8.3s onward).

The secondary voltage magnitudes (in average sense) in Fig. 3.5 have been sequentially changing from zero in induction machine operating mode (as expected for shorted secondary terminals) through DC values (corresponding to the boost voltage) at synchronous speed and then gradually increasing to near 60V in response to desired speed and f_s references according to the executed *V/f* control law formulated by (3.10).
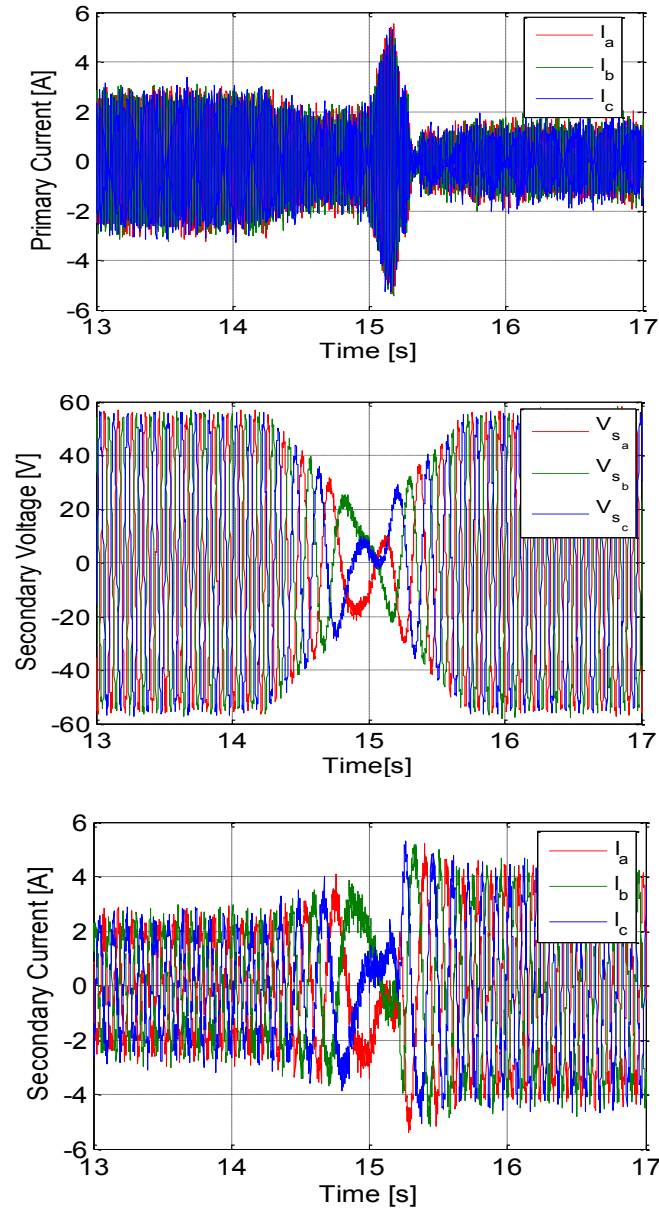
Figure 3.6: Phase sequence reversal in transition from super-synchronous to sub-synchronous mode.

A similar trend can be observed in Fig. 3.6 which clearly illustrates a phase sequence change in both secondary voltage and current waveforms while riding through the synchronous speed. Fig. 3.7 shows the variations of parameters relevant for space-vector PWM of the machine-side IGBT converter (termed as inverter throughout) under the same operating conditions as in Fig. 3.6. The top plot illustrates the PWM step-wise sectorial changes in a stationary reference frame, the bottom graph the respective switching times of the two active voltage vectors defining these individual 60° sectors, and the middle plot depicts the angular positions of the secondary voltage vector obtained by integrating the reference ω_s signal for a desired command speed (Fig. 3.1). These angles have been used by the PWM generator to identify in which sector the voltage vector is located for a given time instant. Note that the sector numbers are in ascending order for the positive phase sequence of the secondary windings (i.e. for super-synchronous operation) when the respective vectors rotate anti-clockwise ($\omega_s > 0$) as the primary winding counterparts (but at line frequency of course). Conversely, in sub-synchronous speed mode, the situation is reversed and the sector numbers are decreasing as the secondary vectors then rotate clockwise ($\omega_s < 0$) i.e. in the opposite direction to the primary vectors.
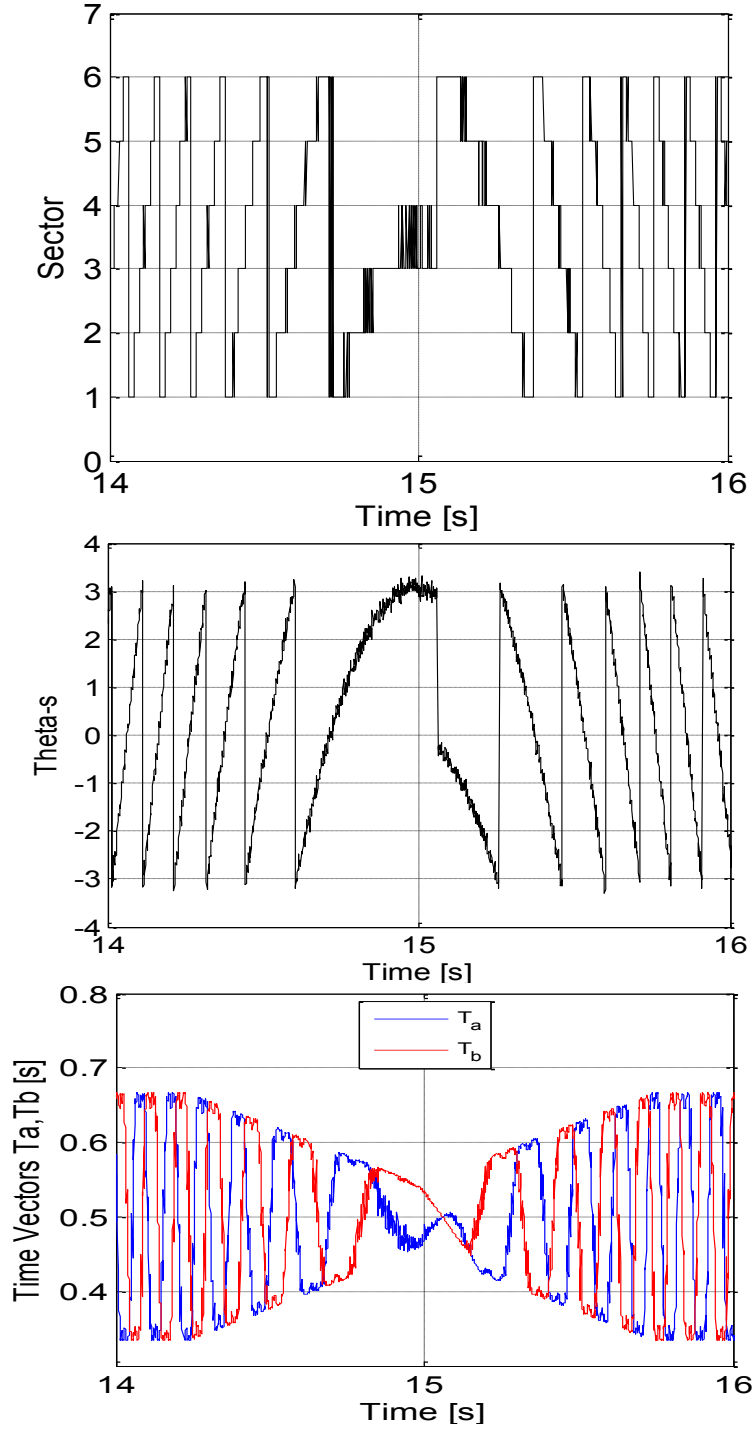
Figure 3.7: PWM space sectors, secondary angular positions and switching times of active voltage vectors bordering particular sectors during BDFRM speed mode reversal in Fig. 3.6

Fig. 3.8 demonstrates the reversibility of the machine operation from motoring to generating through 'idling' unloaded mode at 900 rev/min and 600 rev/min at 6 Nm absolute torques as measured by a torque transducer (see the Appendix for description of the laboratory test facility). Note that the shaft torque is positive in motoring (BDFRM) and negative in generating (BDFRG) regime by default. The specific loading conditions have been achieved by a dynamic dynamometer (i.e. a commercial DC drive feeding an off-the-shelf machine) operated in torque mode as a load or prime mover depending on the machine mode of interest. The speed is kept at desired value through open-loop *V/f* control of BDFRM (G).

It can be seen from Fig. 3.8 that the machine speed response is hardly affected (although some disturbance is visible) by the relatively modest shaft torque variations and that the desired reference can be accurately followed for either BDFRM or BDFRG. For torque changes in a wider range, instability may occur however which is typical for SC. In subsequent experiments, the motoring and generating mode will be independently tested to examine the machine behaviour under speed dependent loading conditions in a limited variable speed range.
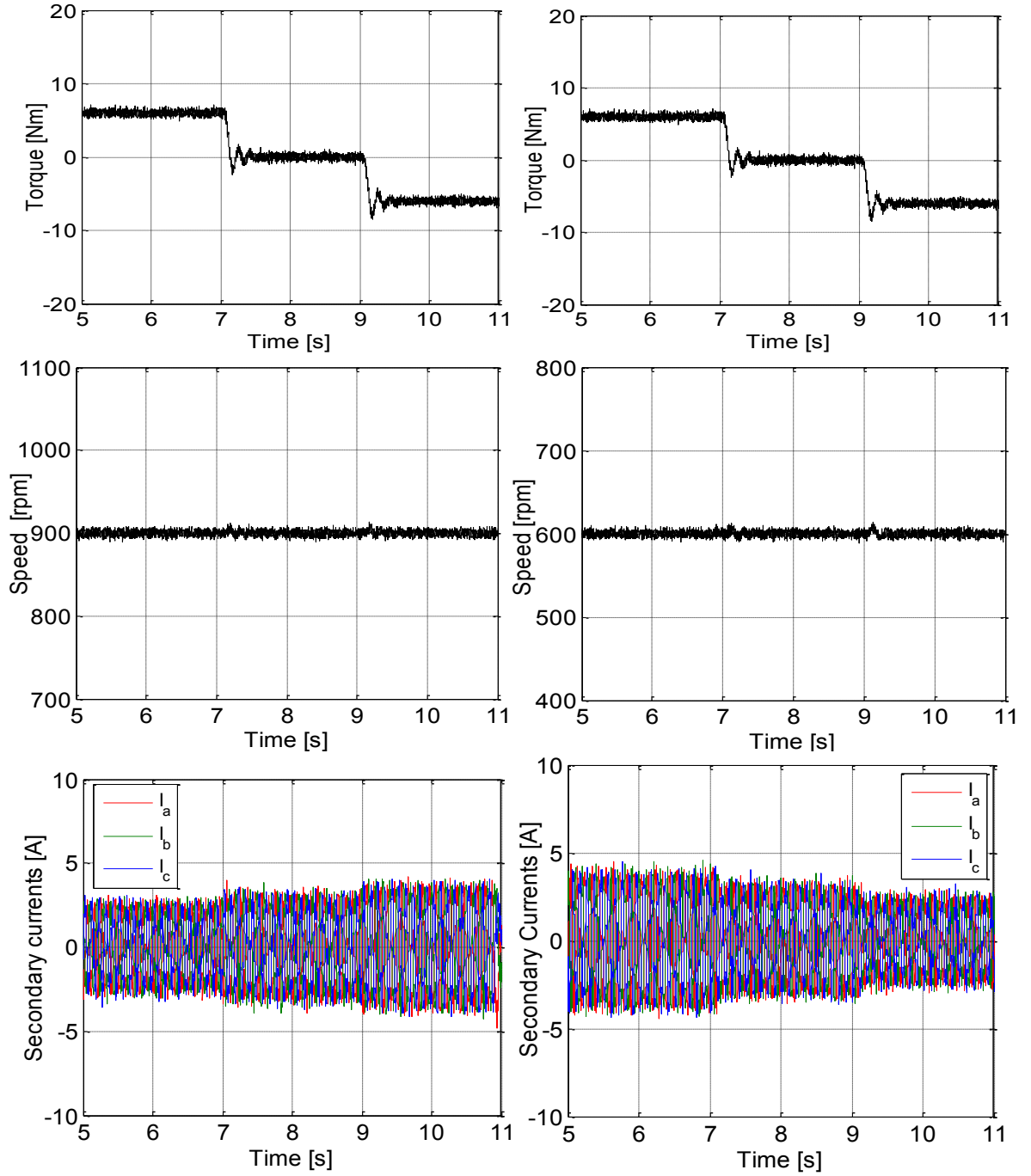
Figure 3.8: BDFRM/G super-synchronous and sub-synchronous operation at 6 Nm shaft torque

3.3.2 Variable Speed and Loading Conditions of the BDFRM /G

The purpose of this section is to present experimental results for speed and loading profiles commonly encountered in the BDFRM(G) target applications: large centrifugal pump-alike drives (e.g. fans, compressors, blowers etc.) or wind turbines with maximum power point tracking (MPPT) for efficient wind energy conversion.

In the aforementioned variable speed motor and generator systems, the shaft torque vs speed characteristic in the base speed region (i.e. from the minimum up to the rated speed) can be represented in generic form as:

$$\frac{T_L}{T_r} = \left(\frac{n}{n_r}\right)^2 \tag{3.11}$$

where n is the actual machine speed, n_r is the rated speed, T_L is the shaft torque, and T_r is the full-load torque of the machine. For the test BDFRM(G) in consideration, (3.11) becomes:

$$T_L = \pm 19.1 \left(\frac{n_{rm}}{1000}\right)^2 \tag{3.12}$$

where '+' refers to the BDFRM and '-' to the BDFRG.

The BDFRM behaviour under variable load condition (Fig. 3.9) is quite similar to that obtained for a fixed load in Fig. 3.4. The speed reference signals are again set in a ramp fashion to minimise troublesome stability problems of scalar control that may occur in case of sudden speed or frequency variations. The notable transient 'glitches' in the torque and speed waveforms in Fig. 3.9 are of the same origin as those in Fig. 3.4 (e.g. due to the voltage boost polarity reversal through synchronous speed). However, having smooth dynamic response is anyway not a necessary requirement in the target BDFRM/G applications as long as the desired

steady-state performance and reference speed tracking are eventually successfully achieved, this clearly being the case in either speed mode judging by the results in Fig. 3.9.

The elevated secondary current levels at sub-synchronous speed (600 rev/min) despite the reduced loading can be largely attributed to the increasing magnetising component in the regenerative operating mode of the secondary winding. This unnecessary reactive current rise can possibly be explained by the SC inaccuracies and excessive voltage applied through the PWM inverter without current regulation, unlike the vector control scenario when only the required amount of voltage is supplied to the secondary terminals to achieve the demanded currents. The copper losses also quantify differently in the power balance on the secondary side for the two speed modes because of the opposite power flow which can be another contributing factor. Similar observations can be made about Fig. 3.4 where the primary current magnitudes are lower than at super-synchronous speed since the primary winding is then required to participate less in the machine magnetisation and therefore in the production of reactive power for this purpose. The same trend can also be seen in the increasing transient secondary currents during the short time interval of speed mode change in Fig. 3.6.

In generating mode (BDFRG), the load torque is shifting to the negative domain (bearing in mind the adopted motoring convention as default), as indicated in Fig. 3.9. In this case, the DC drive used for the emulation of the square torque vs speed profile serves as a prime mover (see Appendix for details). By analogy to the BDFRM start-up procedure, the BDFRG initially operates as a cage induction machine at 780 rev/min (n_{rm}>n_{syn} = 750 rev/min). The control is then enabled and the BDFRG continues to function as an inverter-fed $2p_r$-pole synchronous

machine at desired speeds (e.g. 750 rev/min, 900 rev/min and finally 600 rev/min), in the same fashion as the BDFRM does (left plots in the same figure).

Most of the comments made previously for the BDFRM waveforms in Fig. 3.9 can thus be carried over to the BDFRG operating characteristics except that the power flow is surely different in either speed mode. In fact, the BDFRM super-synchronous operation would correspond to the sub-synchronous operation of the BDFRG and vice-versa, for a given f_s and therefore the secondary voltage magnitude under *V/f = const* law. This duality of the speed modes can obviously be confirmed by the very similar secondary current levels for the BDFRM at 600 rev/min (and 900 rev/min) and the BDFRG at 900 rev/min (and 600 rev/min) respectively when f_s = 12.5 Hz (although with the opposite phase sequence of the two windings) and the direction of secondary power flow (P_s) is also the same. Therefore, the same comparative conclusions and/or observations made for the BDFRM at 600 rev/min would apply for the BDFRG at 900 rev/min (in this case $P_s > 0$ is to the grid) and vice-versa for 900 rev/min (BDFRM) and 600 rev/min (BDFRG) when $P_s > 0$ flow is to the machine.

The investigation of the total copper losses in the BDFRM (G) for various *V/f* ratios deserves a particular attention from an efficiency point of view, and especially for small-scale machines having generally higher resistances (and hence dominant copper losses in most cases) like the BDFRM (G) prototype used for experimental studies. The MTPIA strategy referenced previously should minimise the inverter loading for a given torque reducing so the winding and switching losses on the secondary side, but the question is whether the overall losses in the machine would also be optimised under this condition given the Q producing burden

implications on the primary winding at super-synchronous speeds. This and similar practical issues will be addressed in the following paragraphs.
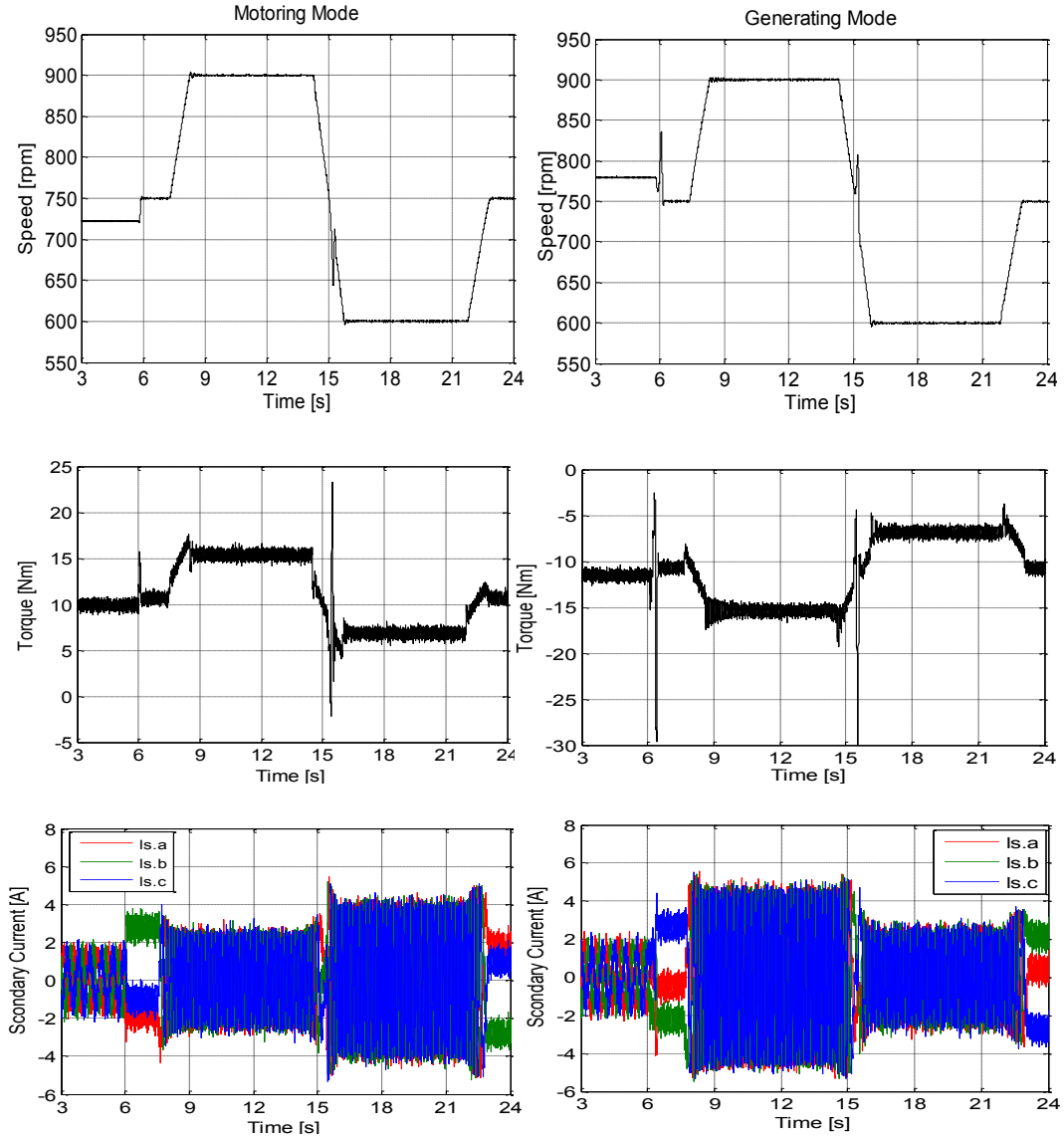
Figure 3.9: BDFRM/G operation under variable speed and loading conditions

3.3.3   BDFRM /GCopper Losses under MTPIA Conditions

The total copper losses in the BDFRM (G) can be calculated from measurements as the sum of the individual copper losses in the primary and secondary windings as follows:

$$P_{Total} = P_{p.cu} + P_{s.cu} = \frac{3}{2} R_p i_p{}^2 + \frac{3}{2} R_s i_s{}^2 \tag{3.13}$$

The main motivation for considering the MTPIA control strategy is an attempt to achieve the same vector control benefits (e.g. reductions in resistive losses of the secondary winding and conduction losses in the inverter power devices) using scalar control of small machines where the core losses are usually negligible compared to the copper losses. In this sense, the 1.5 kW test BDFRM (G) is not an exception. The analysis of copper losses in this section should therefore give us a valuable insight into the machine efficiency in both motoring and generating modes under variable loading conditions in a limited operating speed range of interest to the main target applications – pump drives and wind turbines.

The experimental results presented previously have been generated assuming $V/f \approx 0.8$ according to (3.6). However, this control form expression requires the machine inductance knowledge (e.g. L_{ps}/L_p) which contravenes the claimed parameter independence and versatility of the proposed SC method. In order to retain the latter advantages, an alternative approach should obviously be taken to achieve the same objective but using the nameplate data of a particular machine (refer to Table 2.1 for the test BDFRM specifications).

Applying (3.8) for the machine torque at the rated operating point one can write:

$$T_r = \frac{3}{2} p_r \underbrace{\frac{L_{ps}}{L_p} \lambda_p}_{\lambda_{ps} \approx \frac{V}{f}} i_r \qquad (3.14)$$

Then it is easy to extract the *V/f* ratio for control purposes using the BDFRM ratings from Table 2.1 or the corresponding rated torque value from (3.12):

$$V/f = \frac{2}{3 p_r i_r} T_r = \frac{2}{3*4*2.5\sqrt{2}} * \frac{30*1500}{\pi*750} = \frac{\sqrt{2}}{30} * 19.1 = 0.9 \qquad (3.15)$$

The above *V/f* estimate is slightly higher than that approximated using (3.6) but will be shown to be more representative for the considered machine.

The BDFRM (G) was tested under the same operating conditions as in Fig. 3.9 but for three additional *V/f* ratios: 0.7, 0.9 and 1, to find the most optimal value from an efficiency perspective. The experimental results obtained in motoring mode (BDFRM) are shown in Fig. 3.10, and for the generating operation (BDFRG) in Fig. 3.11. The respective component and cumulative winding losses at steady 900 rev/min (e.g. super-synchronous speed) and 600 rev/min (e.g. sub-synchronous speed) are tabulated for convenience of comparison in Table 3.1 for the BDFRM and in Table 3.2 for the BDFRG. The copper loss distribution for the two operating regimes of the machine in super-synchronous and sub-synchronous speed modes is also illustrated graphically in Figs. 3.12 and 3.13.
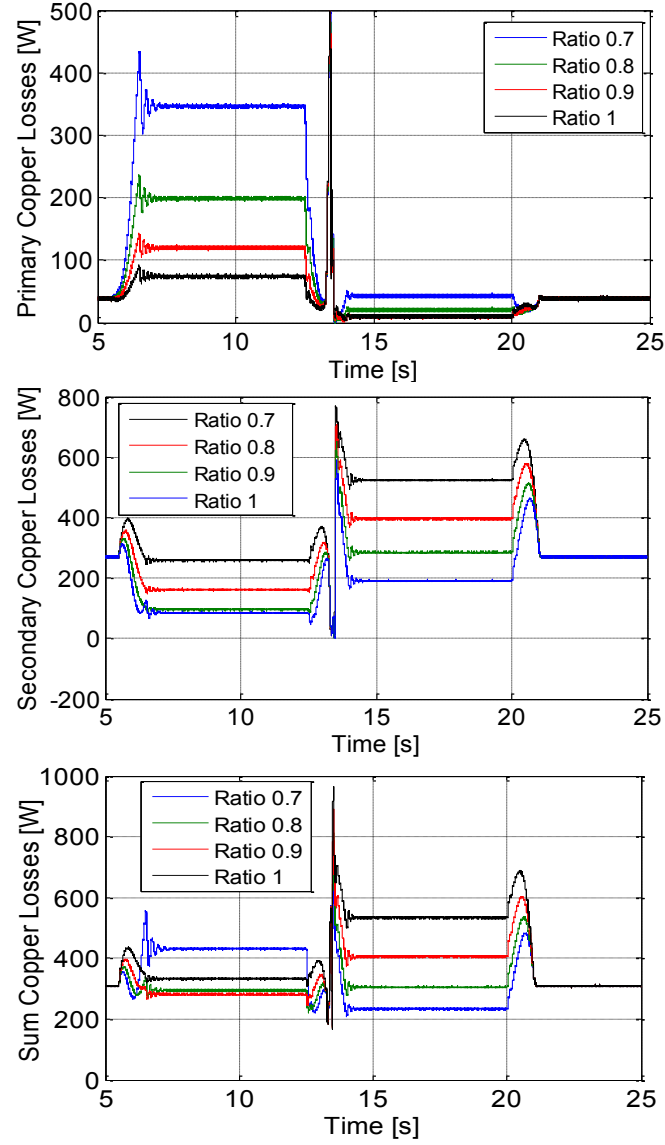
Figure 3.10: Primary, secondary and total losses of the BDFRM at variable load

Table 3.1: Individual and total copper losses of the BDFRM in two speed modes

Ratio	Primary Super-synch	Secondary Super-synch	Total losses Super-synch	Primary Sub-synch	Secondary Sub-synch	Total losses Sub-synch
0.7	340	90	430	40	185	**225**
0.8	200	100	300	25	280	305
0.9	120	160	**280**	10	400	410
1	80	250	330	20	500	520
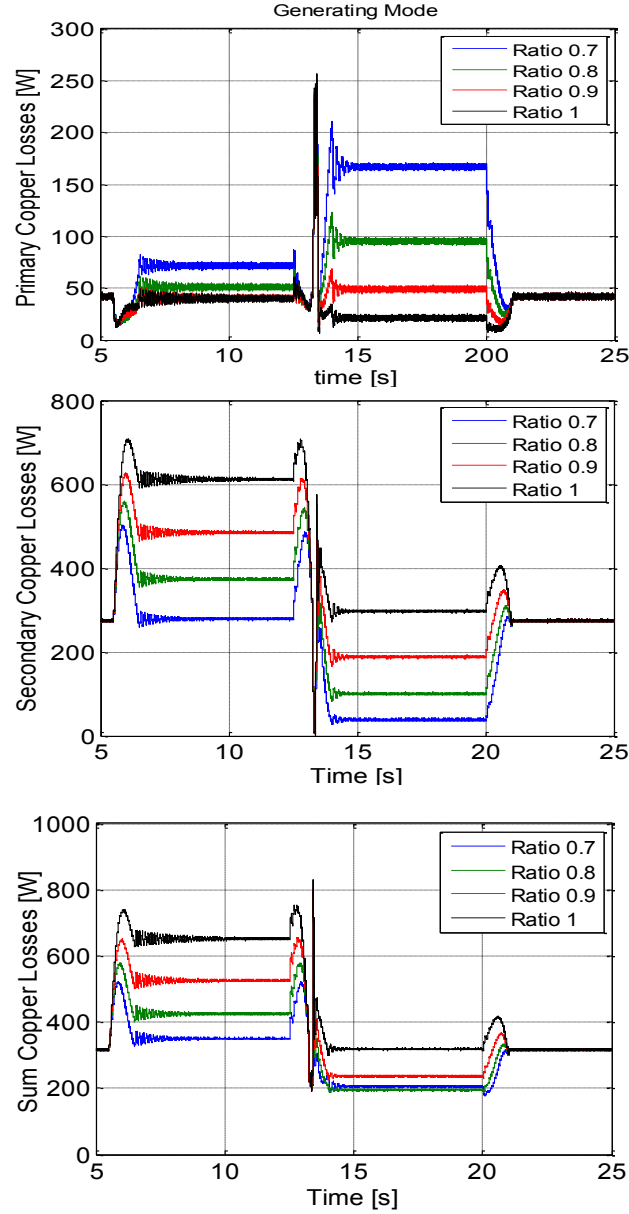
Figure 3.11: Primary, secondary and total losses of the BDFRG at variable shaft torque

Table 3.2: Individual and total copper losses of the BDFRG in two speed modes

Ratio	Primary Super-synch	Secondary Super-synch	Total losses Super-synch	Primary Sub-synch	Secondary Sub-synch	Total losses Sub-synch
0.7	70	280	**350**	165	40	205
0.8	60	370	420	100	100	**200**
0.9	40	500	540	40	190	240
1	30	620	650	10	300	310

50
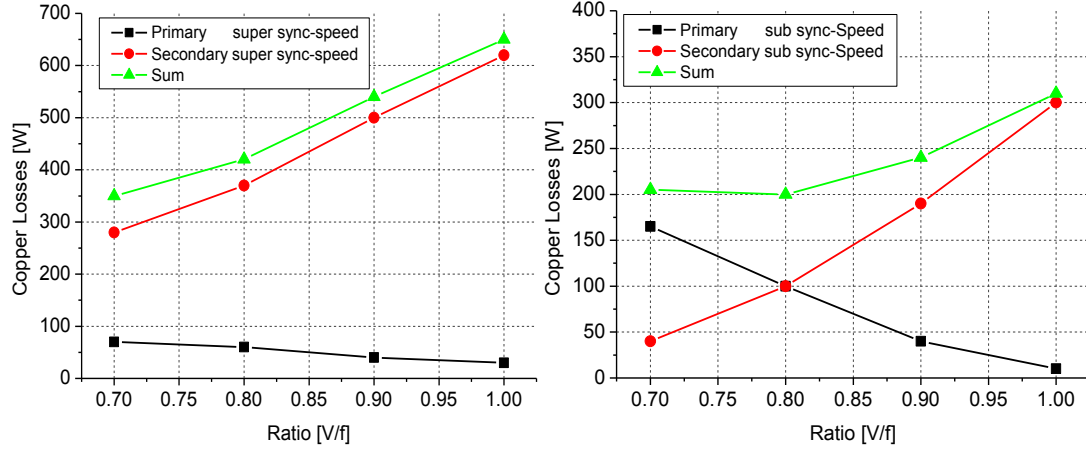
Figure 3.12: Distribution of copper losses inside the BDFRG under VLC
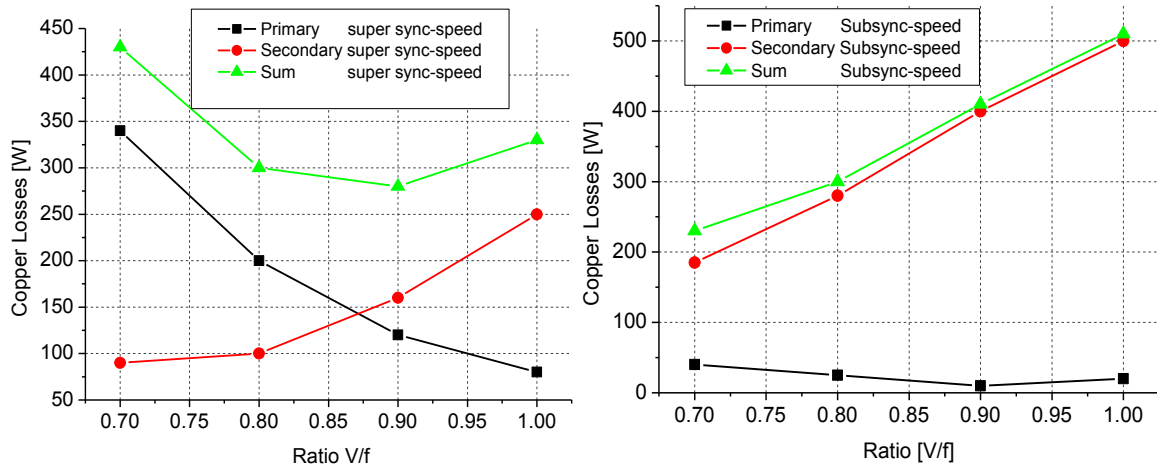
Figure 3.13: Distribution copper losses inside the BDFRM under VLC.

The following important observations can be made from Tables 3.1 and 3.2: (1) The most efficient (i.e. the minimum total loss) points (highlighted in bold) randomly take place at different *V/f* ratios in either operating mode; (2) The secondary power losses are much higher than the primary ones at sub-synchronous speed for the BDFRM and at super-synchronous speed for the BDFRG at any *V/f*. This trend is consistent with the results in Fig. 3.9 for *V/f* ≈ 0.8;

(3) the highest efficiency for BDFRM occurs at $V/f \approx 0.9$ in super-synchronous mode which is encouraging and as predicted by (3.15). However, this is not the case in sub-synchronous mode of the BDFRM or the BDFRG so can't be treated as a general rule.

The issue raised in (2) above should be properly addressed as the secondary currents should be mainly torque producing if the MTPIA conditions have been satisfied and as such should decline in magnitude with decreasing speeds and hence loads. However, this appears not to be quite true which suggests the presence of predominant magnetising component, and especially with the BDFRM. The only logical explanation for this phenomenon, as previously anticipated, is the lack of a current-controlled PWM voltage source and therefore over-voltages applied to the secondary. The solution to this problem has been found in injecting the boost voltage only when absolutely necessary for sustained operation (i.e. at/above synchronous speed for BDFRM and at/below synchronous speed for BDFRG). The results in Figs. 3.14 and 3.15 illustrate the benefits of this alternative voltage boost injection technique. If one compares the waveforms in Figs. 3.14 and 3.15 to those in Fig. 3.9, a significant overall performance improvement and smoother ride-through response through synchronous speed are immediately obvious for both the BDFRM and BDFRG. The current magnitudes are fairly levelled up in the two speed modes in Figs. 3.14 and 3.15 the existing differences being much smaller than in Fig. 3.9 and thus more reflective of the actual loading profiles of the machine. This seems to indicate their mostly torque (power) producing nature as it should be under the MTPIA conditions. The copper losses also appear to be more evenly allocated between the two windings with an apparent efficiency gain over the entire speed range according to the comparative studies presented in Figs. 3.16-3.19 and Tables 3.3 and 3.4.
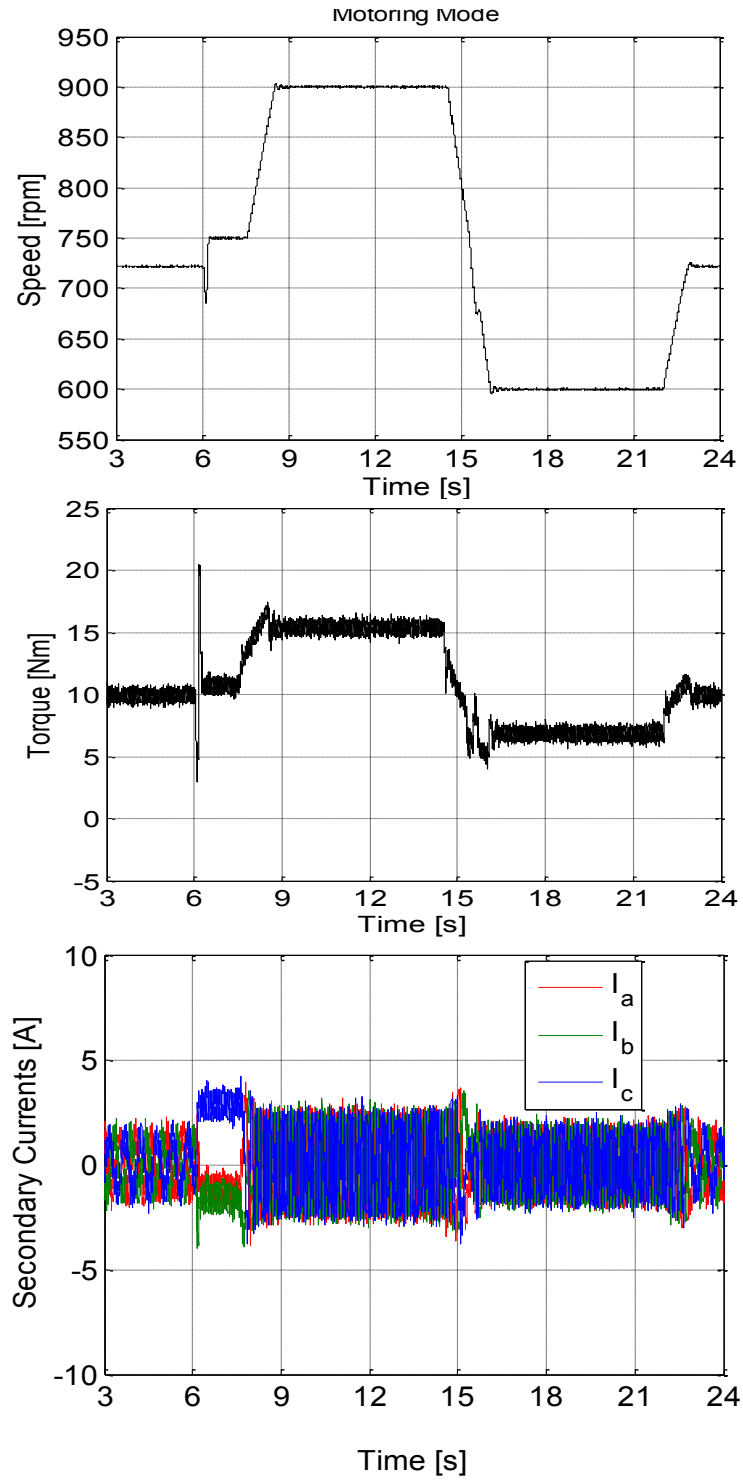
Figure 3.14: BDFRM performance with partial (super-synchronous) boost voltage

53
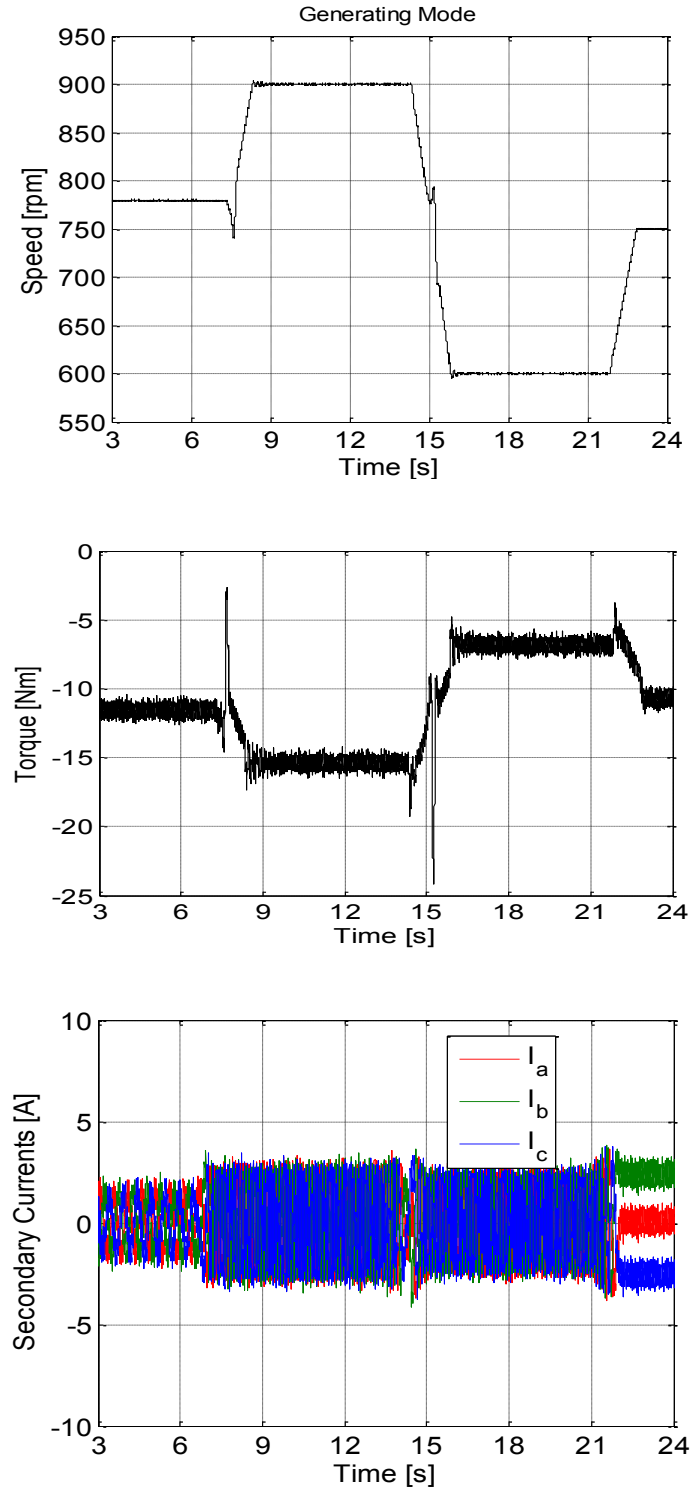
Figure 3.15: BDFRG performance with partial (sub-synchronous) voltage boost.
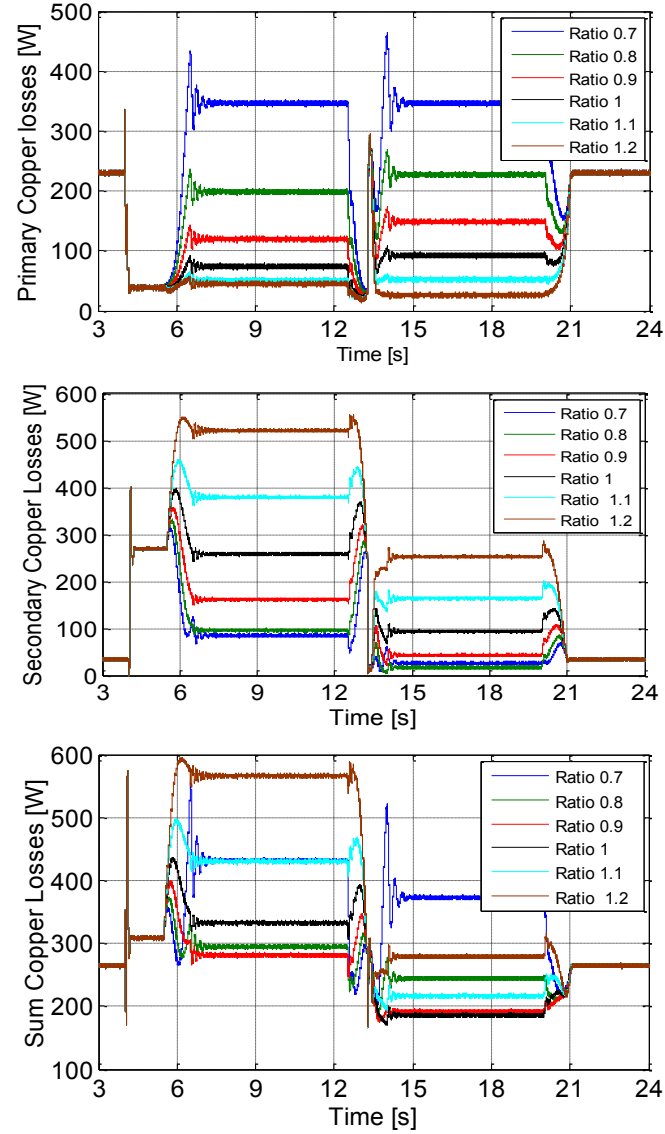
Figure 3.16: Distribution of copper losses of the BDFRM with enhanced SC performance.

Table 3.3: Copper loss levels of BDFRM with partial (super-synchronous) voltage boost

Ratios	Primary Super-synch	Secondary Super-synch	Total losses Super-synch	Primary Sub-synch	Secondary Sub-synch	Total losses Sub-synch
0.7	350	70	420	350	23	373
0.8	200	100	300	220	21	241
0.9	110	170	280	135	43	178
1	70	255	325	90	91	181
1.1	55	370	425	55	170	215
1.2	37	520	557	25	250	275
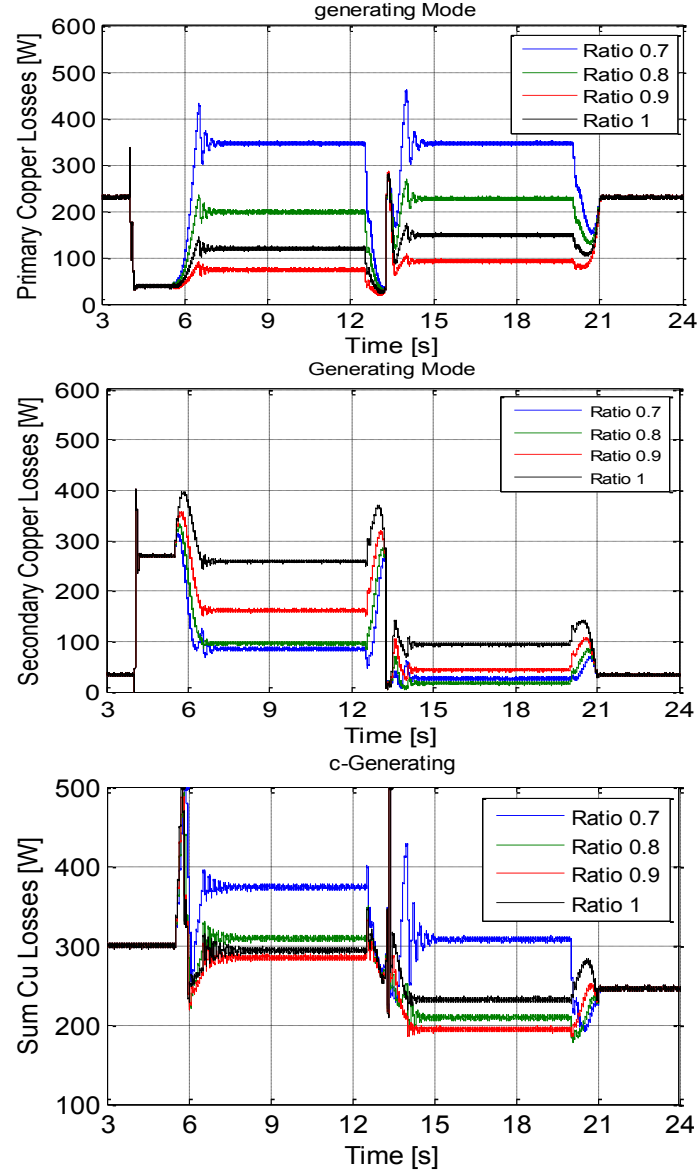
Figure 3.17: Distribution of copper losses of the BDFRG with superior SC performance.

Table3.4: Copper losses of BDFRG with partial voltage boost

Ratio	Primary Super-synch	Secondary Super-synch	Total losses Super-synch	Primary Sub-synch	Secondary Sub-synch	Total losses Sub-synch
0.7	290	75	365	300	23	323
0.8	230	82	312	175	35	210
0.9	150	123	**273**	103	95	**198**
1	110	180	290	50	175	225
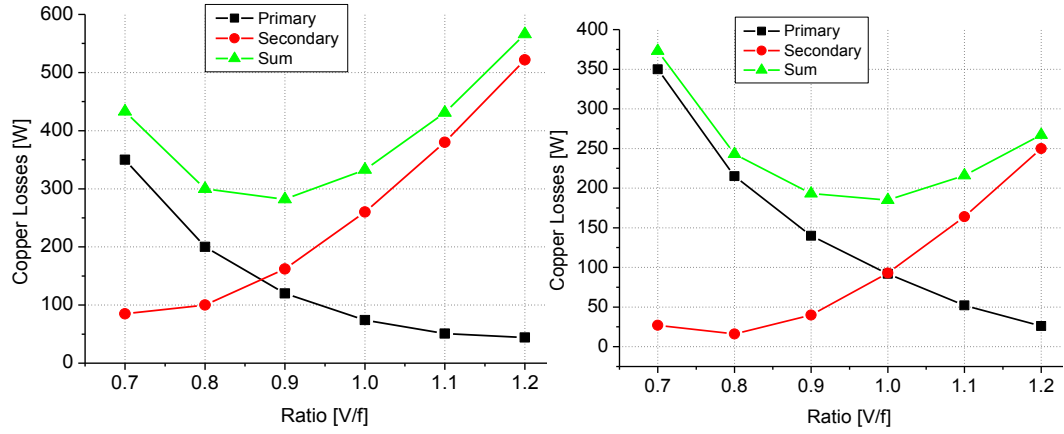
Figure 3.18 : Copper loss allocation of the BDFRM corresponding to Table 3.3.
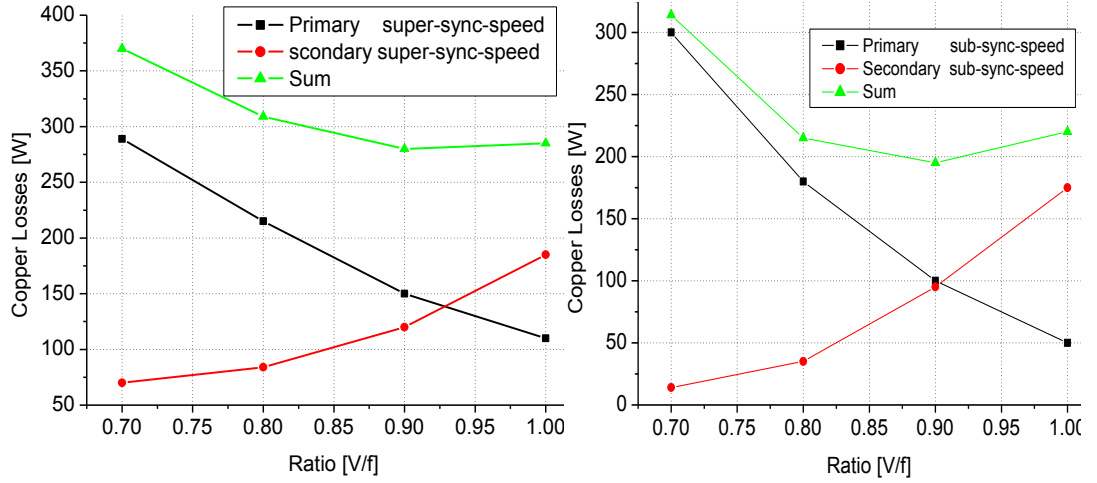
Figure 3.19: Copper Loses Distribution in the BDFRG corresponding to Table 3.4.

The most significant contribution of the alternative voltage boost injection approach to be emphasized is the compliance with the fundamental hypothesis of the best overall efficiency obtainable for the MTPIA *V/f* ratio of 0.9, which is verified by the achieved results in Tables 3.3 and 3.4, and Fig. 20 below for both the BDFRM or BDFRG in either speed mode.
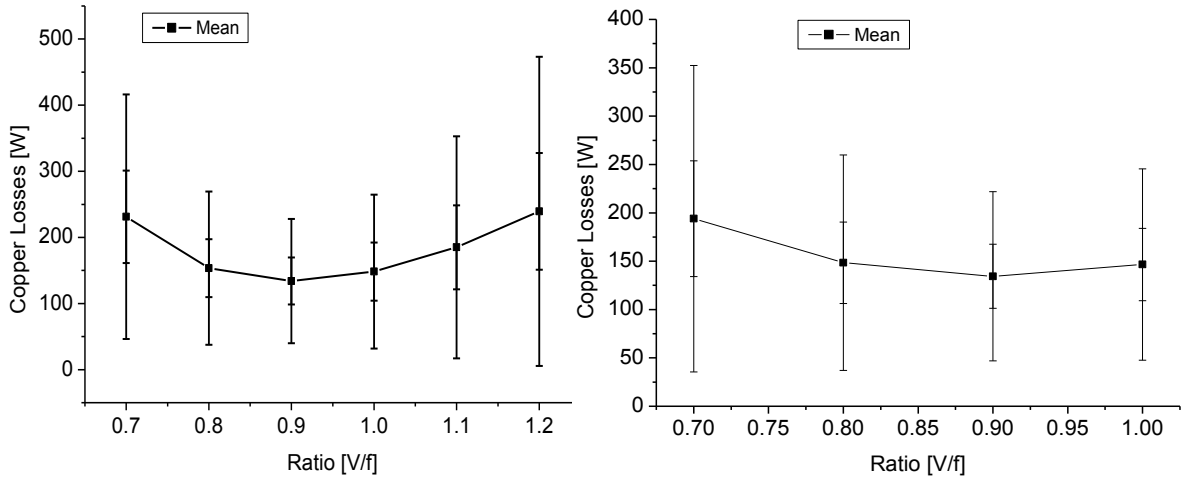
Figure 3.20: The mean copper losses for various *V/f* ratios of the BDFRM (left) and BDFRG(right).

3.4   Conclusions

The main contribution of this chapter is the development and experimental verification of a novel, purely sensorless and entirely parameter independent scalar control (SC) algorithm for emerging brushless doubly-fed reluctance machines (BDFRM). Although SC has been traditionally used for general-purpose applications of conventional cage or wound rotor induction machines, its real-time implementation or simulation studies for the BDFRM has not been reported in the refereed literature on the subject to date. The controller performance has been examined on a small-scale inverter-fed BDFRM prototype which forms a central part of the research test facility for emulation of variable speed drive and generator systems available in the power laboratory using dSPACE® hardware. Good results have been obtained in both motoring (BDFRM) and generating (BDFRG) operating modes of the machine over the limited speed range commonly encountered in the target applications such as centrifugal pump-alike devices (e.g. compressors, fans, blowers etc.) or wind turbines with maximum power point

tracking. The maximum torque per inverter ampere (MTPIA) control strategy has been used as a case study primarily due to the higher-efficiency implications of minimum current loading (and therefore lower resistive and switching losses) obtainable on the BDFRM(G) secondary side.

Another important novelty of the material presented is the design and practical implementation of a viable voltage boost injection technique which has allowed significant control performance enhancement and efficiency improvement of the machine. A comprehensive study of the copper loss distribution in the BDFRM(G) has been carried out clearly demonstrating the possibility to achieve similar performance benefits of vector control under the MTPIA conditions but applying much simpler and inherently more robust open-loop scalar control. The other conclusions and/or observations that can be drawn from the results presented can be summarised in the following:

1. The properties of the proposed scalar controller are ideally suited for the target applications referenced above where only the steady-state control quality is required. It should provide a low cost control solution in these systems compared to vector or field-oriented control.

2. The experimental results have shown that performance optimisation similar to vector control is possible. It has been proven that the highest efficiency can be obtained under the MTPIA conditions which can be derived from the nameplate data of a machine without any need for parameter knowledge or off-line testing procedures.

3. The above performance advantages have been achieved using an alternative voltage boost technique where the DC voltage has been injected to the secondary winding in super-synchronous mode of the BDFRM and sub-synchronous mode of the BDFRG

allowing the secondary currents to become mainly torque producing and hence the copper losses to be more evenly balanced between the two windings of the machine with an immediate efficiency gain.

4. The controller is open-loop in nature (e.g. without speed feedback) and does not require any shaft position sensor or any other voltage or current transducer for control purposes other than a DC link voltage sensor needed for space-vector PWM modulation of the inverter.

Such properties should make the developed low-cost controller very attractive for commercialisation and, given its versatility and inherent robustness, may lead to its potentially wider use for any doubly-fed machine, foremost a conventional doubly-fed slip ring induction machine (DFIM), in low to medium performance applications where only the steady-state operation, and not fast transient response, is of major concern.

Chapter 4 **A Large BDFRG Wind Turbine with Maximum Power Point Tracking**

4.1 Introduction

The earth climate can be seriously influenced by increasing green-house gas emissions from the conventional energy sources (such as oil and coal) as well as the growing concern of depletion of these resources in the near future [58]. Wind energy is certainly one of the most promising alternative environmentally-friendly solutions to this severe problem due to the fact that it is free, safe, clean, sustainable and available world-wide [59, 60].

One of the main electrical problems in terms of quality of generated wind power is the random wind fluctuations. In variable speed wind energy conversion systems (WECS), the maximum power point tracking (MPPT) of a horizontal-axis wind turbine is of great importance for efficient energy production and therefore reduction of pay-back periods of capital investments in such an expensive technology [61]. This chapter presents a sensor-less control method for a large-scale custom designed 2 MW BDFRG wind turbine with MPPT. The use of BDFRG instead of traditional DFIG should bring further cost advantages afforded by the high reliaiblity of its brushless design and hence much lower running costs. The cost benefits can be even more pronounced by applying the same open-loop scalar control, which has been proven by the results presented in the previous chapter to be able to provide satisfactory performance on a small-scale level without a shaft position sensor [62].

Wind turbines have low aero-dynamic efficiency (practical values are about 40% or so), and it is essential to extract as much energy as possible out of the wind for the afore-mentioned economic reasons [63]. Three distinct groups of MPPT methods have been reported in the literature to achieve this objective, namely:

- The Tip Speed Ratio (TSR) control [64] (Fig. 4.1) where the TSR ($\lambda_{opt} = R\omega/V_w$) of a wind turbine is kept at its optimum value (for maximum power coefficient, C_p) by adjusting the turbine (generator) velocity (ω) for a given upstream wind speed (V_w) and a pitch angle (θ) using the manufacturer provided data for a particular wind turbine model i.e. C_p (λ,θ) curves or similar characteristics obtained by off-line testing.
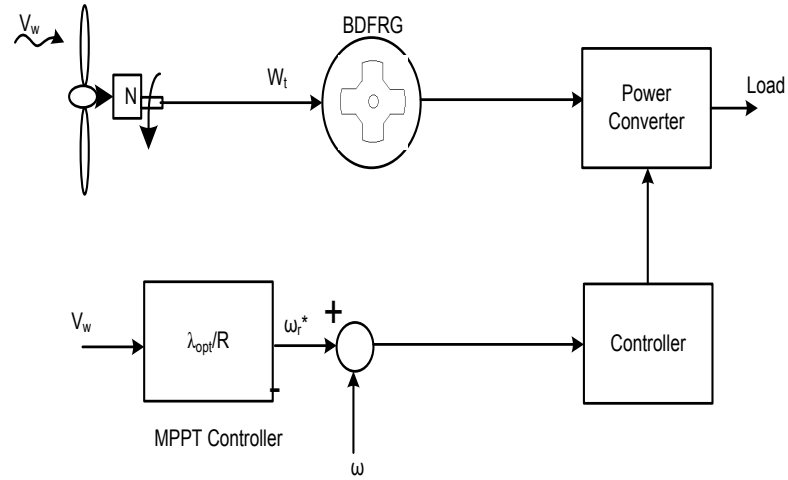
Figure 4.1: A conceptual diagram of a WECS with TSR Control of a BDFRG wind turbine.

- Power Signal Feedback (PSF) control (Fig. 4.2) which requires deep understanding of wind turbine operation and knowledge of the corresponding MPPT curves and trackthis curve through mechanisms. The maximum power curves need to be obtained via simulation or off-

line experiment on individual wind turbines. In this method, reference power is generated either using recorded maximum power curve or using the mechanical power equation of the wind turbine where wind speed or the rotor speed is used as the input.   [65].
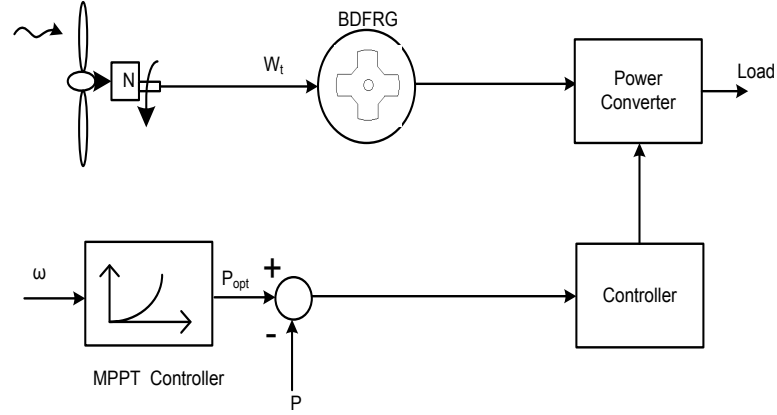
Figure 4.2: The structure of a BDFRG based WECS with PSF control of a wind turbine.

- Hill-Climb Searching (HSC) based on extreme seeking point control (ESC) [66] is attractive as being entirely parameter independent and thus robust. The HCS control algorithm continuously searches for the peak power of the wind turbine. It can overcome some of the problems normally associated with the other two methods. The tracking algorithm, depending upon the location of the operation point and relation between the changes in power and speed, computes the desired optimum signal in order to drive the system to the point of maximum power (Fig. 4.3).
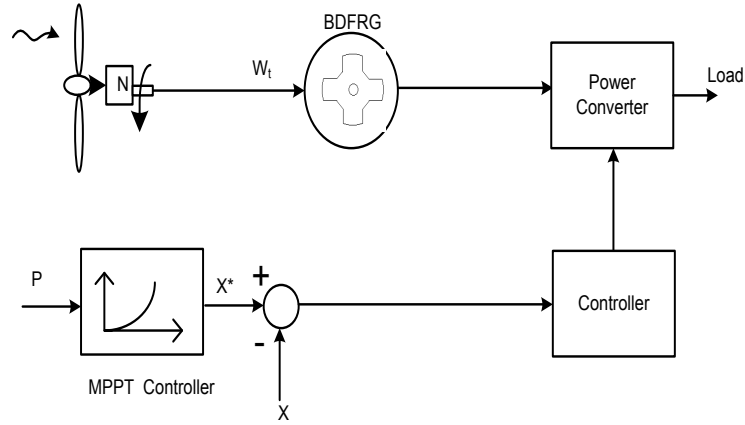
Figure 4.3: A BDFRG based WECS with HSC Control of a wind turbine

4.2   Wind Aerodynamic Model

The MPPT algorithm is applied to find the shaft speed reference for the maximum power extraction from a wind turbine for a given wind speed using the TSR method referenced above as a widely adopted approach in wind power industry due to its simplicity and ease of implementation [67], (refer to Appendix B for further details). The well-known expression for the incident wind power is:

$$P_{wind} = \frac{1}{2} \rho \pi R^2 V_w{}^3 \tag{4.1}$$

Where ρ is the air density, R is the radius (m) of the turbine circular swept area (e.g. the blade length), and V_w is the actual wind speed (m/s). The power captured by the wind turbine is therefore:

$$P_t = \frac{1}{2} \rho \pi R^2 V_w{}^3 C_P (\lambda, \theta) \tag{4.2}$$

The turbine power coefficient, $C_P(\lambda, \theta)$, is a non-linear function of the tip speed ratio (λ) and the pitch angle (θ) , it can be represented in a close form as follows [68]:

$$C_P(\lambda, \theta) = 0.5176 * (116/\lambda_i - 0.4\theta - 5)^{-21/\lambda_i} + 0.0068\lambda \tag{4.3}$$

$$\frac{1}{\lambda_i} = \frac{1}{\lambda + 0.08\theta} - \frac{0.035}{\theta^3 + 1} \tag{4.4}$$

The TSR (i.e. λ) is defined as the ratio between the blade tip speed and the wind speed:

$$\lambda = R\omega_t/V_w \tag{4.5}$$

where ω_t is the rotor angular velocity of the turbine. A family of typical $C_p(\lambda)$ curves that can be plotted using (4.3) and (4.4) for different pitch angles, is shown in Fig. 4.4. Similarly, using (4.2)-(4.5) one can produce the turbine power vs generator shaft speed (e.g. the turbine speed referenced to the high-speed side of the gearbox) graphs in Fig. 4.5 for wind speeds in the base speed region (i.e. from cut-in up to the rated value). The MPPT trajectory for the wind turbine generator is highlighted in red on the same figure.
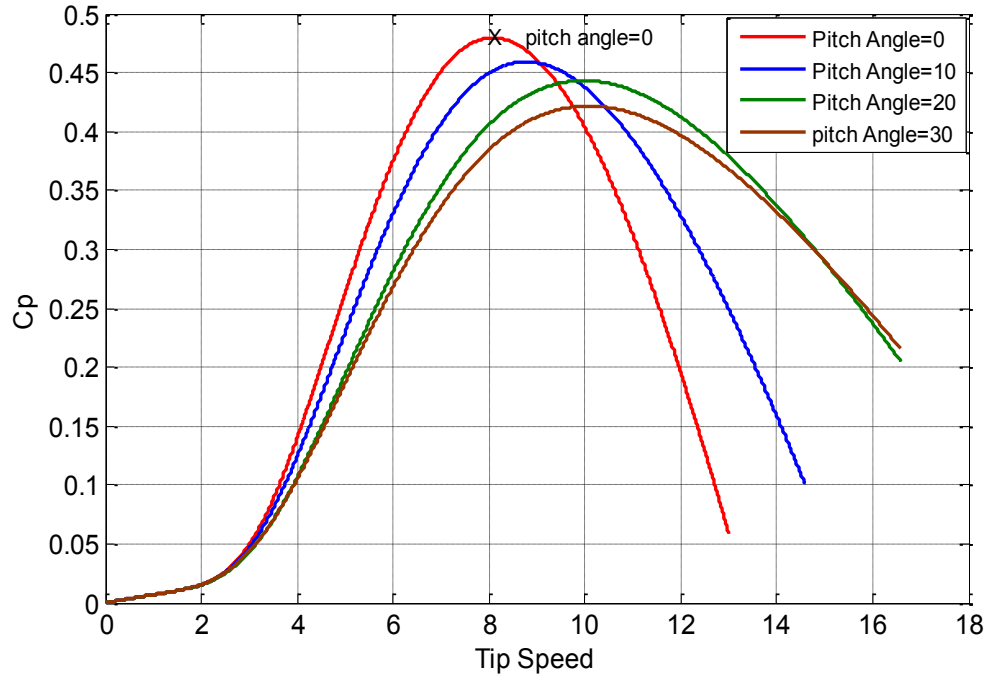
Figure 4.4: Power coefficient vs tip speed ratio characteristics for various pitch angles

4.2.1 MPPT Conditions

Figure 4.4 shows that the maximum power coefficient (i.e. turbine efficiency) of C_{pmax}= 0.48 can be achieved at zero pitch angle (θ = 0) for the optimum tip speed ratio of λ_{opt}= 8.1. Therefore, a variable pitch turbine should be controlled at θ = 0, and its speed should follow a particular wind speed pattern so that λ_{opt}= 8.1 in the base speed region to maximize the efficiency of wind energy conversion at 48% as illustrated by the simulation results in Fig. 4.6 for the BDFRG turbine used as a case study.
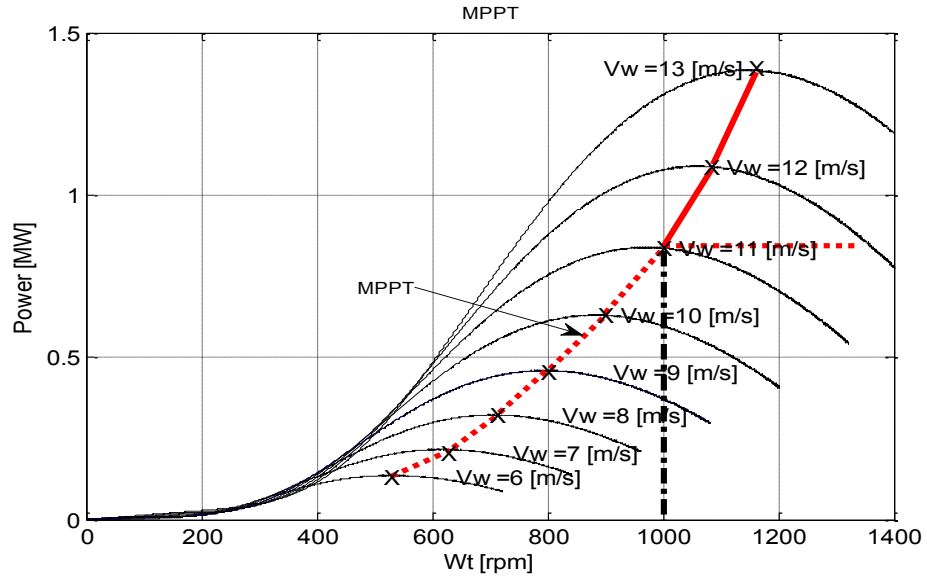
Figure 4.5: Mechanical power vs. speed profiles of a typical wind generator for different wind speeds

Using (4.2) and (4.5), the available ($T_m=P_t/\omega_t$) and optimal (e.g. for MPPT) turbine torque can be written as:

$$T_m = \frac{\rho\pi R^2 V_w^3 C_p(\lambda,\theta)}{2\omega_t} = \frac{\rho\pi R^5 C_p(\lambda,0)}{2\lambda^3} * \omega_t^2 \qquad (4.6)$$

$$T_{opt} = \frac{\rho\pi R^2 V_w^3 C_{pmax}}{2\omega_{t\text{-}opt}} = \frac{\rho\pi R^3 C_{pmax}}{2\lambda_{opt}} * V_w^2 \qquad (4.7)$$

66

where $\omega_{\text{t-opt}} = V_w \lambda_{opt} / R$ according to (4.5). The success of the control process (Fig. 4.7) directly depends on how well the C_p is being kept at its optimal value at randomly fluctuating wind speeds. Otherwise, errors between T_{opt} and T_m may occur. These may be driven to zero (or at least minimised) under both steady-state and especially transient conditions by retrieving the optimal ω_t profile shown in Fig. 4.7 from (J is the turbine-gear box inertia):

$$\omega_{\text{t}} = \frac{1}{J} \int (T_{\text{opt}} - T_{\text{m}})dt \tag{4.8}$$
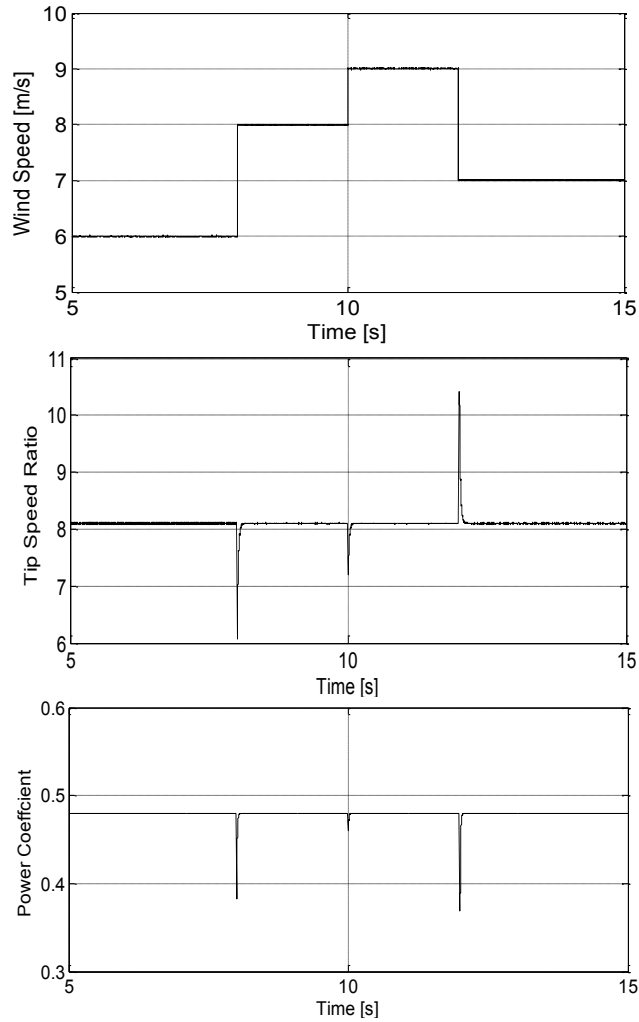
Figure 4.6: wind speed, tip speed ratio (λ) and the coefficient of power
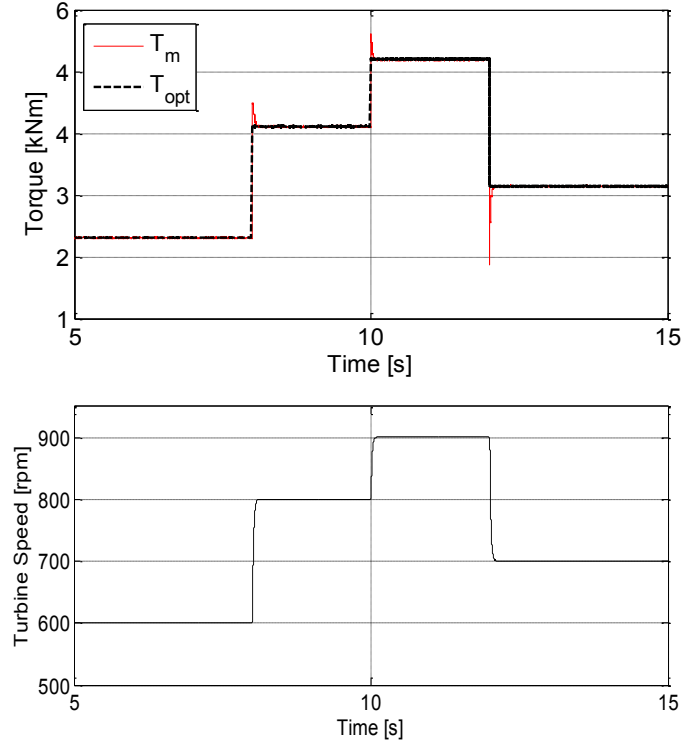
Figure 4.7: Turbine parameter variations in time domain in response to step changes of wind speed
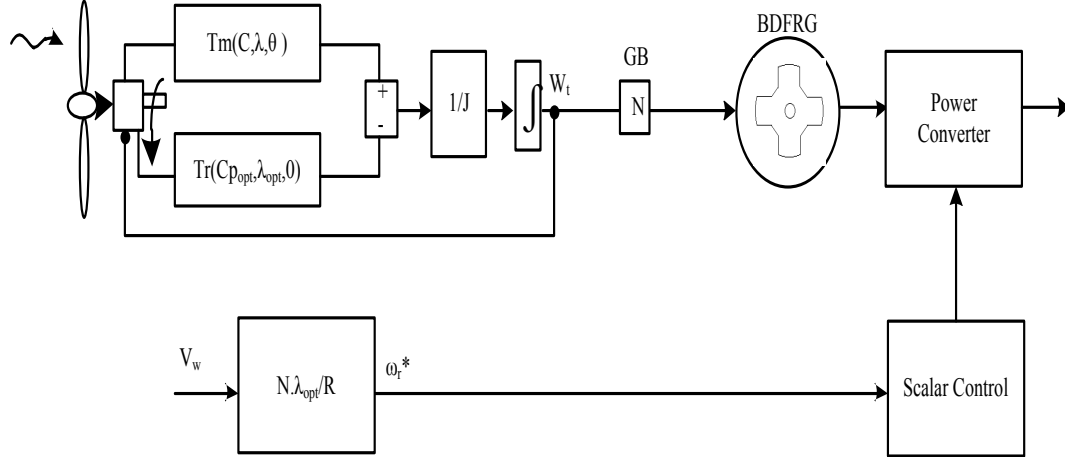
Figure 4.8: A simplified block diagram of the BDFRG wind turbine control procedure

Multi-pole BDFRG designs, similar to bulky and costly synchronous generators for direct drives (e.g. gear-less WECS), have not been reported in the refereed literature yet, so a gear-box of appropriate teeth (gear) ratio (N) is required to match the low turbine speeds with higher BDFRG speeds (i.e. a [500, 1000] rev/min range in our case) by analogy to the DFIG operation. The BDFRG actual and MPPT angular velocities can be therefore formulated as:

$$\omega_r = N\omega_t = NV_w\lambda / R \tag{4.9}$$

$$\omega_r^* = N\omega_{t\text{-opt}} = NV_w\lambda_{opt} / R \tag{4.10}$$

The BDFRG reference speeds for MPPT are tabulated below for the assumed wind speed values in Fig. 4.6 and N=10 in (4.10). These figures should be used as desired input signals to the open-loop scalar controller as shown in Fig. 4.7.

Table 4.1: BDFRG turbine speeds for MPPT

Wind speed V_w [m/s]	Turbine shaft Speed n_r^*[rev/min]
6	600
7	700
8	800
9	900

4.3   Variable Speed Operation Based Scalar Control

4.3.1   Scalar Control Based Step Change Wind Speed

The BDFRG as a promising slip recovery machine features many important advantages such as the possibility of using a proportionally smaller converter (and especially in case of limited speed ranges with geared wind turbines), high reliability of brushless design, and therefore lower running cost compared to the BDFIG, foremost on large-scale level where these favorable properties become increasingly important. These merits, together with its distinguishing low-voltage-fault ride through capabilities discussed in Chapter 6, have largely contributed to the recent revival of interests in the machine as a viable DFIG alternative. The BDFRG potential has already been demonstrated by laboratory tests where competitive performance to DFIG has been achieved [12, 69]. Judging by the preliminary results presented in this chapter for a 2 MW design (Table 4.2), it should be realistic to expect that this trend can be carried over to larger machines as well.

As suggested earlier, a simple, low cost, sensor-less *V/f* scalar controller configuration may be able to provide more than a satisfactory solution to the modest dynamic requirements of wind turbines while offering reasonable steady-state performance as experimentally shown on a small prototype. The dynamic model of the DBFRM has been considered in detail in Chapter 3 where the following fundamental angular velocity relationship for the electro-mechanical energy conversion in the machine has been established (this is repeated in here for convenience):

$$\omega_s = \omega_{rm} p_r - \omega_p \tag{4.11}$$

In the above generic expression, the controllable secondary winding frequency (ω_s) is given as a function of the BDFRG velocity (ω_{rm}) at the fixed line frequency, $\omega_p = 2\pi f_p$, with p_r indicating the number of rotor poles. If a specific generator speed is to be attained (e.g. for MPPT), ω_{rm}^*, the desired secondary frequency can be written in the same form as (4.11):

$$\omega_s^* = \omega_{rm}^* p_r - \omega_p \tag{4.12}$$

The secondary voltage reference for a given grid (primary) voltage magnitude under *V/f* law would then be formulated as:

$$U_s^* \cong \frac{L_{ps}}{L_p} \frac{U_p}{\omega_p} \omega_s^* \tag{4.13}$$

All the benefits of open-loop scalar control work with voltage boost at small-scale level presented in Chapter 3 can be shown to apply to the large BDFRG (Table 4.2) as illustrated by the corresponding simulation results below, (refer to Appendix B for further details). The promising performance and accuracy of this simple control system, as well as its ability to overcome common stability limitations by the narrow operating speed ranges (and hence restricted variations in command secondary frequency), is immediately obvious from Fig. 4.9. This again demonstrates the apparent suitability of this control method for wind power applications, at least in the BDFRG case.
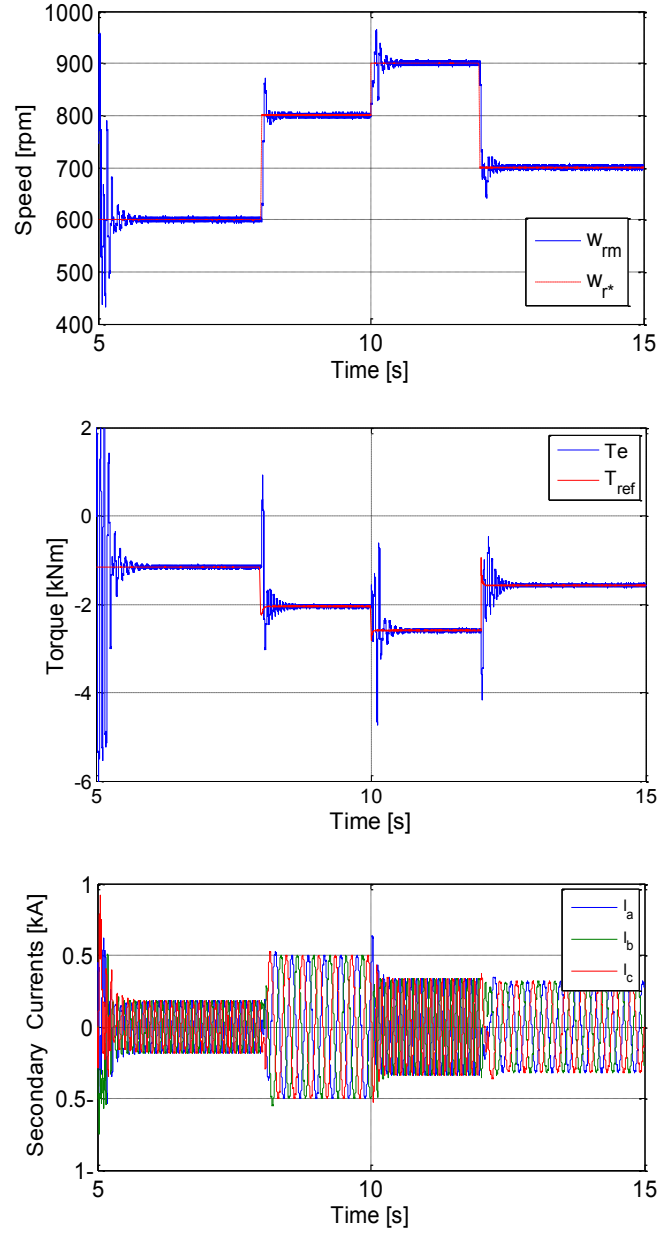
Figure 4.9: A 2 MW BDFRG wind turbine response to a random speed reference signal

An excellent reference speed tracking potential and smoother transient response to sequential speed changes than with the small prototype can be seen in Fig. 4.9. The latter can be explained by the additional damping effects of the large inertia constant table .4.2 and hence the lower speed oscillations. The secondary voltage and current phase sequence reversal while riding

through the synchronous speed (750 rev/min) is also visible from the same figure. expected from The intermediate synchronous speed operation is characterised by the DC voltage and current as (4.12) when $\omega_s = 0$.

Table 4.2: 2 MW BDFRG Design Parameters

Parameter	Value	Definition
f_p	50	Line Frequency [Hz]
V_p	690	Grid voltage [V]
P_r	4	Rotor poles
J	3.8	Total drive shaft inertia [kgm^2]
R_p	0.0375	Primary winding resistance [Ω]
R_s	0.0575	Secondary winding resistance [Ω]
L_p	1.17	Primary winding inductance [mH]
L_s	2.89	Secondary winding inductance [mH]
L_{ps}	0.98	Mutual inductance [mH]

4.3.2 Natural Wind Profile

The concerning challenge facing applied control (in our case scalar control) in general for variable speed WECS applications is the generator ability to track abrupt and highly unpredictable 'natural' wind speed fluctuations, and especially under extreme gusty wind conditions, to achieve the desired MPPT operation or any other performance optimisation of interest. Luckily, even in the turbulent wind circumstances, such seemingly fast variations (at as low as 1s rate) can be classified as 'slow' from a control point of view.

The plots in Fig. 4.10 represent the actual wind speed profile, and the respective wind turbine parameter changes, including the tip speed ratio (λ), power coefficient (C_p) and wind turbine speeds referenced to the generator side of the gearbox (ω_t), in the base speed region (e.g. from cut-in up to the rated speed value). The average MPPT (optimum) tip speed ratio can be shown to be λ_{opt} = 8.1, and corresponding maximum turbine efficiency for zero pitch angle is $C_{p\text{-}opt}$ = 4.8. These data have been used to generate the simulation results in Figs. 4.10-12.
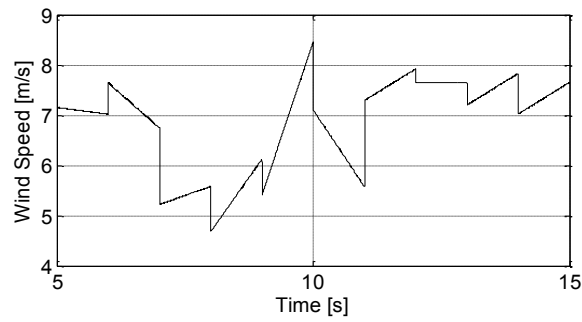
Figure 4.10: Realistic MPPT speed
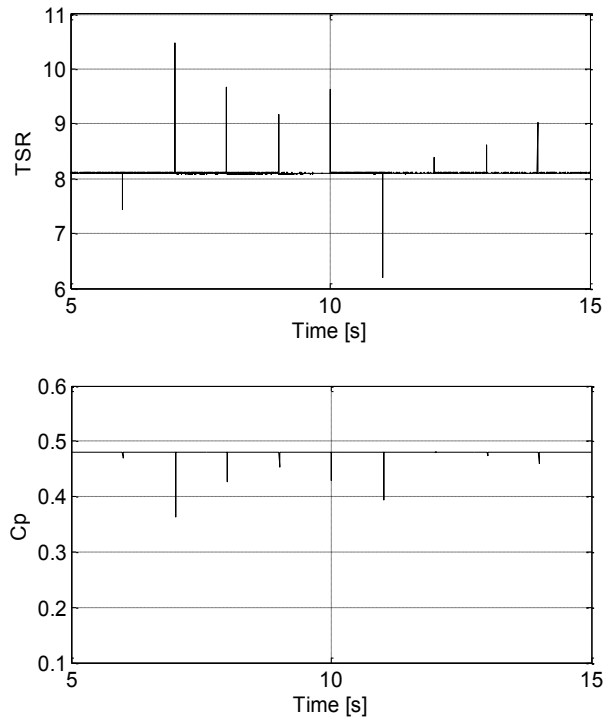
Figure 4.11 : Tip speed ratio Vs Coefficient power.

74
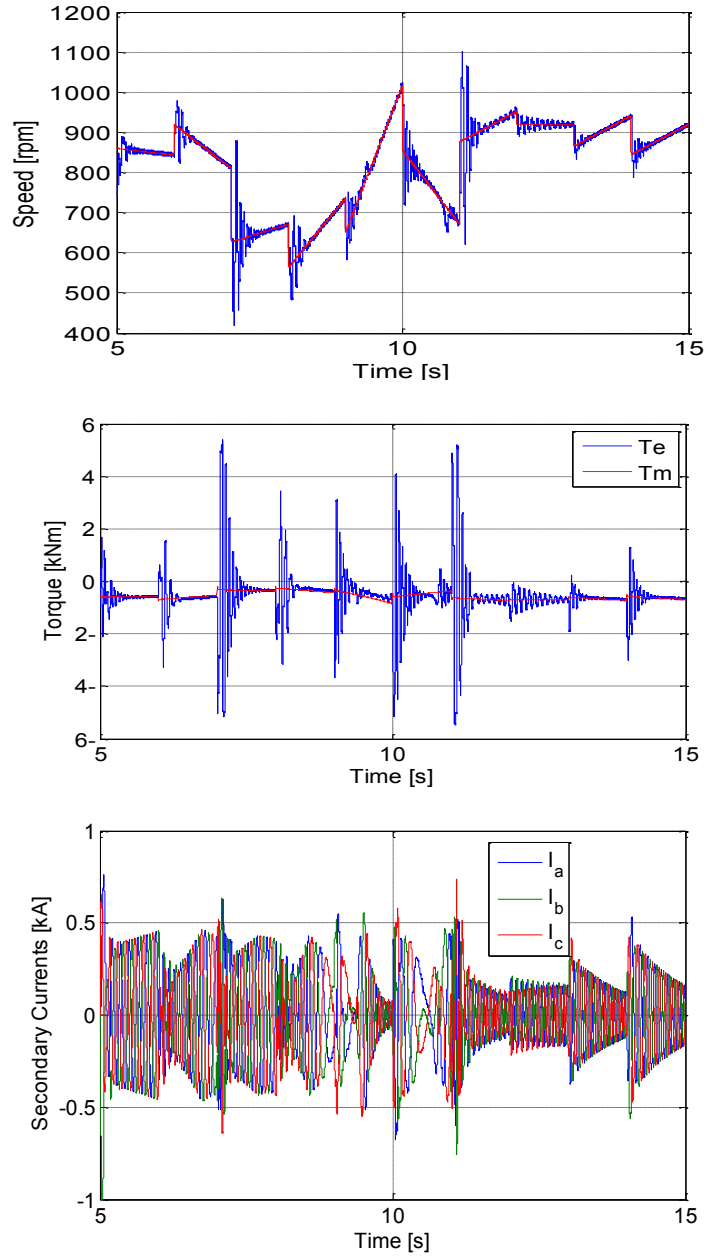
Figure 4.12: A random speed reference trajectory (top), torque, secondary current and speed

The preliminary results in Fig. 4.10 undoubtedly show a good potential of the proposed open-loop scalar controller with voltage boost in the limited variable speed range. The BDFRG is clearly able to reasonably accurately track the desired reference speeds/torques (red lines) despite their highly random nature. No signs of instability in the controller/machine response have been observed.

4.3.3 Flux Oriented Control Fundamentals

This method of control theories achieved a certain accuracy and sharp response to the sudden changes in the machine speed, when it is involved under the impact of non-linear front winds speed [70]. The dynamic model of the BDFRM machine (Fig. 4.13), which is already presented in Chapter 2, proves the following focal rotor angular velocity relationship for the electro-mechanical energy conversion in BDFRG with p_r rotor poles and $\omega_{p,s}$ applied frequency (rad/s) to its primary and secondary winding:

$$\omega_{rm} = \frac{\omega_p + \omega_s}{p_r} = \frac{(1\text{-}s).\omega_p}{p+q} = (1\text{-}s).\omega_{syn} \tag{4.14}$$

where the generalized slip can be defined as $s = -\omega_s/\omega_p$ and $\omega_{syn} = \omega_p/p_r$ is the synchronous speed (for $\omega_s = 0$ i.e. a DC secondary) with super-synchronous speed corresponding to the case $\omega_s > 0$ i.e. $s < 0$ and sub-synchronous speed to $\omega_s < 0$ i.e. $s > 0$ (i.e. the opposed phase sequence of the secondary to the primary winding).
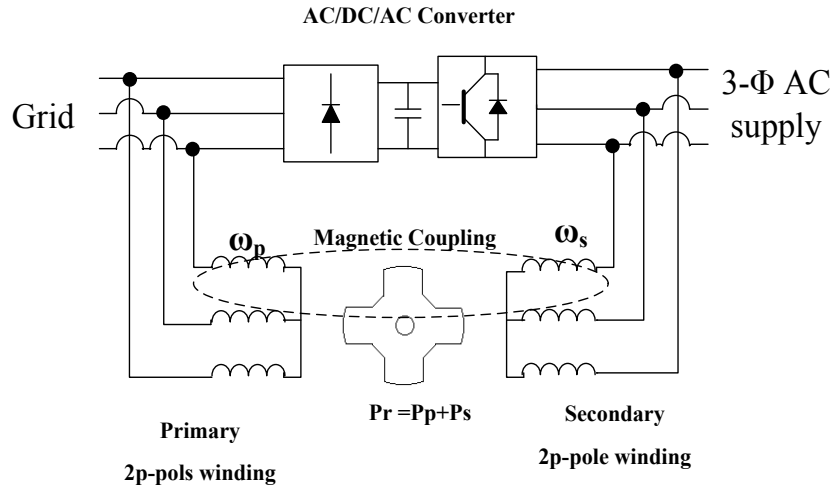
Figure 4.13: BDFRM machine

Implementing the same equation, the mechanical power balance showing individual contribution of each machine winding, assuming motoring BDFRM conversion as default can be presented by:

$$P_m = T_e . \omega_{rm} = \underbrace{T_e . \frac{\omega_p}{p_r}}_{P_p} + \underbrace{T_e . \frac{\omega_s}{p_r}}_{P_s} = P_s .(1-s) \tag{4.15}$$

In the BDFRG case the electromagnetic torque ($T_e < 0$) and thus $P_p < 0$ in (4.15), suggesting that positive power is fed to the grid by the primary winding, while the secondary (slip) power (P_s) flow can be bi-directional subject to the operating speed region as illustrated in Fig. 4.14.
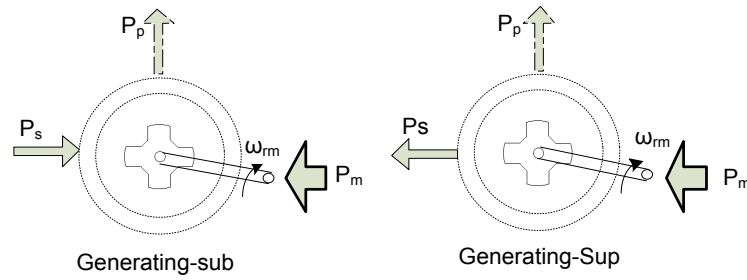
Figure 4.14: Power flow interchange in generating mode

The reference frame relationship between the primary and secondary winding can be estimated depending on primary flux angle technique for FOC algorithm in desecrate form, andthe computing the 3-ph primary active (P) and reactive (Q) power for the control method have been responded to the stationary frame voltage ($v_{\alpha,\beta}$) and ($i_{\alpha,\beta}$) obtained from phase measurements, with control actions being implemented in the secondary d_s-q_s frame rotating at ω_s (Fig. 4.16).
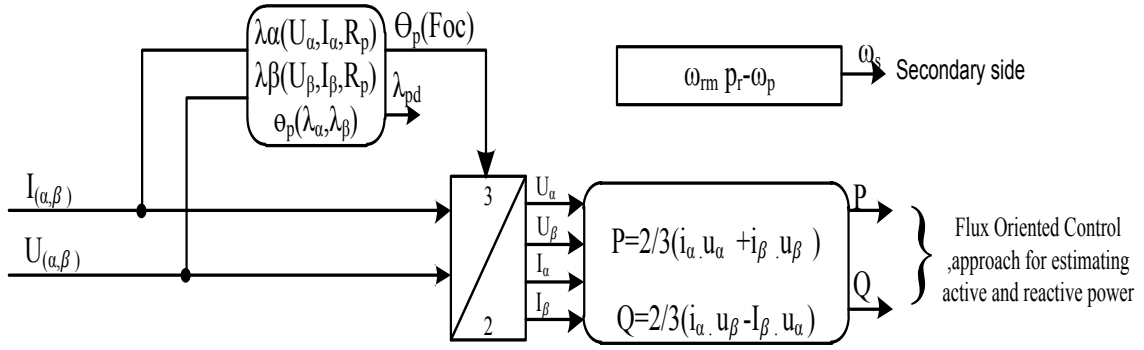
Figure 4.15: Field oriented control approach for estimating active (P) and reactive power (Q)

The conventional expressions for a Y- connected winding with 3-ph sequence applied for power calculations are:

$$\begin{cases} P = \frac{3}{2}(i_\alpha \cdot v_\alpha + i_\beta \cdot v_\beta) \\ Q = \frac{3}{2}(i_\alpha \cdot v_\beta - i_\beta \cdot v_\alpha) \end{cases} \tag{4.16}$$

The reactive power is often set to zero ($Q^*=0$) in case unity power factor and (P^*) in open loop speed (i.e. power or torque) mode of the machine, in variable speed WECS, either ω^*_{rm} or (P^*) may correspond to the maximum power point tracking (MPPT) of wind Turbine (our Target) [12].

The essential flux expression for BDFRG space vector mode, in primary rotating angle ω_p(e.g. d_p-q_p) ω_s (e.g. d_s-q_s for the secondary winding) [71].

$$\lambda_p = \underbrace{L_p \cdot i_{pd} + L_m \cdot i_{md}}_{\lambda_{pd}} + \underbrace{L_p \cdot i_{pd} - L_m \cdot L_{mq}}_{\lambda_{pq}} \tag{4.17}$$

$$\lambda_p = \underbrace{L_s \cdot i_{sd} + L_{md}}_{\lambda_{sd}} + \underbrace{\left(\delta L_s \cdot i_{sd} + L_{mq}\right)}_{\lambda_{sq}} = \delta L_s \, i_s + \underbrace{\frac{L_m}{L_p}\lambda_p^*}_{\lambda_m} \tag{4.18}$$

In (4.17), the magnetizing current (i_m) and primary flux λ_p in the ω_p frame whereas the i_s as a secondary currents and λ_m in equation (4.18) in $p_r\omega_{rm}$-$\omega_p = \omega_s$ frame, as a natural frame.
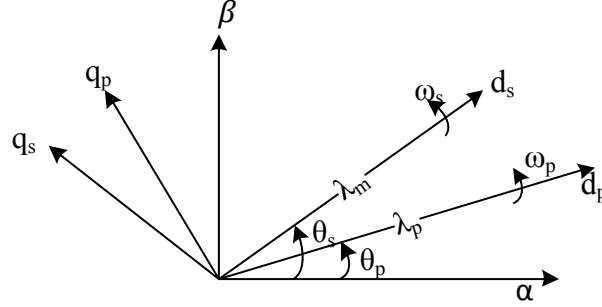
Figure 4.16 reference frame vectors based FOC

The conventional power expression for apparent power can be presented as:

$$S = P_p + j\,Q_p = \frac{3}{2}j\omega_p\lambda_{pi_p^*} \tag{4.19}$$

By substituting (4.17) and (4.18) into (4.19), the following torque and active/reactive power relationships can be developed:

$$T_{evc} = \underbrace{\frac{3}{2}p_r\lambda_{md}i_{sq}}_{T_{foc}} - \frac{3}{2}p_r\lambda_{mq}i_{sd} \tag{4.20}$$

$$P_{pvc} = \frac{3}{2}\frac{T_{evc}}{p_r} = \underbrace{\frac{3}{2}\omega_p\lambda_{md}i_{sq}}_{P_{pfoc}} - \frac{3}{2}\omega_p\lambda_{mq}i_{sd} \tag{4.21}$$

$$Q_{pvc} = \underbrace{\frac{3}{2}\omega_p\left(\frac{\lambda_p^2}{L_p}i_{sq} - \lambda_{md} \quad i_{sd}\right)}_{Q_{pfoc}} - \frac{3}{2}\omega_p\lambda_{mq} \quad i_{sq} \tag{4.22}$$

79

The complementary FOC forms (e.g. with the d_p-axis aligned with the λ_p as in Fig. 4.15) are:

$$T_{efoc}=\frac{3}{2}\frac{L_m}{L_p}p_r\lambda_{md}i_{sq}=\frac{3}{2}p_r\lambda_m i_{sq}=\frac{3}{2}p_r\lambda_p i_{pq} \qquad (4.23)$$

$$P_{efoc}=\frac{3}{2}\omega_p\lambda_m i_{sq}=\frac{3}{2}\frac{L_m}{L_p}\omega_p\lambda_p i_{sq} \qquad (4.24)$$

$$Q_{efoc}=\frac{3}{2}\frac{\omega_p\lambda_p}{L_p}(\lambda_p-L_m i_{sd})=\frac{3}{2}\omega_p\lambda_p i_{pd} \qquad (4.25)$$

The FOC control expression display the power correspondence with the secondary currents in term of using P,Q control strategy in MTPIA and satisfying from decoupling advantage over vector control strategy, when the coupling side clear in (4.20)-(4.22) as torque and power. The situation is better in FOC when the torque and power are correspondence with one of i_{sd}, and i_{sq} current otherwise the d_p-axis lies along the λ_p, then the corresponding d_s-axis of the secondary currents aligned with λ_m such a usual frame-flux vector mapping is inherited with FOC control strategy (Fig. 4.16).

The dynamic model for FOC control more related with primary side than vector control[70]. The design adopted in this investigation satisfied from the speed loop control which involved to this algorithm to create specific torque correlated with reference current i_{sq} (23) as the outcome from first stage controller. Other branch can estimate i_{sd} by comprehensive open loop strategy between the desired and actual reactive power (Q,Q^*) established from the primary side. The cascade FOC theory will decrease the fluctuation in transient period and the PI controller adjusts and limits of the currents and out coming reference voltage V_d, V_q.

Satisfying from the turbine control income Fig. 4.17 that can develop the wind speed to the certain shaft turbine rotation match the operating speed (sync-speed) of BDFRG and introduce

as well negative torque, offers the shaft sufficient acceleration, that's enable the electrical generator close energy production loop base WECS application. The torque and speed are the main production of sensor less TSR control methods, and the rotating shaft speed w_t can be developed after gearbox normalizing gain "N" to the desired (reference) speed ω_r^*.
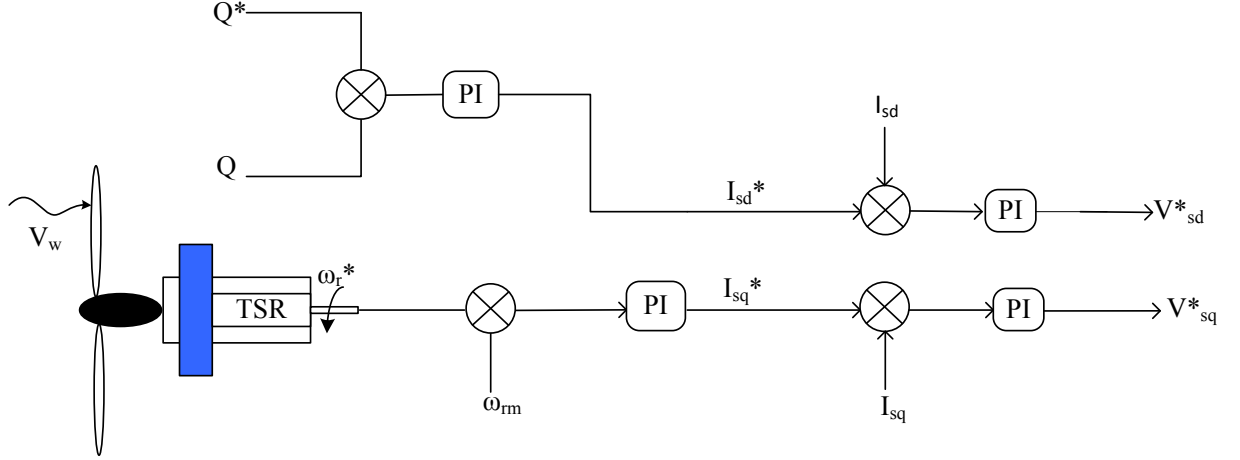
Figure 4.17: FOC system configuration

The generator adopt in this investigation is the same BDFRG that used previously in the scalar control application with same parameters but the control theory will take deferent trends by adopting stator field orientation control FOC. One of interesting approach adopted as well in this control theory is the speed loop control correlating with our data demand from the turbine in form rotating shaft speed and negative torque. The i_{sd}^* current reference can be developed from desired reactive power and estimating reactive power from the primary side based on (4.25) Based open loop approach.

The other current reference can be achieved from the speed loop control following the Equation (4.15) in case electromagnetic balance when the:

$$P_{foc} = P_m = \omega_{rm}.T \tag{4.26}$$

The comparison between the desired speed and actual speed for the generator will drawn the appropriate torque taking into account the inertia, which can be normalized by the suitable PI controller to produce the reference current i_{sq}. When the rotation of shaft turbine matches the synch speed $\omega_r^* = \omega_{rm}$, the first control stage is presented by the following formulae:

$$I_{sq}^* = PI\left(\omega_{rm}^* - \omega_{rm}\right) \tag{4.27}$$

$$I_{sd}^* = PI\left(Q^* - Q\right) \tag{4.28}$$

The reference frame relation can be coupled from the primary side as expressed below:

$$\theta_s = \theta_r - \underbrace{\tan^{-1}\frac{\lambda_\beta}{\lambda_\alpha}}_{\theta_p} \tag{4.29}$$

The reference voltage that established according to the comparison between the first stage reference current and actual d-q secondary current (i_{sd}, i_{sq}) through step up PI controller, developed after inverse park transformation to appropriate time vector to emulate the SVPWM to produce switching time to drive through IGBT gates.

$$V_{sq}^* = PI\left(I_{sq}^* - I_{sq}\right) \tag{4.30}$$

$$V_{sq}^* = PI(I_{sd}^* - I_{sd}) \tag{4.31}$$

4.3.4 Simulation Results under Step Change of Wind Speed

Step change variations related to the wind speed gives us strictly mechanical change which followed by the same schedule harmony of electrical side changes of BDFRG.
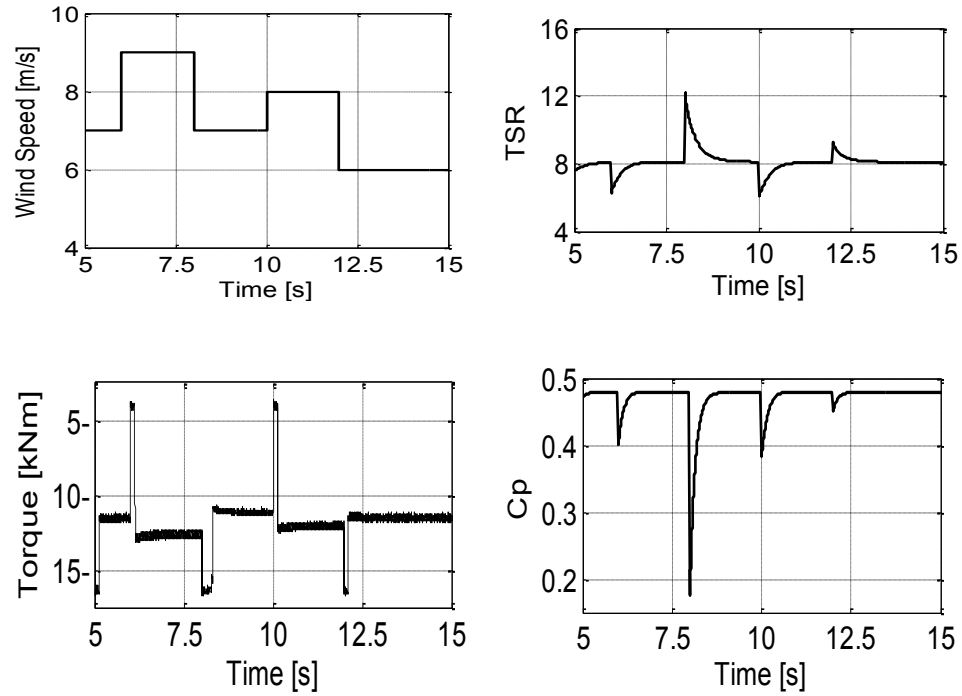
Figure 4.18: Wind turbine parameters
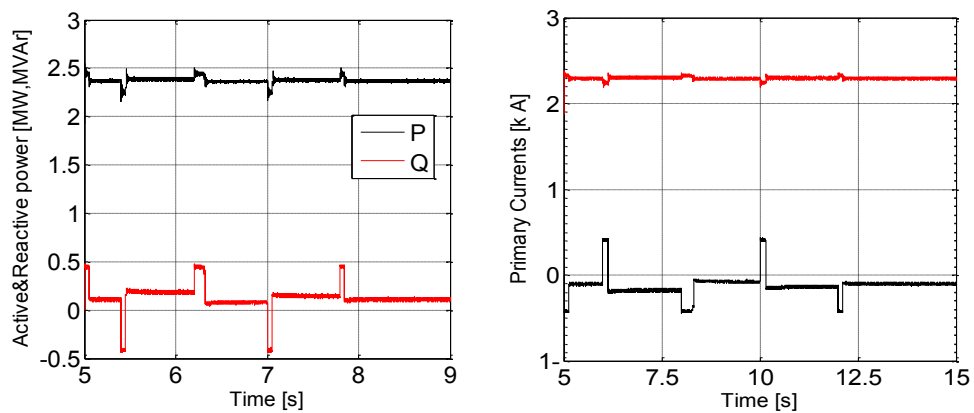
Figure 4.19: BDFRG simulated FOC characteristics for the parameters in Fig. 4.12
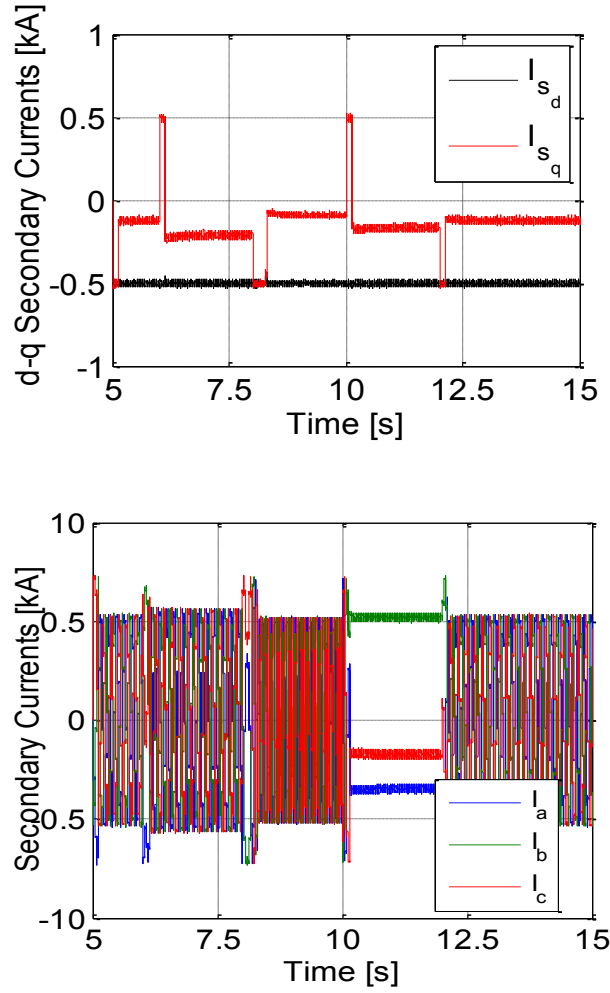
Figure 4.20: Generator (d-q secondary and Phase) currents

Figure 4.18 explains the nature of step change response of the turbine for high performance Field oriented control (FOC) when the wind speed expressed as a reference change in variable step from (6-9) m/s. The tip speed ratio achieve expected ratio 8.1, power coefficient 4.8 and the torque is negative as gained torque from the turbine side. The machine behave in generating mode, power with current in Fig.4.19 are following power unity strategy when the reactive power is close zero i.e. $I_{pd} \sim 0$ and I_{sd} Rated. The Fig. 4.20 illustrated the response of the secondary side BDFRG to the stapes change of the wind speed, the advantage of FOC is clearly

presented by decupling l_{sd}, I_{sq} secondary side currents and fine response to the wind speed. The intermediate synchronous speed operation is characterised by the DC currents when $\omega_s = 0$.

4.3.5 System Conversion under Non-Linear Wind Speed

The rhythms of the wind speed variations, in actual condition change rapidly following non-linear behaviour of the wind speed so the tracking of this change requires high performance control algorithm, the optimal power conversion is achieved by following every single change in wind speed to match reality MPPT for the system control. Therefore, the assessment of the situation comes from the results gained simulation such as these developed result under non linearity instruction. The turbine side control reflect the higher flexibly and optimum tracking to the wind variation reflected in torque coupling between the mechanical (turbine) and the electromechanically (generator), tip speed ratio accomplish 8.1 with power coefficient 4.8and the negative torque as well reflects the generating mode process Fig. 4.21. The superior performance of the system control is clearly illustrated in the behaviour of the power and the currents levels in primary side machine Fig. 4.22 and advantage of decoupling side of secondary currents in Fig.23.
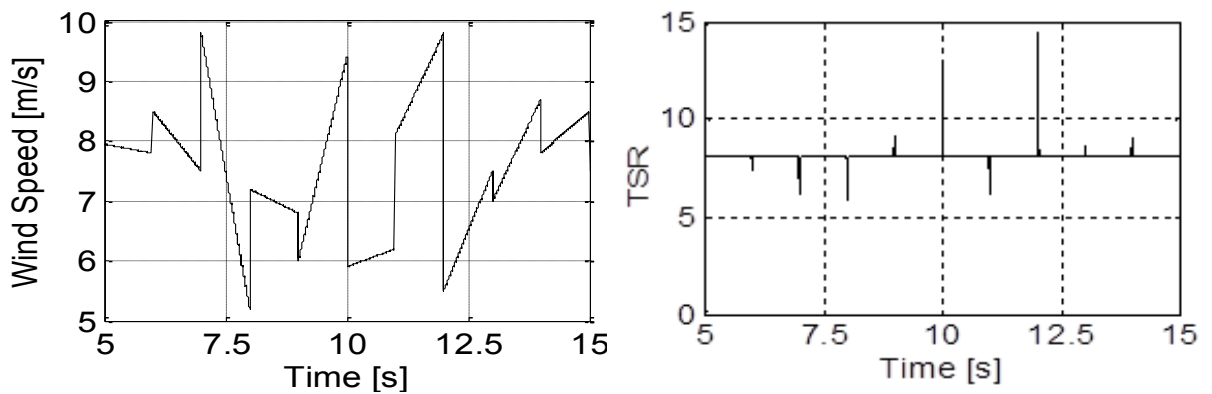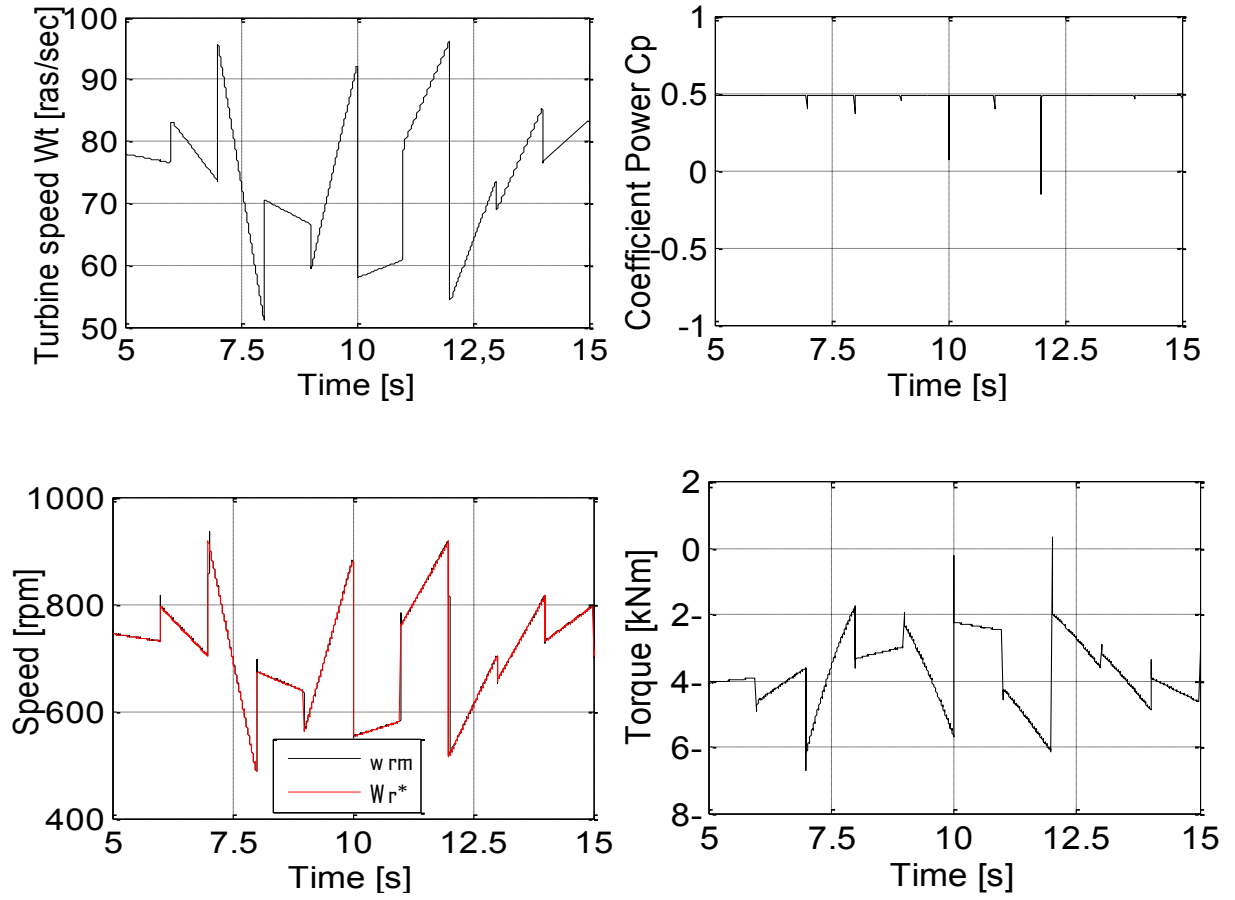
Figure 4.21: Turbine Parameters
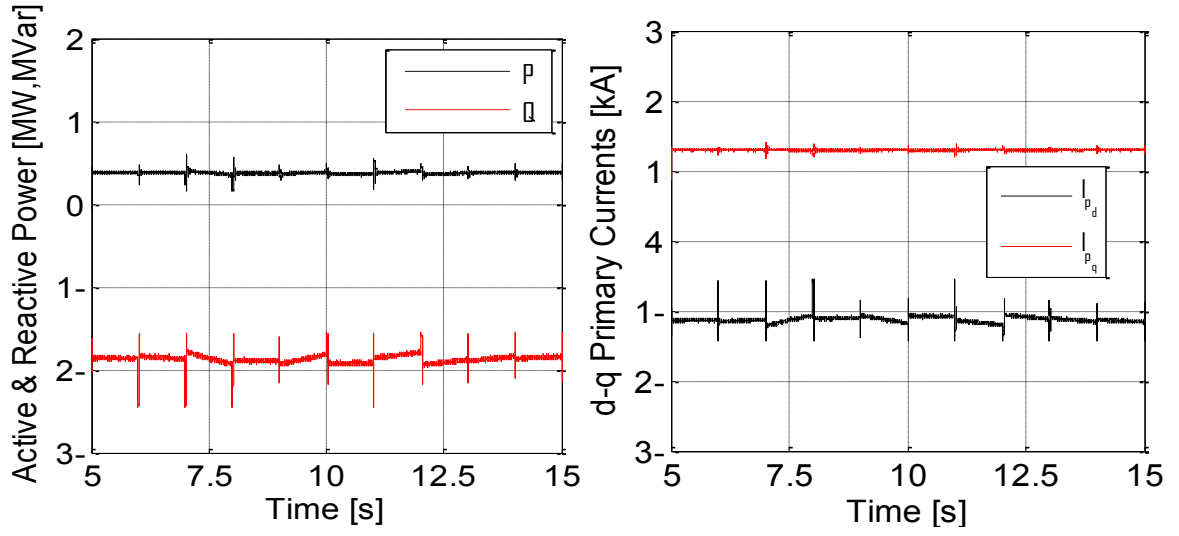
Figure 4.22: Generator side parameters
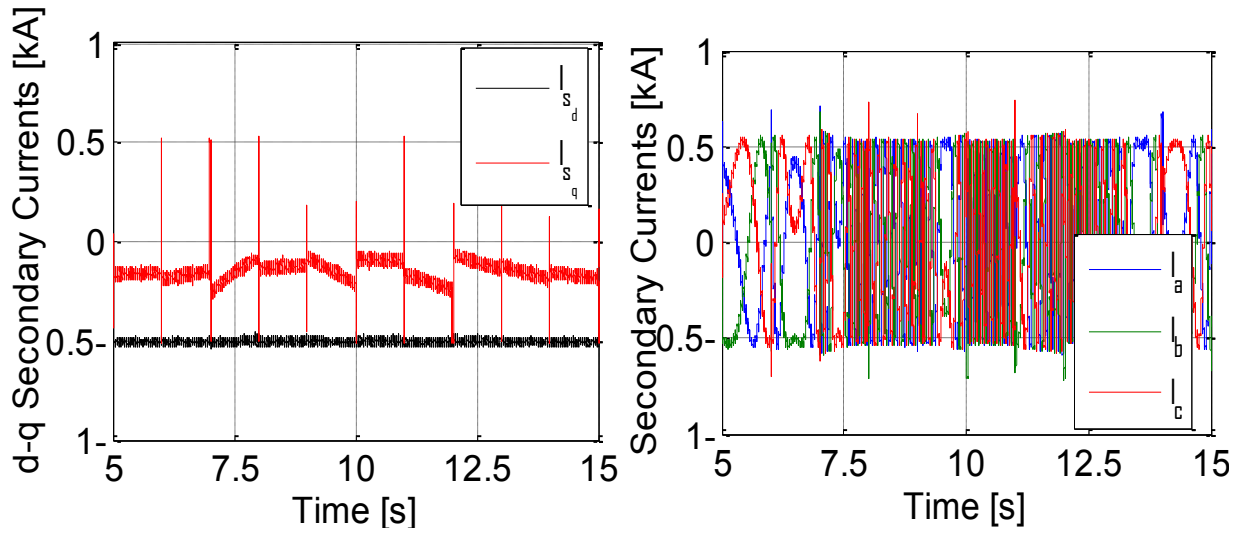
Figure 4.23: Generator (d-q secondary and phase) currents

4.4   Conclusions

Program design represents the capability of large scale generator based accurate parameters and its behaviours as wind generator to overcome the nonlinearity nature of the variable wind speed. The feature and ambitious program to employ this emerging technology within wind application was successful as well as, the permitted performance under coupling condition between the mechanical turbine and electrical generator in control strategy. The purpose of the study is to demonstrate the eligibility large scale emerging BDFRG to deal with the circumstances and conditions those accompanying power electrics. The study was conducted using two appropriate methods of control, proven them effective tracking in simulation and practice as well; that they scalar control and flux oriented control. The degree of response to these methods and their performance is uneven for several reason as the precision, simplicity and speed response but the scalar and FOC control always match the target .The results have been encouraged reflects properties of the machine design backed by the results of simulations based on reliable expertise and precision.

Regarding the V/f open loop scalar control, the response was reasonable and promise, and portability control method to follow the desired speed was convenient, even when the turbine subjected to the nonlinear speed waves. The system maintained its hardness and the extracted results prove the stiffness of open-loop control strategy and its reliability to serve as a trusted backup control in critical situations.

The results obtained under distinct analysing of the turbine performance, supported by profiles; graphic curves and aerodynamic equation explain the evolution of the potential wind energy. The sensor less methods adopted in these Simulations built on the dialectical relationship

between the machine and the turbine without the need to reference information from the generator side. That's make this valued study more attractive according to predictable advantages and scalability of generator, which is considered the second conversation state in the power plant.

The high performance FOC strategy is achieved when the mechanical shaft rotation is within the scope of the sync-speed of the BDFRG. The recommended notice to the researchers is to take time to set the appropriate turbine parameters to emulate suitable rating speed suitable to the maximum power point tracking (MPPT) energy match with the BDFRG parameter to achieve target performance. So the N (Gearbox) Ratio considered fundamental value to normalize the speed from low speed shaft side to the high speed shaft side as (desired rotation). After providing all these requirements, supported with appropriate coupling between the turbine and generator side's that appear obviously when the speed of the generator chasing the turbine speed, with corresponding loaded torque to the mechanical torque as negative load. The BDFRG as a power generator, capable to be practical and sensible alternative technology, operate in the wind energy field with an innovative advantage such high performance, robust and reliable in the wind energy field even based simplest control application such open lop control algorithm or high performance and complex methods when perform with the FOC.

- The accuracy and the capability to track the non-linear wind speed tend to side flux oriented control.
- The system in FOC is stable and the transformation speed from the super synchronous speed to sub synchronous speed is smooth and free-disturbance and obviously considers a big advantage, over the scalar control algorithm.

- The maximum properties can be achieved from FOC with high rate stability, which is characterized control method.

- The economy technology and the simple design further than the robustness system with the ability to meet the same target accounted as advantage to the scalar control algorithm.

Chapter 5 **Vector Control of BDFRM**

5.1   Introduction

There is no doubt that the precision, efficiency and flexibility is what distinguishes vector
control algorithm which is considered the common algorithm to control induction machine, at
the expense of the economic cost and complexity [72]. Furthermore, the drive system ensures
high accuracy speed control over a wide range [73]. Recent progress in the field of power
electronics and micro-electronics has made it possible to develop and produce such systems
based on the introduction of machine complete control of transient and steady-state behaviour of
the machine being achieved by means of appropriate feedback loops [74]. This method does not
only deal with rated voltage, but it also concerns about building appropriate frame angle based
primary voltage vectors, which is evaluating the power flow performance and complaining
between both side machine due to ease interchange of energy between satisfying from the
cascade control stage to provide appropriate d-q reference voltage and phase to the secondary
side machine [25, 75]. The adopted d-q references frame based on park transformation theory
responsible to provide suitable currents through cascade control stage and exiting frame based
voltage and currents requirements [76]. Vector control authorized short time period of transient
response and smooth performance compared to the scalar control. Since the control is being
executed in each of the two axes in a synchronously rotating d-q reference frame, a diversion of
stationary frame measurements (e.g. voltages and currents) is required and the algorithms

themselves are more complicated than scalar control counterpart [77].For this reason, a vector control scheme is more comprehensive and needs digital signal processing knowledge of fast micro-processors to achieve high control rates necessary for good dynamic performance. Nowadays, space vector pulse width modulator (SVPWM) featuring low harmonic injection and reduced switching losses [78], with hardware implementation is commonly used in vector control schemes (although sinusoidal alternative PWM with high-frequency carriers offering similar advantages is also popular). The accuracy and effectiveness of this control method are highly pronounced flexible to deal with the variables involved in vector control algorithms. Stator primary voltage oriented vector scheme will be implement for the machine side converter (MSC) and grid side converter both of conventional design allow the bi-directional power converter of the BDFRM through the secondary winding side in either motoring or generating mode. Both controllers have inner and outer loop currents and power loop respectively. Vector control MSC requires measurements of primary, secondary d-q currents primary voltage and position angle in the form of rotating angle through shaft decoder, suitable park conversation unit and PI controller to adjust the primary and secondary currents in both stage controls further than reference d-q voltage as the upcoming voltage from the control unit.

P&Q VC Control
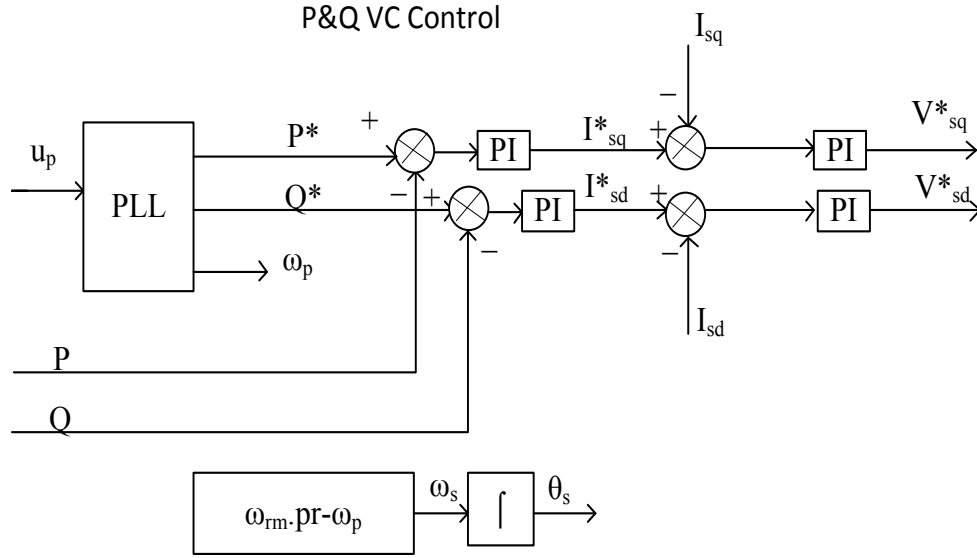
Figure 5.1: Block Diagram for Machine side converter control

5.2   Machine Side Vector Control (MSVC) according to active and reactive power

Providing the mathematical model equation adopting vector control method featuring an extra reliability to establish the simulation models which interpret behavioural and dynamic performance of the system and its ability to highlight the distinctive characteristics and accuracy performance illustrated above in Fig. 5.1.The main goal of this section is to examine the viability to minimize the coupling side between the quadrate current in the secondary side machine as a controllable quantity to observe the power flow inside the machine.

The simulation software has been built to proof the control machine behaviour based accurate vector control strategy. The main voltage supply is 690V (V L_L) and 563.4 V as rated voltage and dc voltage 850 V. In order to achieve amount of stability in term of the transient periods, the control unit includes two cascade stage the outer loop deal with the actual power in the form

(P,Q) and the reference power (P*,Q*) involved to achieve required reference current (i^*_{sd}, I^*_{sq}) taking advantage of the PI controller as compensating unit to offer appropriate reference secondary currents reference current I^*_{sd}, I^*_{sq} has significant influence on the operating secondary d-q currents which are obtained from the machine side as a feedback loop, to set up their values according to the load requirements. The operating mode, which the machine obtained and the value of desired speed can be identified following load torque.The second stage control (inner Loop) interested in, pursue reference currents (both axis) which are gained from the first stage control, compared to the actual secondary currents (i_{sd}, i_{sq}), and developed the error during the dominant PI controller to the appropriate U_d, U_g voltages Equation (5.8). Inverse park transformer unit converts the d-q voltage form into a form 3-phase voltage using inverse park unit and θs as key word to build suitable secondary voltage based power electronics applications.

The role of DC voltage to draw proper voltages to the secondary side machine,justify the tracking behaviour for the nominated variable through the control action respected to dynamic equations which govern the repetitive variation through control stage.

5.2.1 Inner loop (Currents loop)

According to dynamics model of the machine the secondary side voltage identified as:

$$U_s = \frac{d\lambda_s}{dt} + j\omega_s \underline{\lambda}_{ps} \tag{5.1}$$

Secondary flux vector illustrates as follow:

$$\lambda_s = L_s \underline{i}_s + L_{ps} \underline{i}_s^* \tag{5.2}$$

The secondary flux equation above will be developed according to the following equation:

$$\lambda_s = \sigma L_s \underline{i}_s + \frac{L_{ps}}{L_p} \lambda_p^* \tag{5.3}$$

Further development will link mutual flux with the secondary flux as

$$\lambda_s = \sigma L_s \underline{i}_s + \lambda_{ps} \tag{5.4}$$

σ presented here as a coefficient coupling and we can express the ω_s as the secondary side frequency

$$U_s = R_s \underline{i}_s + \sigma L s \frac{di_s}{dt} + \frac{d\lambda_{ps}}{dt} + j\omega_s \sigma L s i_s + j\omega_s \lambda_{ps} \tag{5.5}$$

The steady state forms of the equation above.

$$U_s = R_s \underline{i}_s + j\omega_s \sigma L s \underline{i}_s + j\omega_s \lambda_{ps} \tag{5.6}$$

The Equation (5.6) declares the proportional relationship between the secondary voltage and secondary current with constant flux linkage offset component. Developing the equation in d-q form will give as an essential approach to the vector control algorithm.

$$\begin{cases} U_{sd} = R_s i_{sd} + (\omega_s \sigma L s i_{sd} + \omega_s \lambda_{psd}) \\ U_{sq} = R_s i_{sq} + (\omega_s \sigma L s\, i_{sq} + \omega_s \lambda_{psq}) \end{cases} \tag{5.7}$$

Pena [79] and some of researchers adopted the Equation (5.7) as compensating branches for more accuracy, but the simulation declared that's not quite vital to achieve the target, and fed back satisfying from PI controller can fill this gap.

$$\begin{cases} U_{sd}^* = PI(i_{sd}^* \text{-} i_{sd}) \\ U_{sq}^* = PI(i_{sq}^* \text{-} i_{sq}) \end{cases} \tag{5.8}$$

5.2.2 Power Loop Derivation

In another procedure the relation between the active and reactive power and the corresponding secondary d-q currents can be proved mathematically by the following equations;

$$\lambda_p = L_p \underbrace{i_{pd} + j i_{pq}}_{i_p} + L_{ps} \underbrace{i_{sd} . j i_{pq}}_{i_{sm}} \tag{5.9}$$

$$S_p = \frac{3}{2} U_p I_p{}^* \tag{5.10}$$

Where i_{sm} consider magnetizing secondary current .Avoiding coupling relation between the the d-q current as expected in conventional VC control the electromagnetic force(*emf*) related to the disturbance should be compensated for improving the performance by substituting (5.9) in (5.10)assuming the $i_{sm} = i_s$ in respective frame would lead to the following relationships for primary mechanical (i.e., $P_{electrical}$ −Losses) and reactive power. One can develop the following important VC relation for torque and active and reactive power

$$T_{evc} = \underbrace{\frac{3}{2} p_r \lambda_{md} i_{sq}}_{T_{foc}} - \frac{3}{2} p_r \lambda_{mq} i_{sd} \tag{5.11}$$

$$P_{pvc} = \frac{3}{2} \frac{T_{evc}}{p_r} = \underbrace{\frac{3}{2} \omega_p \lambda_{md} i_{sq}}_{P_{pfoc}} - \frac{3}{2} \omega_p \lambda_{mq} i_{sd} \tag{5.12}$$

$$Q_{pvc} = \underbrace{\frac{3}{2} \omega_p \left(\frac{\lambda_p^2}{L_p} isq - \lambda_{md} \quad i_{sd} \right)}_{Q_{pfoc}} - \frac{3}{2} \omega_p \lambda_{mq} i_{sq} \tag{5.13}$$

where the λ_{md}, λ_{mq} consider the magnetising flux component. As can be seen in the above expiration, VC of P_p and Q_P is coupled as both the i_{sd} and i_{sq} secondary current appear in (12)
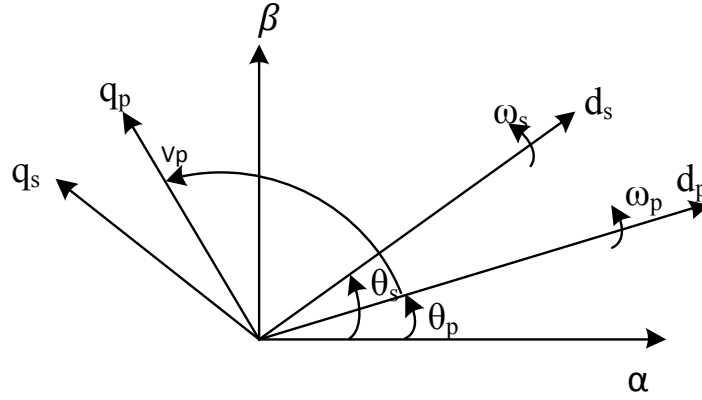
Figure 5.2. Reference frame based Vector control

and (13), reducing this coupling can be achieved by aligning q_p-axis of the reference frame to the primary voltage vector as proposed in Fig 5.2, in this case λ_p would be phase shifted ahead of the corresponding d_p-axis, depending on the winding resistance which is generally smaller in large machine. For this reason the reference frame of the VC should be similar to the FOC control and the equation (5.12) and (5.13) can be developed as:

$$P_{vc} \approx P_{efoc} = \frac{3}{2} \omega_p \lambda_m i_{sq} = \frac{3}{2} \frac{L_m}{L_p} \omega_p \lambda_p i_{sq} \tag{5.14}$$

$$Q_{vc} \approx Q_{efoc} = \frac{3}{2} \frac{\omega_p \lambda_p^2}{L_p} - \frac{3}{2} \omega_p \lambda_{ps} i_{sd} = \frac{3}{2} \frac{\omega_p \lambda_p}{L_p} (\lambda_p - L_{ps} i_{sd}) = \frac{3}{2} \omega_p \lambda_p i_{pd} \tag{5.15}$$

With the λ_p, λ_{ps} magnitude fixed by primary winding grid connection at line frequency (ω_p) the P_P will be respective to the i_{sq} and Q_p versus i_{sd}.

$$\begin{cases} i_{sq}^* = PI(P^* - P) \\ i_{sd}^* = PI(Q^* - Q) \end{cases} \tag{5.16}$$

5.3 Vector Control based Speed Loop.

This control method is appropriate control to practise work due to ease building the reference frame, and torque based actual machine rotation. The inner loop is the current loop (one for each axis). The outer control responded to speed development to the appropriate torque developed by compensating PI controller to the necessary q component of the secondary current Isq* presented in Equation (5.16) below.

$$i_{sq}^*{\sim}T_e=PI\ (\omega_r^*{-}\omega_r\ ) \tag{5.17}$$

To produce the required torque desired d-q secondary voltages to be applied to the BDFRM. $(U_{sd}*, U_{sq}*)$ are output of the current loops Fig.5.3. After the inverse park transformation, the signals are passed into the pulse width modulation PWM generator to convert them in an appropriate switching pattern.
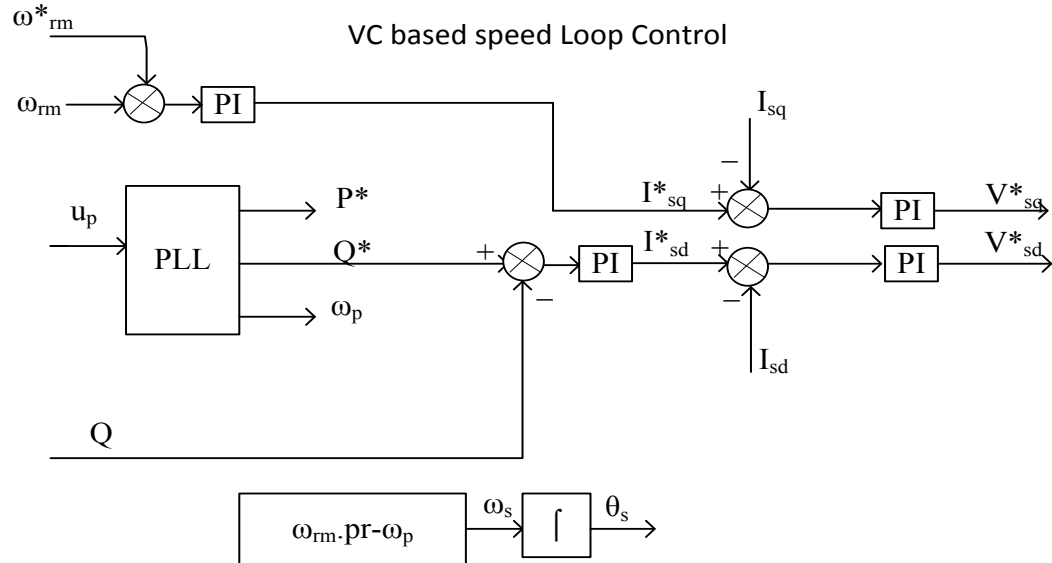
Figure 5.3: The Configuration block diagram for the vector control based speed

The results can be presented in both work modes (generating and motoring) to give superior depicting of the nature machine behaviour based accurate software taking into account all the features and parameter mentioned in Chapter 2, during the implemented modes separately. The control proceed in this attempt established based on the unity power factor when the reactive power equal zero that's mean the machine is synchronising with grid and consume the inverter side satisfying from the control sensors .

5.3.1 Motoring Mode

A simulation of BDFRM vector model based speed loop, system control shown below in order to focus on the behaviour of the drive. The theory assumes that the rotation of machine ω_{rm} can be developed to i_{sq} current as torque production then according to equation 5.15 presented in this case main active power indications. The analysis of this mode explained the positive route of the torque Fig. 5.4, through the simulation process and that indicate producing power from the grid. The i_{sd} = 1830 A in Fig.5.5, and i_{pd} = 0 complimentary to the Q= 0. Fig. 5.6 illustrates the stability of the machine through transient period (when the machine mod change from the supper synchronous speed to sub synchronous speed) associated with power electronics parameter.
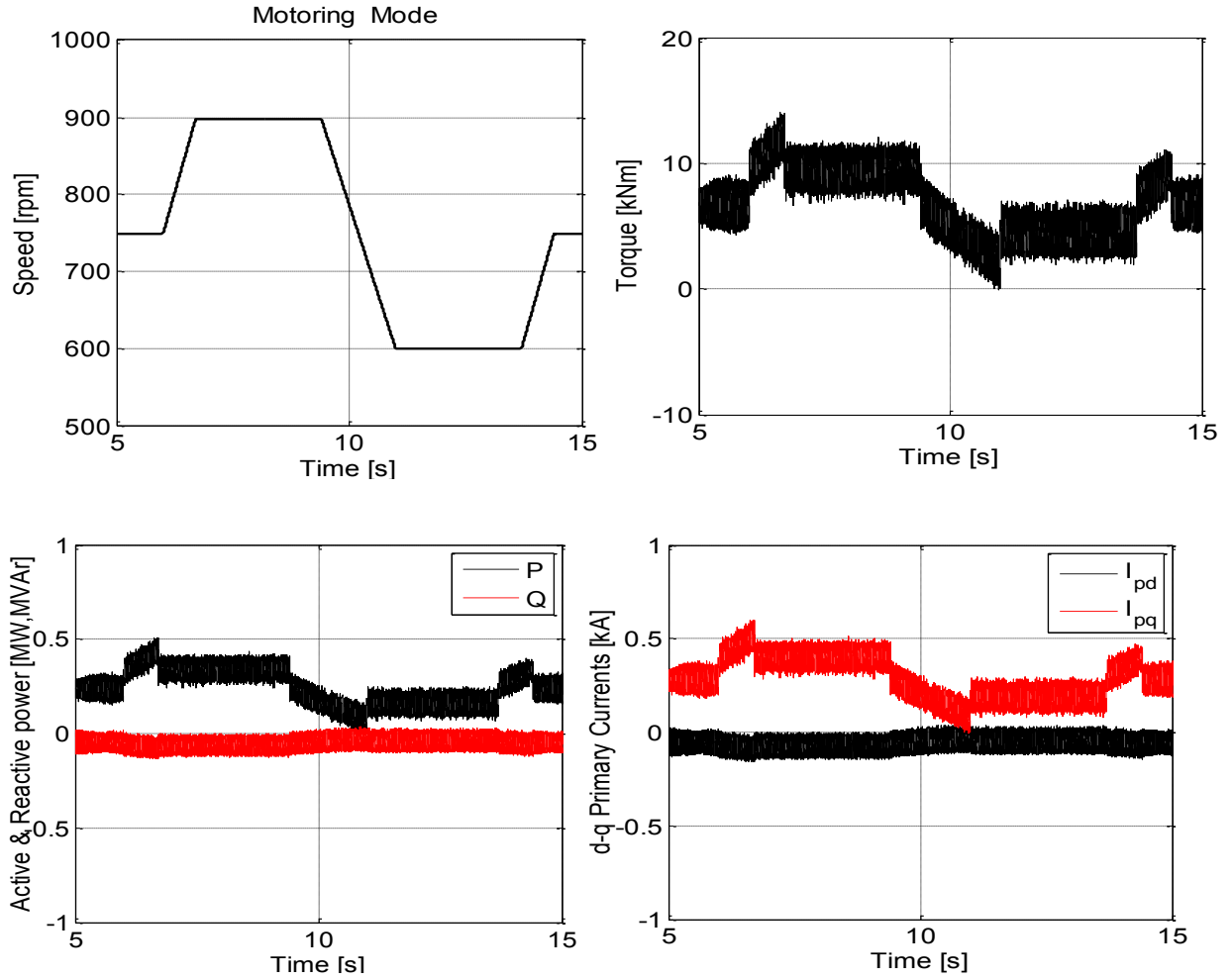
Figure 5.4: Speed, Electromagnetic Torque and PQ, with d-q primary current
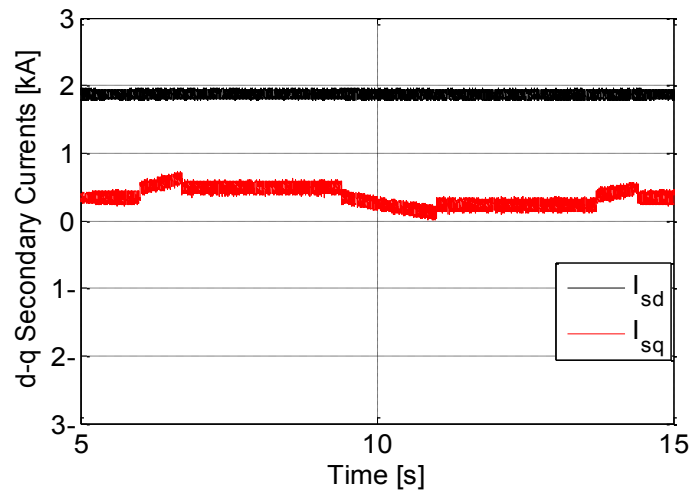
Figure 5.5 : d-q Secondary Currents

100
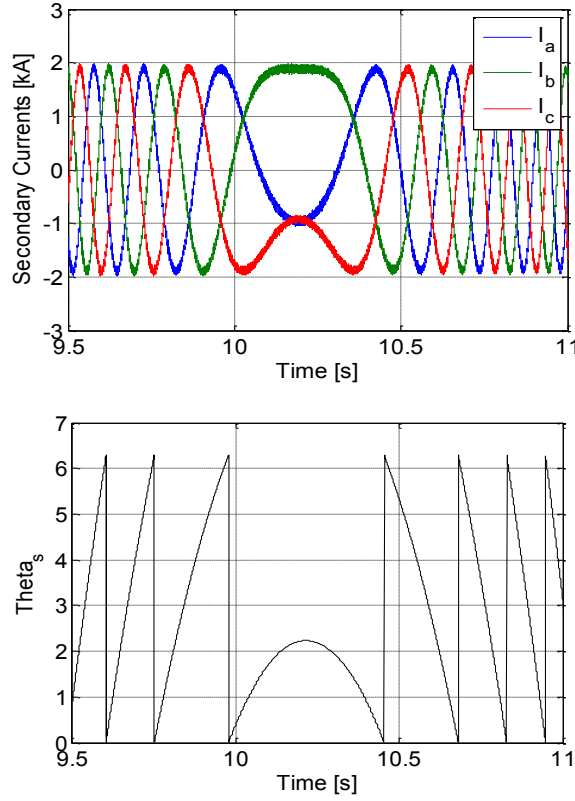
Figure 5.6: transient transaction period between the super and sub sync machine

5.3.2 Generating Mode

The resent trends of the wind conversation systems are adopting alternative free maintenance generators technology under consideration of long term operating work. The BDFRG generator consider[12, 14] the new technology can achieve this advantages with acceptable response and partially dealing with power electronics, with high performance capability to follow deferent control algorithms .The mechanical coupling between the wind turbine shaft and machine prime mover considered in real condition as imported torque (negative) developed by BDFRG to suitable electrical energy.
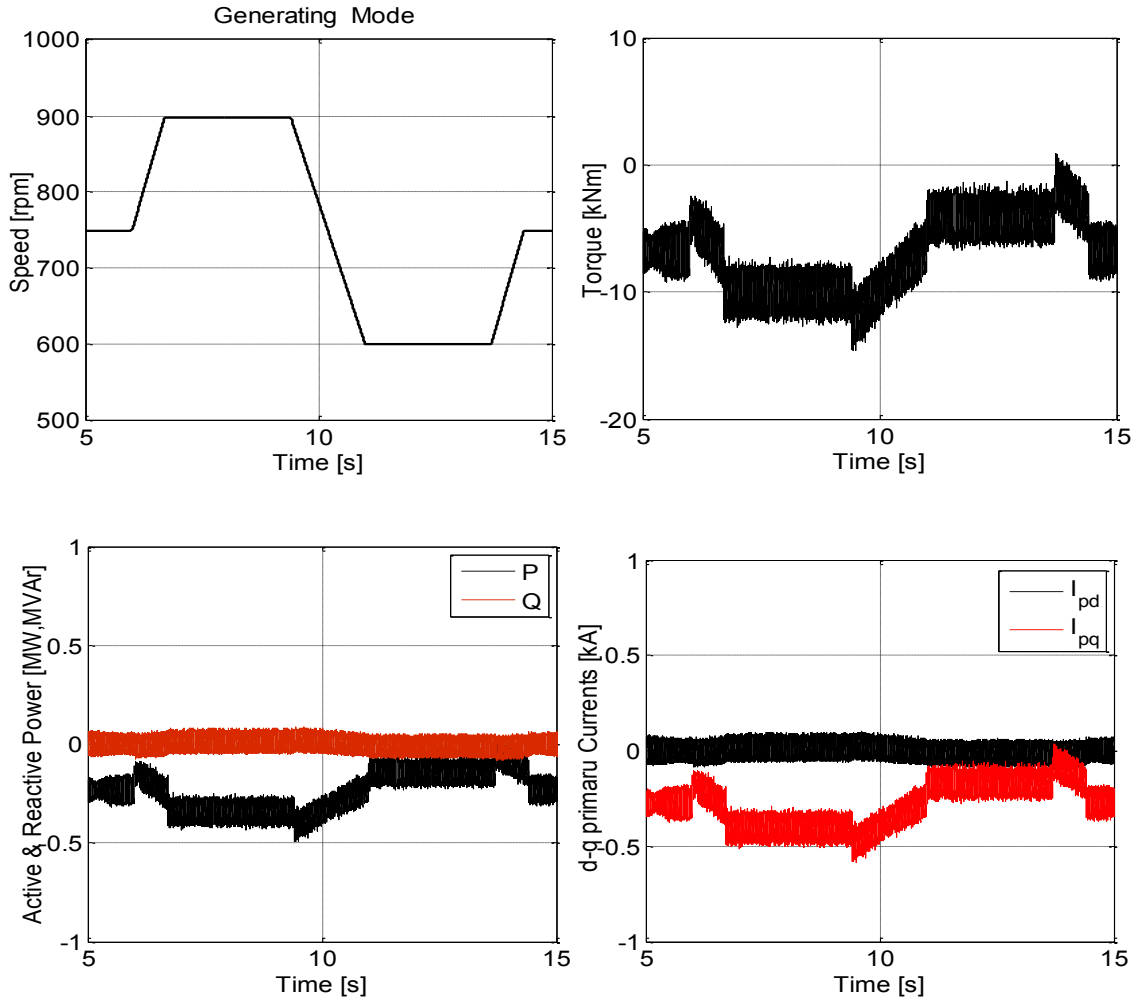
Figure 5. 5.7: Speed, Torque, Activ**e** and Reactive power in generating process
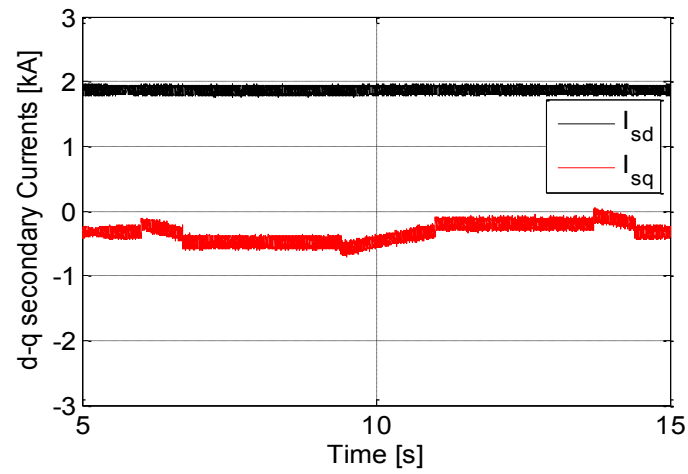
Figure 5.8: Secondary d-q currents based generating mode
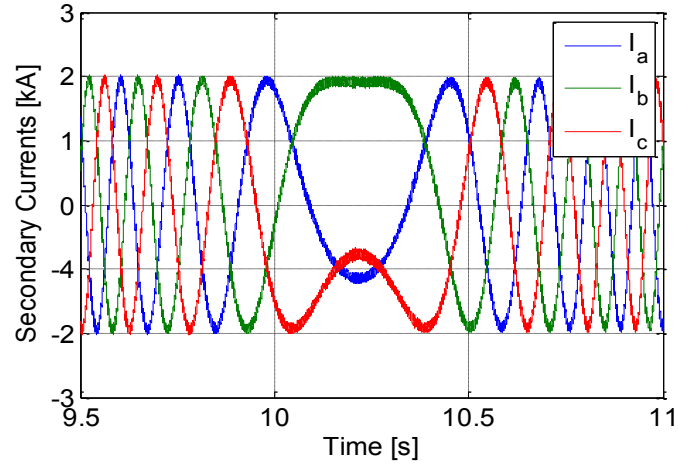
Figure 5.9: Transition period of the phase secondary currents
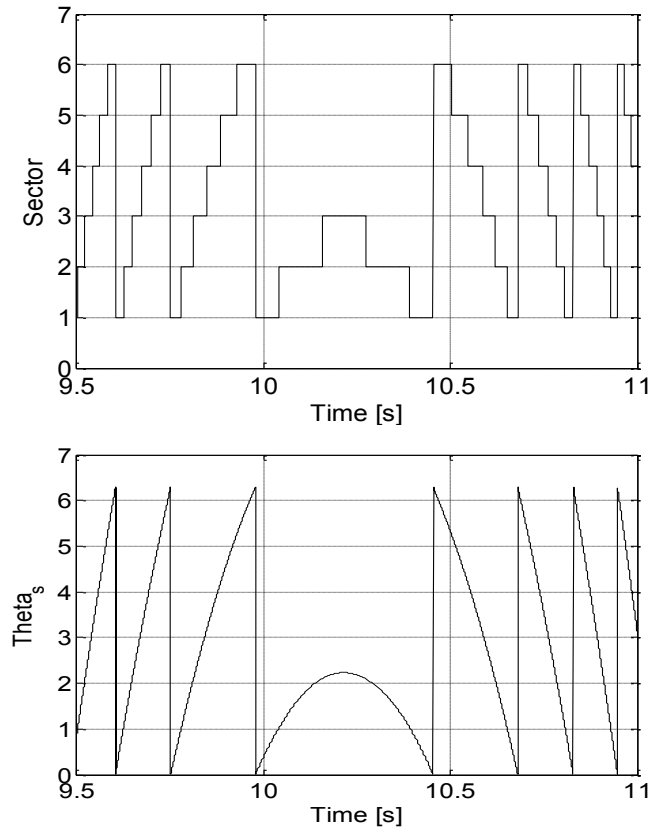
Figure 5.10: Power electronics parameter associated VC, transient period, sector top plot and theta-s

The route of torque is negative corresponding to the gaining power the generating mode from the wind turbine as motivating mechanical load. Route of currents and power will responds to this change, identifying absorbing power Fig 5.7. The speed in both procedures (motoring, generating) has a typical speed trajectory starting as synchronous mode 50 Hz, 750 rpm and then climbing to the 900 rpm as a super synchronous speed, then descending to 600 rpm (sub Synchronous speed) and settle down to 750 rpm. The load applied, followed the torque-speed Equation (3.13) chapter 3,when the amount of load correlated to rotation machine. The positive behaviour of secondary currents in term of variable speed condition superior from the scalar control especial in transient period as illustrated in Fig 5.9 complimentary with power electronics parameter in Fig.5.10.

5.4   Vector Control of Grid Side Converter (GSC)

Figure 5.11: Conventional vector control Grid Side converter.

Variable speed generator produces variable frequency and voltage that have to be converted to appropriate frequency and voltage to match the constant grid frequency because that variable speed generator is connected to grid through power electronics converters [80, 81]. More popular is the back to back ac/dc/ac converter [30, 81-83] by means of pulse-width-modulation (PWM) rectifier-inverter systems with dc-link voltage contains of two loops of control which depend on the connection side such as control grid side [21]. Both types of control loops have many variables that deal effectively with their requirements. The control grid side circuit can be thought of as voltage source inverter connected to the power grid as shown in Fig. 5.11. The suitable equations that govern this relationship listed in following section deals with Inner and outer loop control.

5.4.1 Inner Side GSC Control

Nowadays converter fed electrical AC drive is used in industry in numerous applications and in large numbers, basic type used in power range from less than KW to 2000 KW and more [84, 85]. The DC supply voltage can be provided by the rectifier from an AC supply or directly from a DC source as battery. The capacitor is necessary to supply the high frequency currents produced by the inverter switching action where the rectifier produce DC voltage, the capacitor also acts to smooth the low frequency rectifier voltage ripple [82, 86]. The grid side converter control requires the measurements for all the variables, which related to it as grid side currents, primary voltage, DC voltage, and q components to the line side current. Similar to the machine side, the GSC conclude two-loops control Inner loop and outer loop derivation. In order to simplify the inner control relation starting from;

$$I_L = \frac{1}{Z}(U_p - U_c)$$ (5.18)

$$U_c = (U_p - ZI_L) \tag{5.19}$$

The proportional relationship between the converter voltage (Uc) and line side current I_L as shown in equation (5.19) justify the control equation which govern inner side loop control.

$$\begin{cases} U^*_{cd} = PI\ (\ I_{Ld}{}^* - I_{Ld}) \\ U^*_{cq} = PI\ (\ I_{Lq}{}^* - I_{Lq}) \end{cases} \tag{5.20}$$

5.4.2 Outer Side Converter Control

This loop depends on power flow through the grid side converter, especially between the apparent power S_g, and line current I_L and primary side voltage:

$$S_g = P_g - JQ_g = \frac{3}{2}(U_{Pd}\ I_{Ld} + U_{pq}\ I_{Lq}) - J(I_{Ld}\ U_{pq} - I_{Lq}\ U_{pD}) \tag{5.21}$$

Consequently to the primary voltage orientation (i.e. $U_{pd} = U_p$, $U_{pq} = 0$)

$$\begin{cases} P^*_g = U_p\ I_{Ld} \\ Q^*_g = U_p\ I_{Lq} \end{cases} \tag{5.22}$$

To achieve unity power factor on the grid side $I_{Lq} = 0$ then the expression (5.20) can develop to:

$$I^*_{Ld} = PI\ (\ U_{dc}{}^* - U_{dc}) \tag{5.23}$$

Fig. 5.12 reflects the extraordinary importance of quadrate line current on the driving DC-link voltage in weather minimising of afforded V_{dc} voltage to get maximum magnetising current from the source voltage.
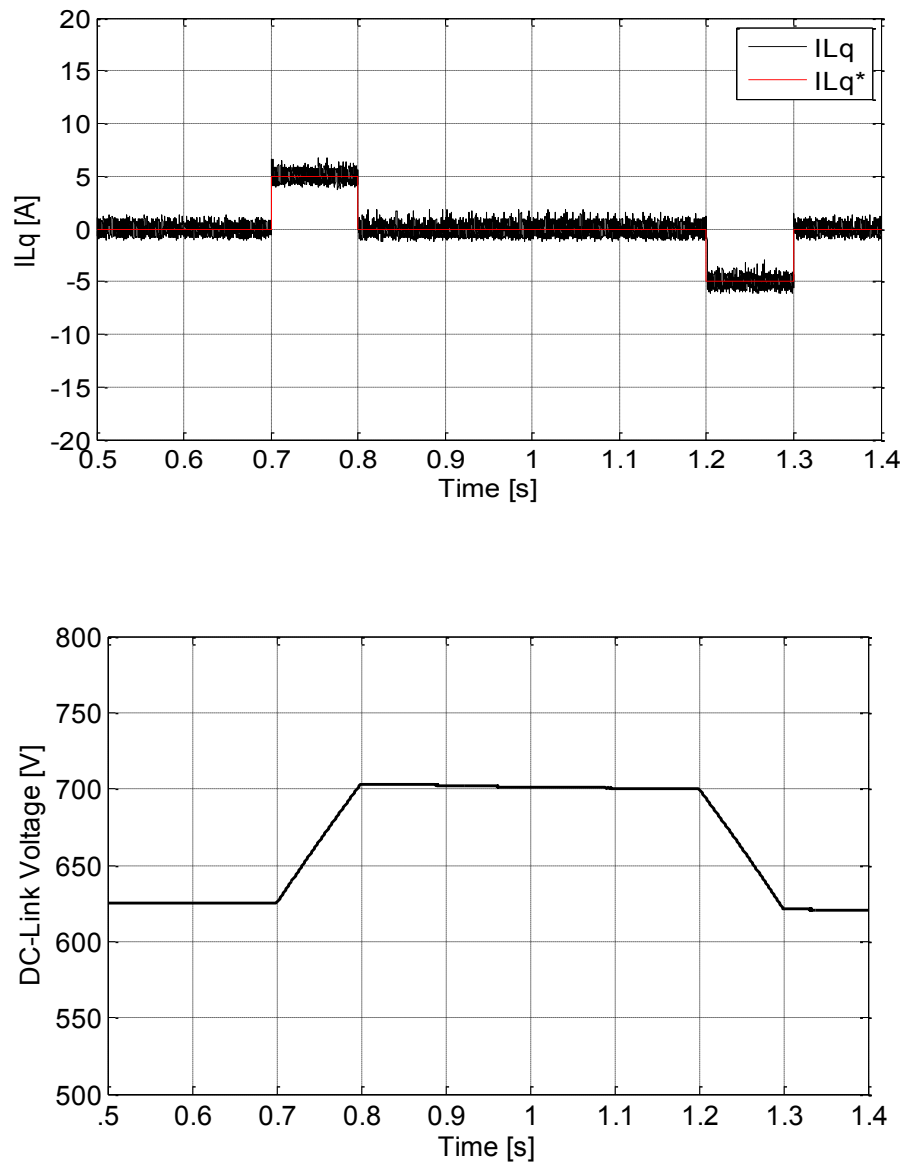
Figure 5.12: Quadrature line current and the producing DC voltage
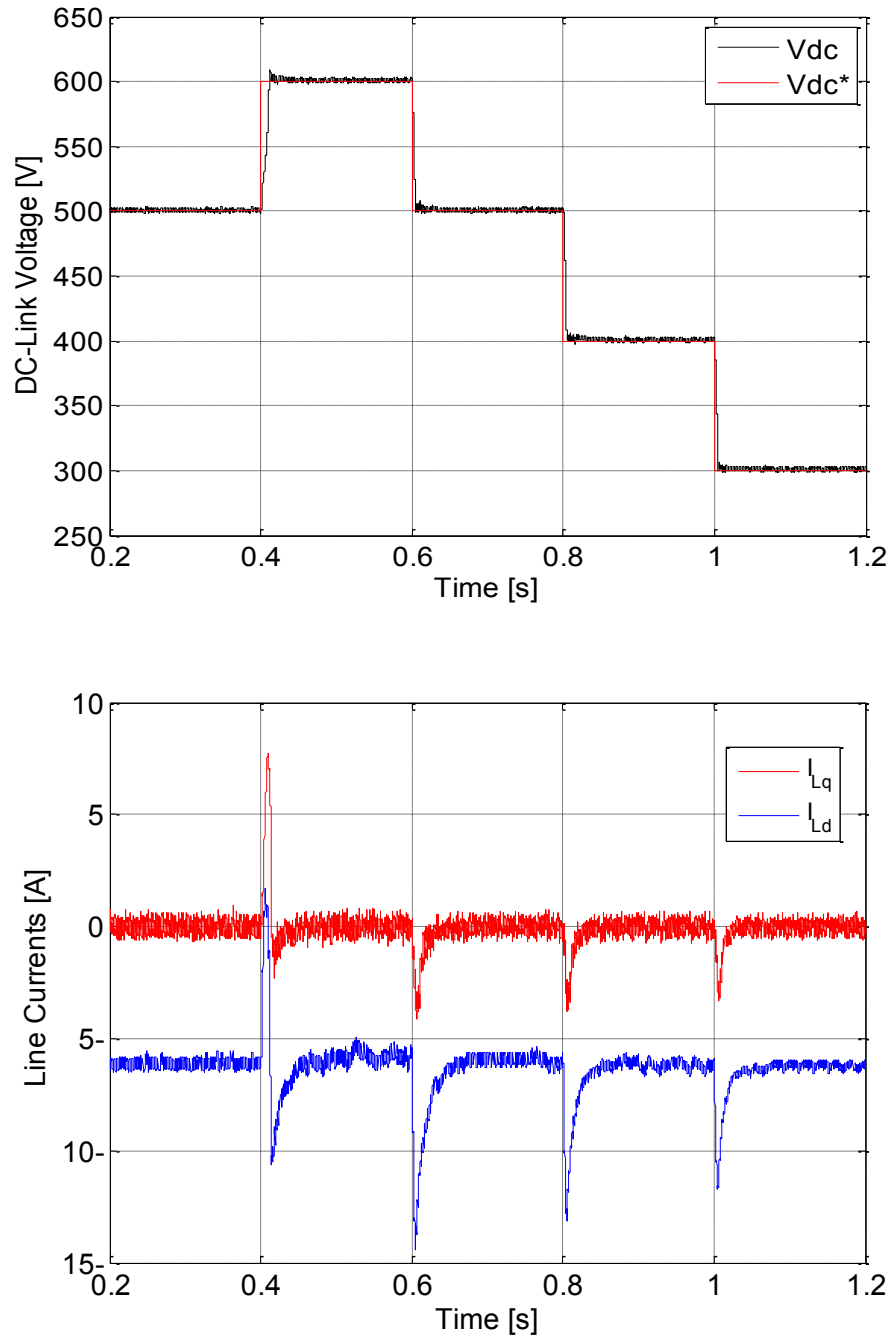
Figure 5.13: DC –link Voltage and line currents

Fig. 5.13 proves the equation (5.23) in order to achieve unity power factor strategy, the $i_{Lq}=0$ and the direct current i_{Ld} responded to the step change of desired DC-link voltage. The smooth

change in the line current reflects the stability of control system (vector control) to observe and regulate the variation of V_{dc} voltage over i_{sd} currents.

5.5 Conclusions

Vector control active and reactive power control based Generating and motoring mode and trusted drive application has been presented and evaluated. The performance BDFRM under various speed regimes included the synchronous speed illustrated in the reliable results above, and the processing done correlated to specific case condition. The vector control based speed loop controller reflects the preferred algorithm in practise work to reflect the actual behaviour of the machine under variable speed condition which makes it compelling for industrial applications. The previous vector control strategy developed for machine side converter (MSC) reflected the success and compatibility brushless doubly feed machine to follow the high performance application and demonstrate its efficiency to achieve optimum dynamics and features. The stability of GSC is addressed the urgent request for maintaining the proper control algorithm handling of the electric grid connection. The simulation results in Fig. 4.12 and Fig. 5.13 confirm the superiority of VC to drive the DC-link Voltage dealing with the symbiotic relationship between the line currents and Voltage to establish the stable grid side outcome.

Chapter 6 **Low Voltage Ride Through of a BDFRG Wind Turbine**

6.1 Introduction

The installation of wind power plants is growing rapidly as the main or supporting generating stations, but suffers from the weakness of inadequate power production to satisfy increasing demands for energy [87, 88]. The continuous penetration of wind plants over the recent years has provided a basis to integrate wind with other energy resources in a power generation system. In order to facilitate this development, a new set of stringent regulations, named as grid codes, have been stipulated nationally to ensure the necessary quality of energy distribution[89-91]. The grid code specifies the capability of wind generators to support the power system by supplying ancillary services, such as voltage control [92], to assure a safe and reliable power system operation. Power electronics based solutions for grid interfacing of wind turbines seem to be a very promising technology able to satisfy these strict grid requirements. So, grid interaction related issues of wind generators have become increasingly important worldwide and qualitatively can be understood as follows. If most of the wind generators would be disconnected from the grid in case of a fault, the network voltage recovery time would be extended and the power system stability would be severely compromised [93] with immediately obvious adverse implications. The trend is therefore to establish safe conditions for as many wind turbines to stay on-line during fault occurrence (e.g. to allow them to ride through the fault) and provide the necessary reactive power support to help restore the system voltage in the shortest possible time.

6.2   National Grid Codes

With the perspective of wind farms integration, the E.ON Netz fault response code has already set requirements for the behavior of the wind generator protection as mentioned in [67, 94-96]. Instead of disconnecting them from the grid, the wind generators should be able to follow the characteristic shown in Fig. 6.1.
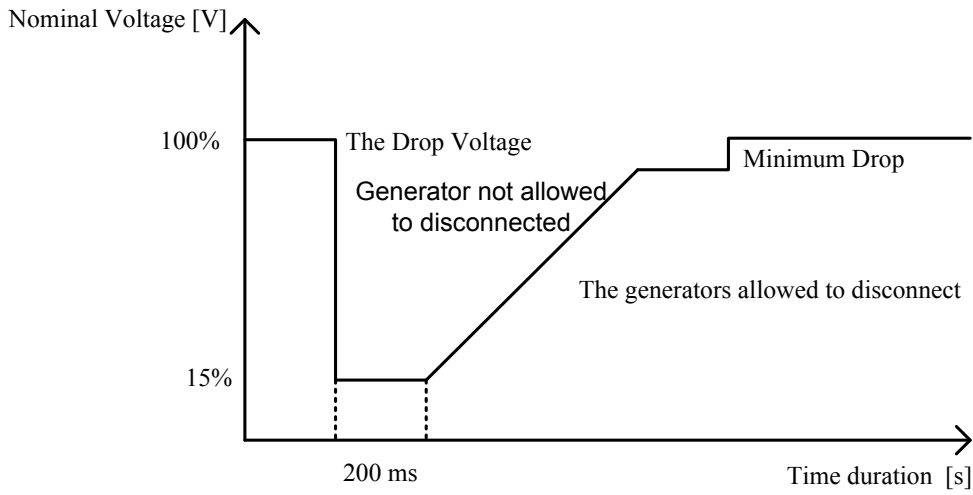
Figure 6.1: E.ON fault response requirements

The proposed method, which makes it possible for BDFRG wind generators to remain grid connected during symmetrical faults, has been developed in this chapter based on a dynamic model of the machine. In assessing the generator capability to ride through a symmetrical fault, the study takes into account the stability of the DC link focusing on the machine performance evaluation in terms of the secondary winding current levels in order to establish measures to by-pass the inverter or at least prevent its over-currents during the fault interval. The E. ON grid codes requirements should present the Fault Ride Through (FRT) capability to allow the generator or wind farm terminal voltage to stay above the pre-defined limit according to the

Time-Voltage characteristic in Fig. 6.1. In the region below the boundary line, the protection can trip and take the generator off-line. Another clause of the E.ON grid code is the demand for reactive power injection during voltage dips, which should also follow a certain specified curve. This requirement, by improving the voltage profile in the electric grid under a fault condition, has added benefit in effectively increasing the generator ride-through capacity given Fig. 6.1. The generating farms therefore must support the grid voltage with appropriate reactive current on the line side of the matching transformer during the voltage sag with the control actions taking place within 200 ms interval following the fault inception as indicated in Fig. 6.1. A reactive power output of at least 100% on rating must be possible if necessary based on the E.ON specifications.

6.3   Low Voltage Ride Through (LVRT) Fundamentals

The LVRT is defined as the ability of a generator to remain grid-connected operating dynamically stably and offering network support throughout the voltage disturbance period by supplying sufficient amount of reactive power [97]. Grid faults, even far away from the wind turbine location, can cause voltage sags at the connection point of the BDFRG with transient stability phenomena similar to classical synchronous generators. Such a voltage dip results in a mechanical input- electrical output power imbalance of the generator accelerating its rotor and producing both the primary, and hence the secondary (through magnetic coupling), high in-rush currents which may damage the back-to-back (dual bridge) converter. Another immediate harmful effect is the DC-Link voltage disturbance of the converter [98]. In the past, the affected wind generators were disconnected under these circumstances to prevent the power electronics

failure. Nowadays, however, they have to operate on-line by supplying reactive power to the system and safely ride through the fault [99, 100].

6.4   LVRT of BDFRG

With the introduction of the grid codes, LVRT control strategies for commercial DFIG and other competitive variable speed technologies (e.g. multi-pole wound field or permanent-magnet synchronous generators), have started to be widely investigated and a commonly adopted solution to protect the machine converter have been to use a crowbar to short the rotor winding during the fault. Doing so, the rotor and converter over currents can be diverted away through the crowbar short-circuit resistance [101-103].

Following the recent LVRT line of research on symmetrical faults of the DFIG, similar studies have been carried for its promising brushless alternative from the same slip power recovery family of machines, the brushless doubly-fed induction generator (BDFIG) [98, 104-106]. This significant work has clearly demonstrated the superior LVRT capability to DFIG in terms of the BDFIG's ability to ride through the fault without a crowbar. This distinguishing property can be attributed to the higher leakage inductances, and hence the lower fault current levels, compared to the DFIG. However, no publications on this subject have subsequently appeared in the refereed literature on the BDFIG reluctance rotor, the BDFRG, despite its apparent performance and control advantages over the former. This chapter will attempt to fill this void by presenting a comprehensive analysis of the LVRT capabilities of the BDFRG for both symmetrical and more common asymmetrical faults, which will be shown to be in many respects similar to BDFIG's, and as such also preferable to traditional DFIG's. This distinctive feature, together

with the other merits identified earlier, should make the BDFRG a viable cost-effective candidate to DFIG in the target wind power applications.

6.4.1 FOC Principles and Procedure

Adopting Primary Flux (Field)-Oriented Control (FOC) for the BDFRG to overcome a symmetrical fault on the line side, has been mainly motivated by the inherently decoupled nature of the primary real power (P) (or electro-magnetic torque) and primary reactive power (Q) control. This advantageous FOC property comes from the reference frame selection and the flux vector (λ_p) alignment choice shown in Fig. 6.2.
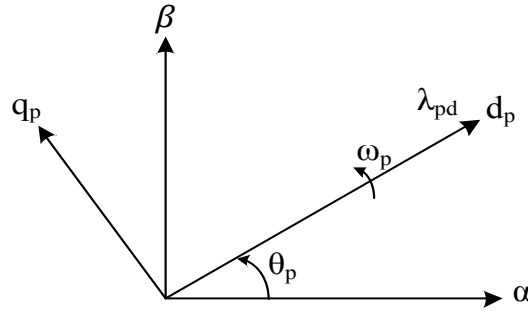
Figure 6.2: A reference ω_p rotating d-q frame and primary voltage/flux vector positions for FOC

Under the above frame-flux alignment conditions, the following obvious equalities apply:

$$\lambda_{pd}=\left|\lambda_p\right| \text{and } \lambda_{pq}=0 \tag{6.1}$$

The angular position of the magnetising d-axis for control purposes in a stationary α-β frame (with the α-axis overlapping the phase-A space location of the primary winding), θ_p, can be

found from the respective voltage, current and flux $\alpha\beta$ components (deduced from the voltage and current phase measurements) in a standard manner as follows:

$$\lambda_{p\alpha} = \int (U_{p\alpha} - R_p i_{p\alpha})\, d\theta \tag{6.2}$$

$$\lambda_{p\beta} = \int (U_{p\beta} - R_p i_{p\beta})\, d\theta \tag{6.3}$$

$$\theta_p = \tan^{-1}\left(\frac{\lambda_\beta}{\lambda_\alpha}\right) \tag{6.4}$$

The above estimation technique is presented graphically in Fig. 6.3 for convenience.
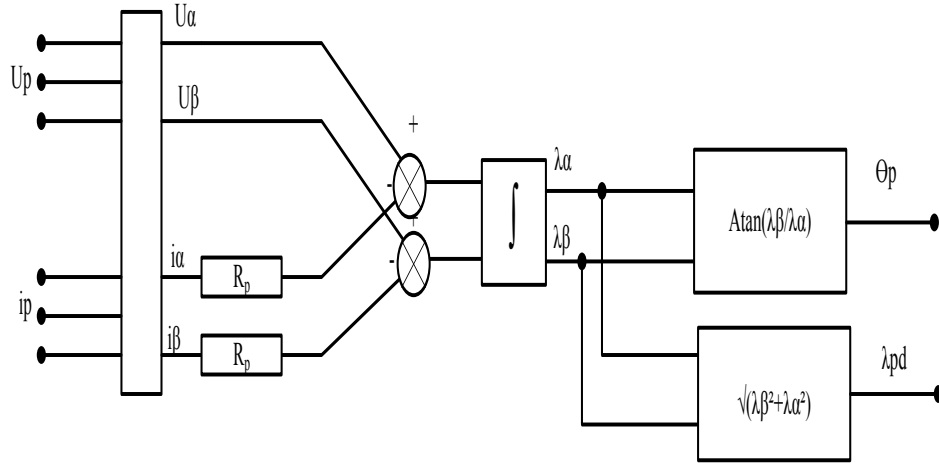
Figure 6.3: Estimation of primary flux vector orientation in a stationary frame.

The control (secondary) frame d_s-axis angle (θ_s) relative to the stationary α-axis can now be obtained from the measured rotor position (θ_{rm}) using the equivalent form of the fundamental velocity relationship:

$$\theta_s = \underbrace{\theta_{rm} p_r}_{\theta_r} - \theta_p \tag{6.5}$$

The Q control logic can be derived starting from the following conventional equation for the primary apparent power (Fig. 6.4):

$$P+jQ=\frac{3}{2}\mathbf{u}_p\mathbf{i}_p{}^*=\frac{3}{2}\left(u_{pd}i_{pd}+u_{pq}i_{pq}\right)+j\frac{3}{2}\left(u_{pq}i_{pd}-u_{pd}i_{pq}\right) \tag{6.6}$$

Substituting for $\boldsymbol{\lambda}_p$ from (2.3) into the respective voltage equation (2.1) of the BDFRG dynamic model introduced in Chapter 2, the latter can be manipulated as follows:

$$\mathbf{u}_p=u_{pd}+ju_{pq}=R_p(i_{pd}+ji_{pq})+\frac{\partial(\lambda_{pd}+j\lambda_{pq})}{dt}+j\omega_p\,(\lambda_{pd}+j\lambda_{pq}) \tag{6.7}$$

or resolving further into the corresponding d-q components as:

$$u_{pd}=R_pi_{pd}+\frac{d\lambda_{pd}}{dt}-\omega_p\lambda_{pq} \tag{6.8}$$

$$u_{pq}=R_pi_{pq}+\frac{d\lambda_{pq}}{dt}+\omega_p\lambda_{pd} \tag{6.9}$$

Substituting for (6.8) and (6.9) and rearranging the Q expression of (6.6) one obtains:

$$Q=\frac{3}{2}\left[\underbrace{\left(R_p\,i_{pq}+\frac{d\lambda_{pq}}{dt}+\omega_p\lambda_{pd}\right)}_{u_{pq}}i_{pd}-\underbrace{\left(R_p\,i_{pd}+\frac{d\lambda_{pd}}{dt}-\omega_p\lambda_{pq}\right)}_{u_{pd}}i_{pq}\right] \tag{6.10}$$

The general steady-state equation of (6.10) then becomes:

$$Q=\frac{3}{2}\omega_p(\lambda_{pd}i_{pd}+\lambda_{pq}i_{pq}) \tag{6.11}$$

or in FOC form, bearing in mind the fundamental assumptions in (6.1), it can be written as:

$$Q_{foc}=\frac{3}{2}\omega_p\lambda_{pd}i_{pd}=\frac{3}{2}\omega_p\lambda_pi_{pd} \tag{6.12}$$

Hence, a linear relationship clearly does exist between the reactive power and primary current i_{pd}, which is in turn nearly proportional to the controllable i_{sd} counterpart through the FOC equivalent of (2.3), $\lambda_p = L_p i_{pd} + L_m i_{sd} \approx$ *const* (by the primary winding grid-connection at fixed line frequency, ω_p). The reactive power loop can therefore be conceptually drawn as:

$$i_{sd}^* \approx i_{pd} = PI(Q^* - Q) \tag{6.13}$$

The use of PI controller in (6.13) is therefore more than justified by the above observations. This approach does not require any parameters knowledge as all the inaccuracies or unknown variations of parameters should be effectively taken care of by appropriate tuning of PI gains Fig. 6.4.

6.4.2 Speed Controller Design

Speed control principles are virtually the same as with Vector Control (VC) strategy described in Chapter 5.The essential mechanical torque equation using standard notation is:

$$T_e = J \frac{d\omega_r}{dt} + B\omega_r + T_L \tag{6.14}$$

where the electro-magnetic torque of the BDFRG with p_r rotor poles, using the rotating frame dq components in the respective frames (i.e. the primary quantities in ω_p frame, and the secondary counterparts in $\omega_s = p_r \omega_{rm} - \omega_p$ frame), can be generally expressed as:

$$T_e = \frac{3 P_r L_m}{2 L_p} \left(\lambda_{pd} i_{sq} + \lambda_{pq} i_{sd} \right) \tag{6.15}$$

The FOC form of (6.15), considering the (6.1) conditions i.e. $\lambda_{pq} = 0$, is therefore:

$$T_e = \frac{3P_r L_m}{2L_p}\lambda_{pd}i_{sq} = \frac{3P_r L_m}{2L_p}\lambda_p i_{sq} \tag{6.16}$$

Given the above proportional relationship, the PI speed control law can be formulated as:

$$i_{sq}^* \sim T_e = PI\,(\omega_r^* \text{-} \omega_r) \tag{6.17}$$

One can conclude from (6.13) and (6.17) that under FOC, the d-axis currents are actually magnetizing in nature and responsible for flux production, while the respective q-axis components are torque/power producing and there is no cross coupling between the respective expressions (unlike vector control). Actually, control variables are the dq secondary currents, the primary counterparts having complementary consequential effects. Using the secondary voltage equation (2.2) in Chapter 2, simple PI control can be shown to be also applicable to the individual d-q current loops of the torque/power controller, which can be structurally represented in a similar fashion to Q and speed:

$$u_{sd}^* = PI\,(i_{sd}^* \text{-} i_{sd}) \tag{6.18}$$

$$u_{sq}^* = PI\,(i_{sq}^* \text{-} i_{sq}) \tag{6.19}$$

The generic parameter independent configuration of the entire speed controller for healthy (normal) operating conditions is shown in Fig. 6.5. This arrangement is versatile and can be used for both FOC and primary voltage-oriented (vector) control (VC) elaborated in Chapter 5.
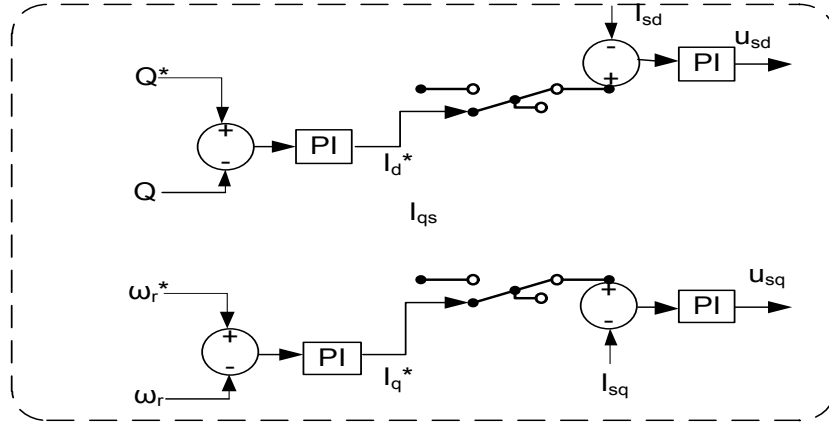
Figure 6.4: FOC (VC) arhitecture for normal variable speed operation of the BDFRG.

6.5   Analysis of BDFRG Symmetrical Faults

Large wind generators in a MW range have negligible winding resistances and in this sense the considered 2 MW BDFRG is not an exception according to the resistance values in Table 4.2. Ignoring R_p for simulation and practical studies is therefore a valid and very common approximation, and especially at the power system level. In this case, the FOC forms of (6.8) and (6.9) in steady-state can be simplified to:

$$u_{pd} \approx -\omega_p \lambda_{pq} = 0 \tag{6.20}$$

$$u_{pq} \approx \omega_p \lambda_{pd} = \omega_p \lambda_p \tag{6.21}$$

The corresponding power relationships (6.6)in the fault voltage and current terms can be written as:

$$P = \frac{3}{2} \left(u_{pd} i_{pd} + u_{pq} i_{pq} \right) \approx \frac{3}{2} u_p i_{pq} \tag{6.22}$$

$$Q = \frac{3}{2}\left(u_{pq}i_{pd} - u_{pd}i_{pq}\right) \approx \frac{3}{2}u_p i_{pd} \tag{6.23}$$
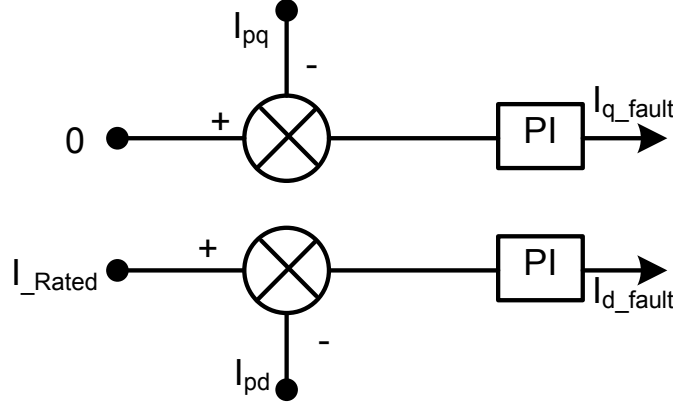
Figure 6.5: Desired primary current magnitudes and the corresponding secondary current references for maximum reactive power injection during fault occurrence.

Therefore, by analogy to the normal FOC, P is also determined by the i_{pq} and Q by the i_{pd} during the fault for a given voltage sag magnitude, u_p. The primary qd currents are regulated indirectly through the proportional and controllable i_{sq} and i_{sd} variations, so that the respective P and Q responses satisfy the grid code requirements as specified in Fig.6.1. In order to maximise the Q support from the grid for faster voltage recovery in the network, the primary winding side should behave as close as possible to an ideal capacitor, which means that most (if not all) of the primary current should be made reactive in nature. In other words, the power producing secondary i_{sq} component should be controlled so that $i_{pq}=0$, and the complementary magnetizing i_{sd} in a manner to ensure that the i_{pd} counterpart is rated. The outputs of the primary current PI control loops in Fig. 6.5 represent the desired reference values, i_{q_fault} and $i_{d\_fault,}$ to achieve this objective. Although the controller in Fig. 6.6 has to operate in power (i.e. open-loop speed) mode in this case, the rotor speed is unlikely to change much in a short 200ms fault interval

anyway by the heavy inertia of the 2MW turbine drive shaft. This conjecture will be confirmed by the simulation studies in the next section.
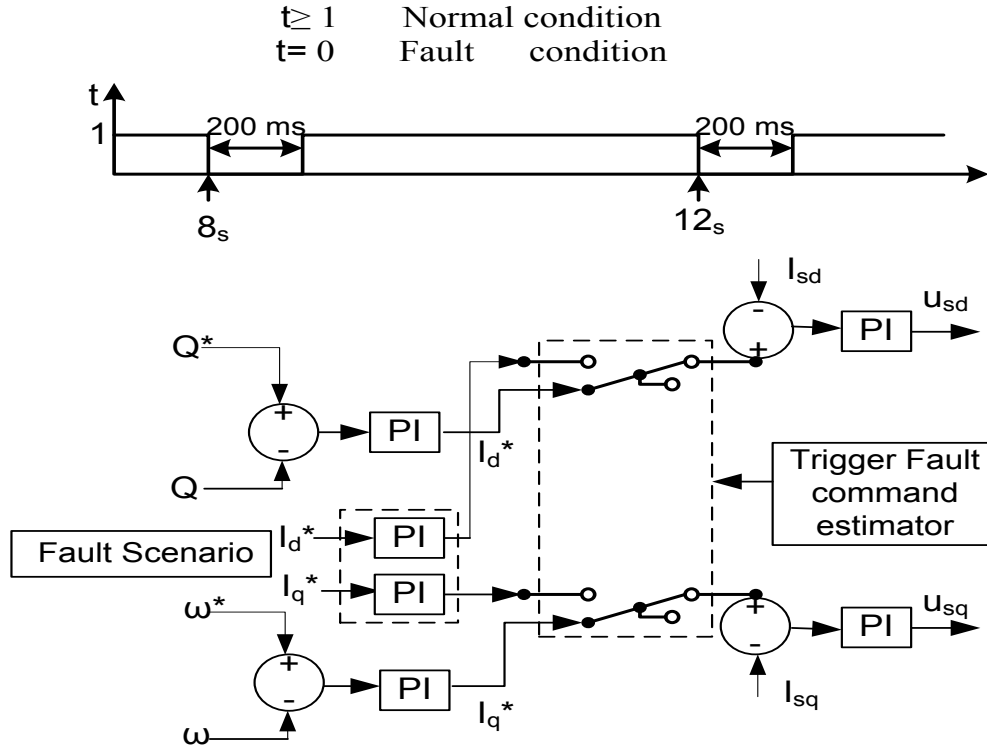
Figure 6.6: Simulated FOC strategy with a control selector for normal or faulty BDFRG operation

The variable currents used in the measurement drawing the final shape change of the electrical quantity during the fault interval. Actual active and reactive power will be extracted from the grid side the inner control loop adopted this operation responded to the fault command and the intersection loop addressing the validation of the low voltage ride through for BDFRG. The fault command demanded (timer), generate fault order(0,1),cooperating with 3 switching units installed according to their location in the source voltage, and other two switches installed

inboth control branches to trigger fault case as maintained in Fig. 6.7 to change the root of the supporting reactive power exclusively from $I^*_{sd}=I_{dfault}$and $I^*_{sq}= I_{qfault..}$

Terminal Voltage will be descended by 15% of the rated voltage the duration of fault limited to 200 ms. The machine performance in this period is responding to fault condition when the i_{dfault} and i_{qfault} start to inject reactive power to recover the voltge drop. The behaviour of machine during this period is our target of investigation. The requirement of network code was done by linking the first stage of controller to the primary side and starts to inject reactive power to recover power absence. In the second stage of the control unit, the secondary current will be present as usual in the meantime to build the appropriate voltagesu_{sd}, u_{sq}, cooperating with the injected fault currents, which is in this case considered as a secondary reference currents (I_{sd}^* I_{sq}^*), through (6.18) and (6.19).

6.6   Simulation Results

The BDFRG testing under normal and faulty conditions is a significant step to further understanding of the BDFRG behaviour and capability to recover fault challenge. One of the characters can be added as a positive feature is the BDFRG capability to handle the drop of voltage up to a 15% margin of rated voltage using grid code requirements.

2MWBDFRG forced under symmetrical fault, when main supply unit drop to 15% of rated voltage. The generator capability to ride through symmetrical fault has been evaluated under three-fault conditions; first operating procedure under the principles unsupported reactive power Q to assess the natural capability of BDFRG to ride through the fault based on the reference secondary currents $i^*_{sq}=0$, $i^*_{sd}=15$ % of rated current and Q=0. The second approach, following

the low voltage ride through requirements or (supported mode) when the $i^*_{sq}=0, i^*_{sd}=$rated

current,the reactive power in this case Q maximum supported. The third approach can be

implemented save mode behaviour of the BDFRG machine which is maintained as one superior

characteristic over rest cascade machine in fault condition by short circuiting the secondary

winding and bypassing the converter. The nominal grid voltage is 690 V L-L and rated voltage

is 563.4 V, DC-Link voltage is limited to 850 V. The BDFRG Running in variable speed at 900

rpm (e.g. super synchronous speed) and 600 rpm in sub-synchronous speed mode. The

symmetrical fault (drop in 3 Phase, voltage to 15% of the source voltage) will hit the system at

8s time instant when the machine acts in the super synchronous mode and second 12s in the

period of sub synchronous mode. The duration of the fault in both cases is 200 ms and the

clearance of the fault; depend on the taste circumstance, which the system faced.

The 3PH voltage drop is the main interest in this case presented in the primary side of the

machine and the behaviour of the machine, case unsupported reactive power Q=0 and the

second approach under supporting reactive power LVRT requirements when the reactive power

injected to the grid as Maximum .The last approach taking in account the advantage of the save

mode of the machine and the expected benefit of this mode in the same fault duration (200 ms).

6.6.1 Unsupported Mode Fault Condition

Figures 6.7-6.9 illustrate the complete control process starting as normal mode and triggered in

8s and 12sdepending on the machine mode. The normal control strategy built corresponding on

unity power factor requirements when i_{sd}=1830 A and i_{pd} = 0, i_{sq} has certain values depending

on the loaded condition (half loaded machine). In faulty period (200 ms) as un-supported

approach the rated voltage 563.4V and i_{sd} current dropped to 15%, then i_{sd}= 274 A, therefore, in

this condition the machine lacks support $Q \approx 0$, $i_{sq} = 0$ then the produced torque descended to zero this difference occurs between the electrical and mechanical torque cause the acceleration in the speed through duration fault in both super-sub synchronous mode.
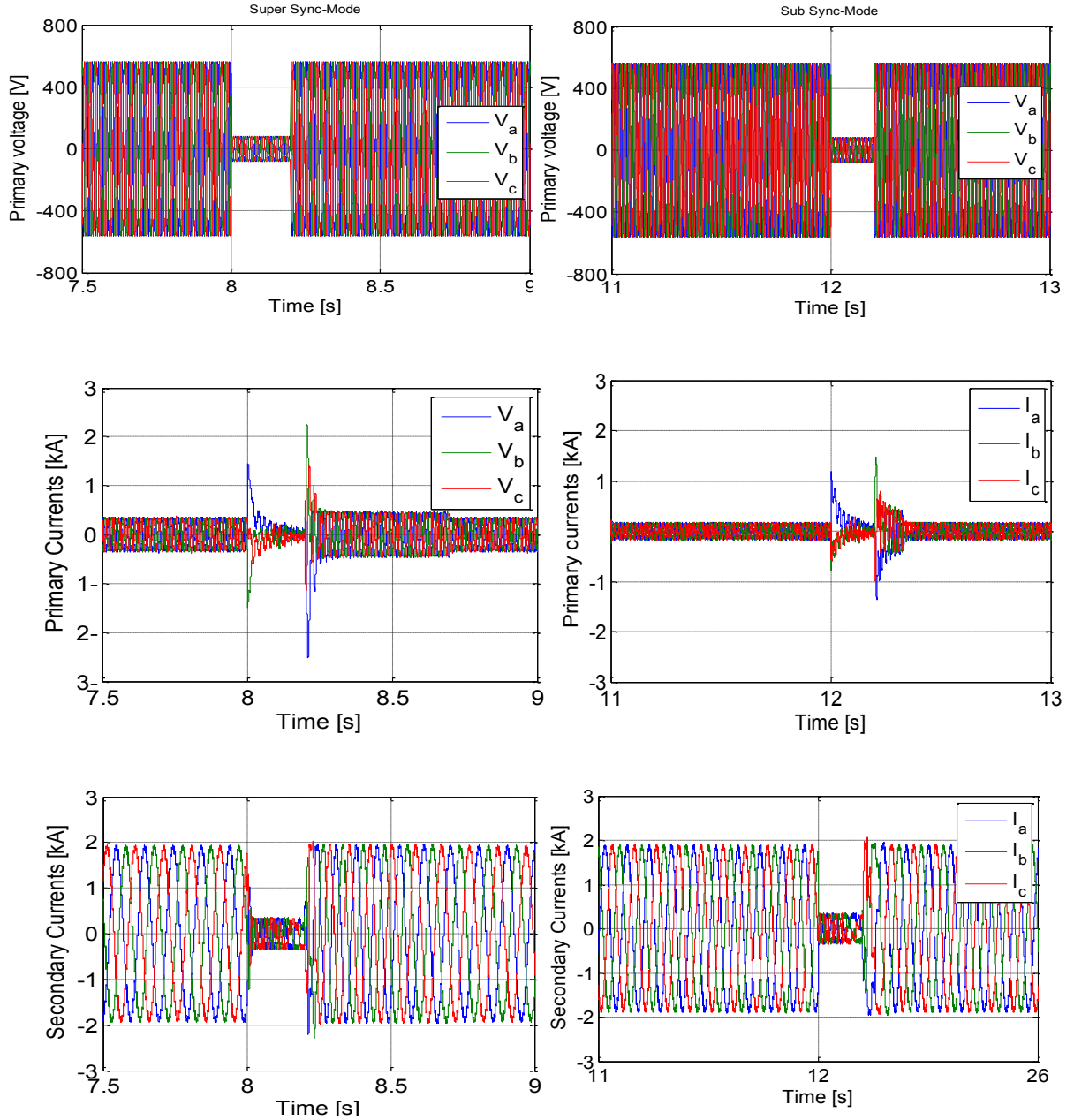
Figure 6.7: From the Top: Primary Voltage, primary current and secondary current in both sync-modes under symmetrical fault without injection reactive power.
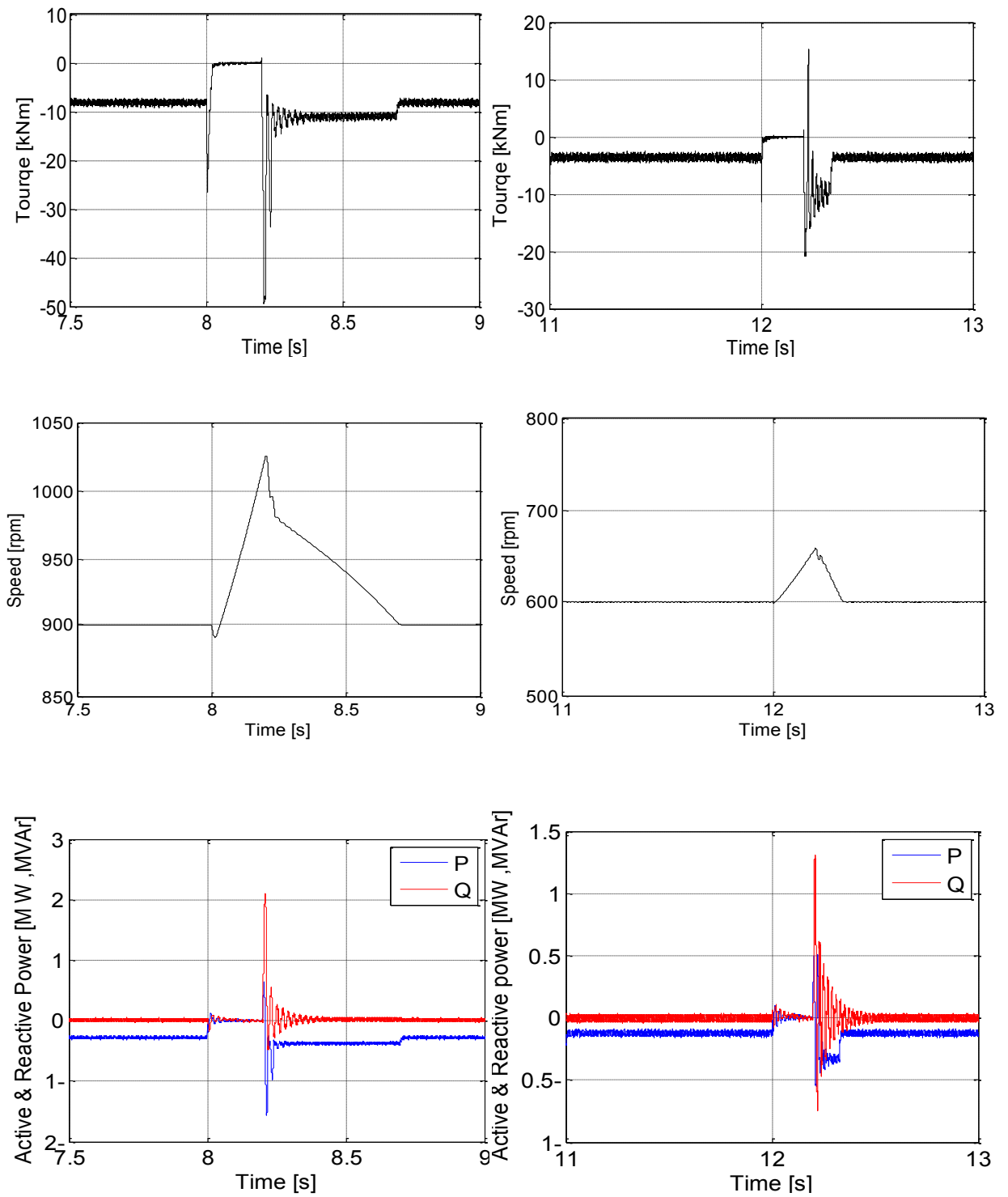
Figure 6.8: Torque, Speed, Active and reactive Power P, Q in both modes under symmetrical fault.
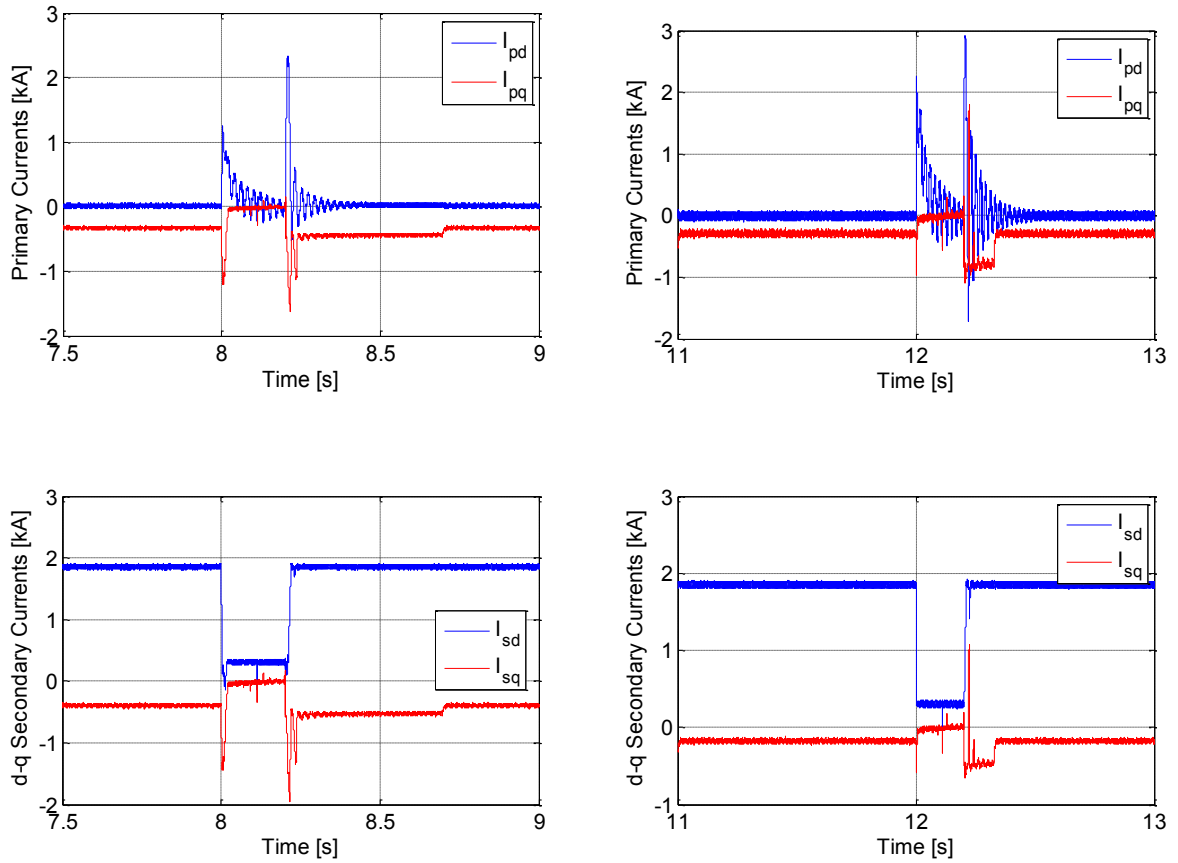
Figure 6.9: Primary and Secondary Currents both sync- modes under symmetrical Fault.

6.6.2 Fault under low voltage ride through requirements(supporting mode)

The second procedure applied is the LVFRT theory which is carried out under the E.ON

requirements and the following results extracted under the same control system, however, the

objective in this case is supporting reactive power to the grid under faulty command, to help the

system to recover the symmetrical fault. The changes in the behaviour of the control strategy is

the main aim to assess the machine capability to ride through symmetrical faults as depicted in

Figs. 6.10-12, as well as the machine capability under the fault occurrence.
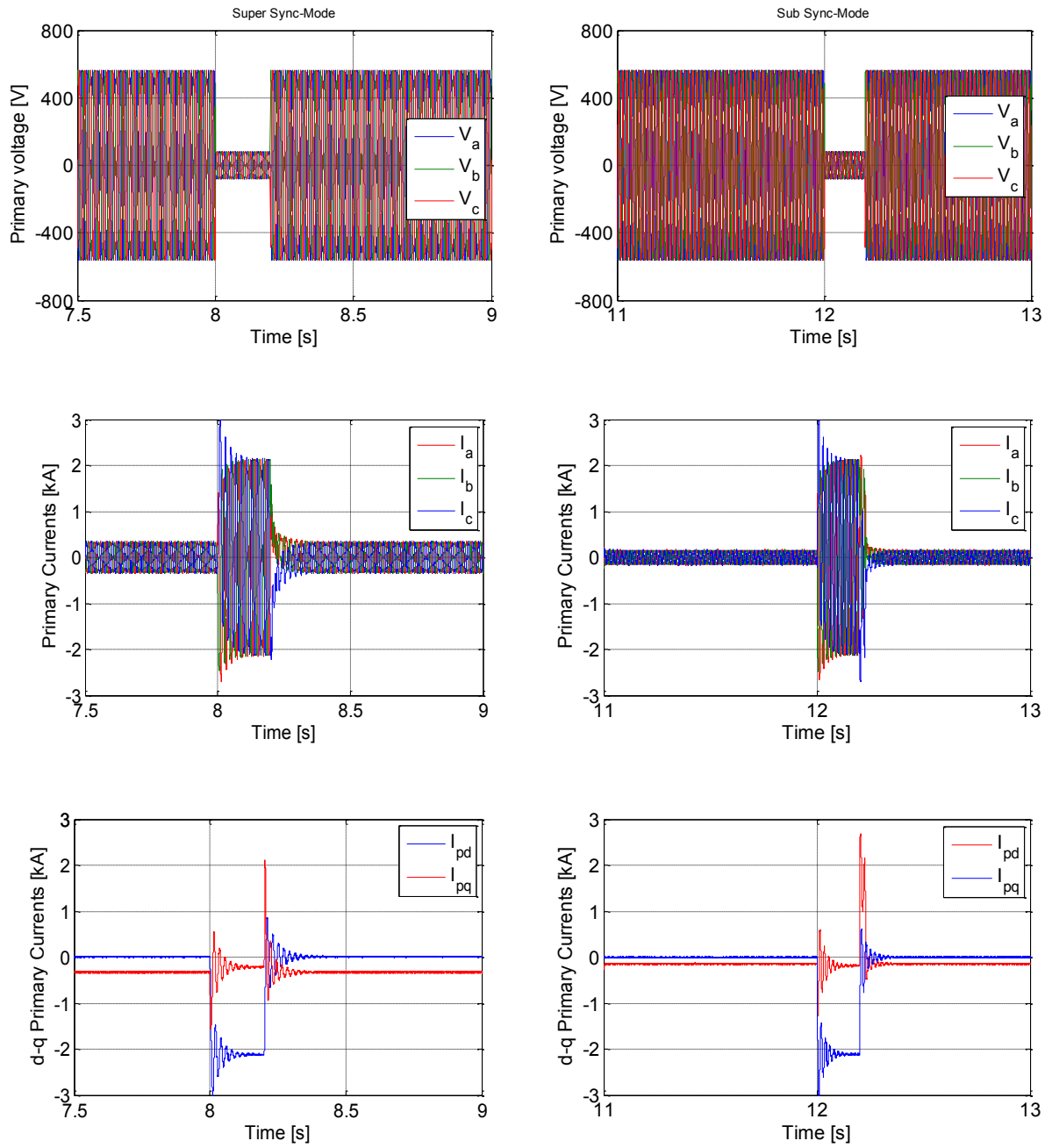
Figure 6.10: From the top: Primary Voltage, Primary & d-q primary currents under LVRT Condition.
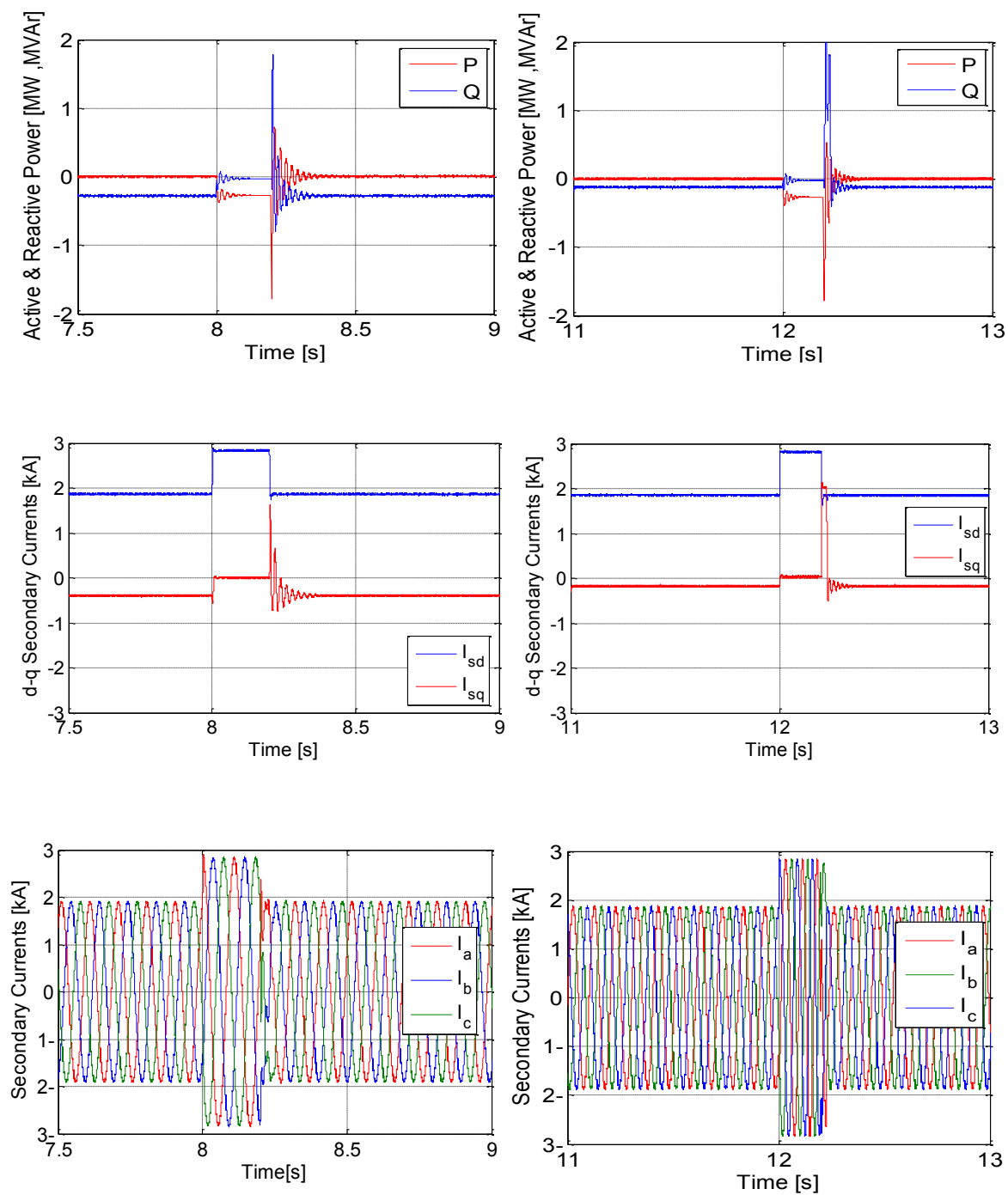
Figure 6.11: From the Top: PQ power,d-qSecondary Current, 3 ph Secondary Currents responded to LVRT Requirement.
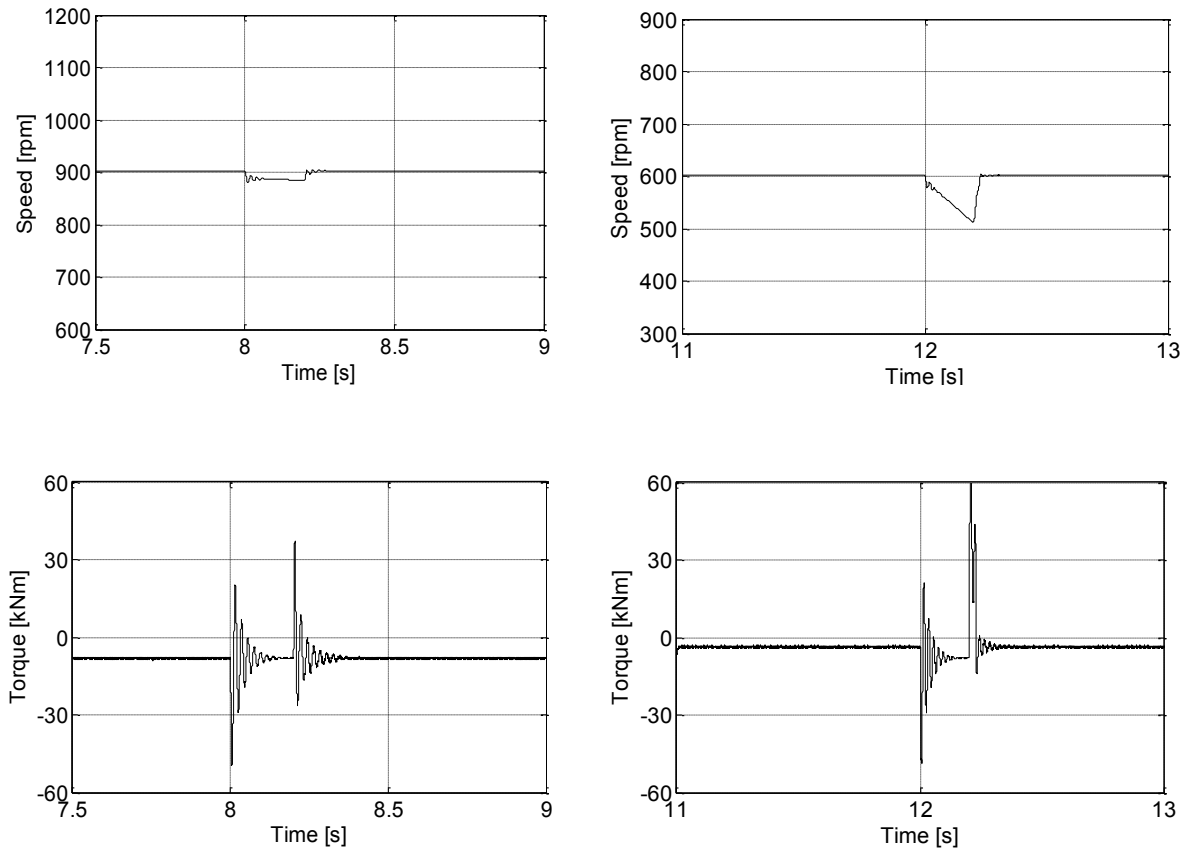
Figure 6.12 :Speed and Torque under LVFRT.

The fault ride through requires injection of maximum reactive power Q_{max}, where the i^*_{sq}=0 and i^*_{sd}= rated current which equal to 2830 A shown in Fig.6.11. This condition is applied when the primary voltage exposed to voltage sag about15% of rated voltage correspondence to grid code the trigger fault change the route of control to allow the fault unit to support reactive power proportional to i^*_{sd} =$i_{sdfault}$ to help the machine to recover the dip voltage in grid during fault duration. The results in Figs. 6.10-6.12 illustrate the capability of the BDFRG to act in accordance with this aforementioned operating procedure consequently. The reference current $i_{sdfault}$=2830 A injected though the fault period, where certain negative reactive power Q appear in the primary side as injecting power to the grid, as well as i_{pd} current through the primary side

appears in Fig. 6.11and the secondary currents are maximized Fig. 6.12. The torque in this section not match 0 as expected, even when i_{sq}= 0 due to many reasons such the half loaded machine, the applied inertia further than the coupling issue between d-q secondary currents related to the similarity in behaviour between the FOC and VC, which allow i_{sd} to take role and develop transient torque Fig.6.12, and speed in both mode machine differs from controlled speed. The smooth behaviour of the control operation and the ability to inject the reactive power requirement is considered a real success for BDFRG machine to ride through the symmetrical fault.

6.6.3 The Fault under Save Mode Condition

One of advantages of brushless doubly fed reluctance machine(BDFRM) over other cascade machine is the ability to protect the machine from the voltage sag and transient disturbance , using the failed save mode by short circuiting the secondary side of the machine and operate as an induction machine. This mode operation utilized through lab works as start mode to avoid overloading inverter in transition situation by by-passing the inverter setting (i.e., operating sector as 000 or 111). Implementation the same procedure of fault with bypassing the inverter in the same fault duration time (200 ms) considers the back-up protection to protect the secondary side of the machine as well. Actually the system is not injected any reactive power through fault duration, there is only one action done through this period by isolating the inverter when the rated voltage drop to 15%, occur then secondary voltage u_{sd}, u_{sq} switched to zero.

The magnitude of primary and secondary currents in save limit as shown in Fig.6. 13-14, and short circuiting the secondary winding are avoiding overloaded the inverter that's prove the

validation of the save mode to substitute the complicated solution for sudden dip voltage in the

grade side machine and using crowbar less save mode.
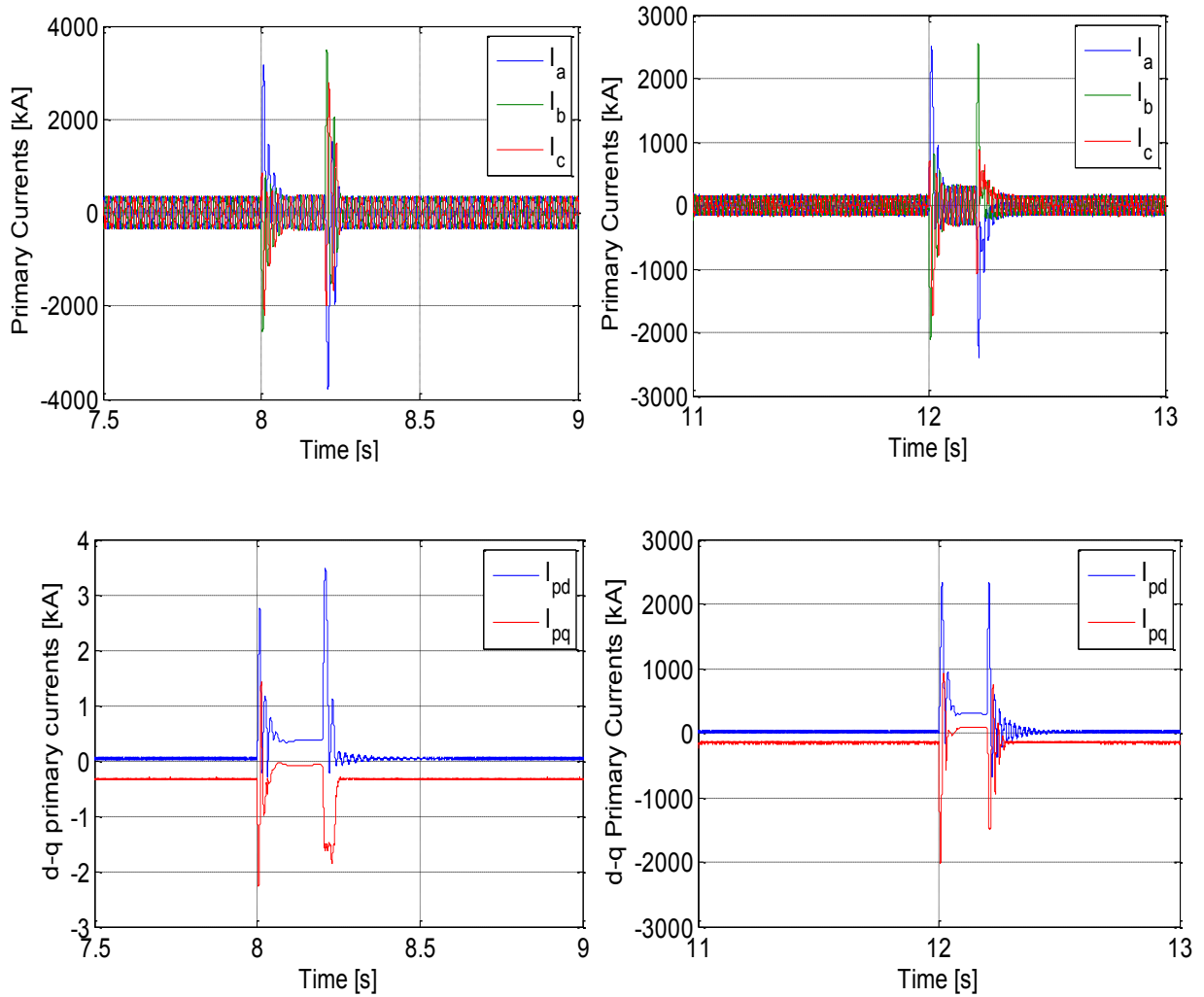
Figure 6.13 : The primary currents under save mode condition.
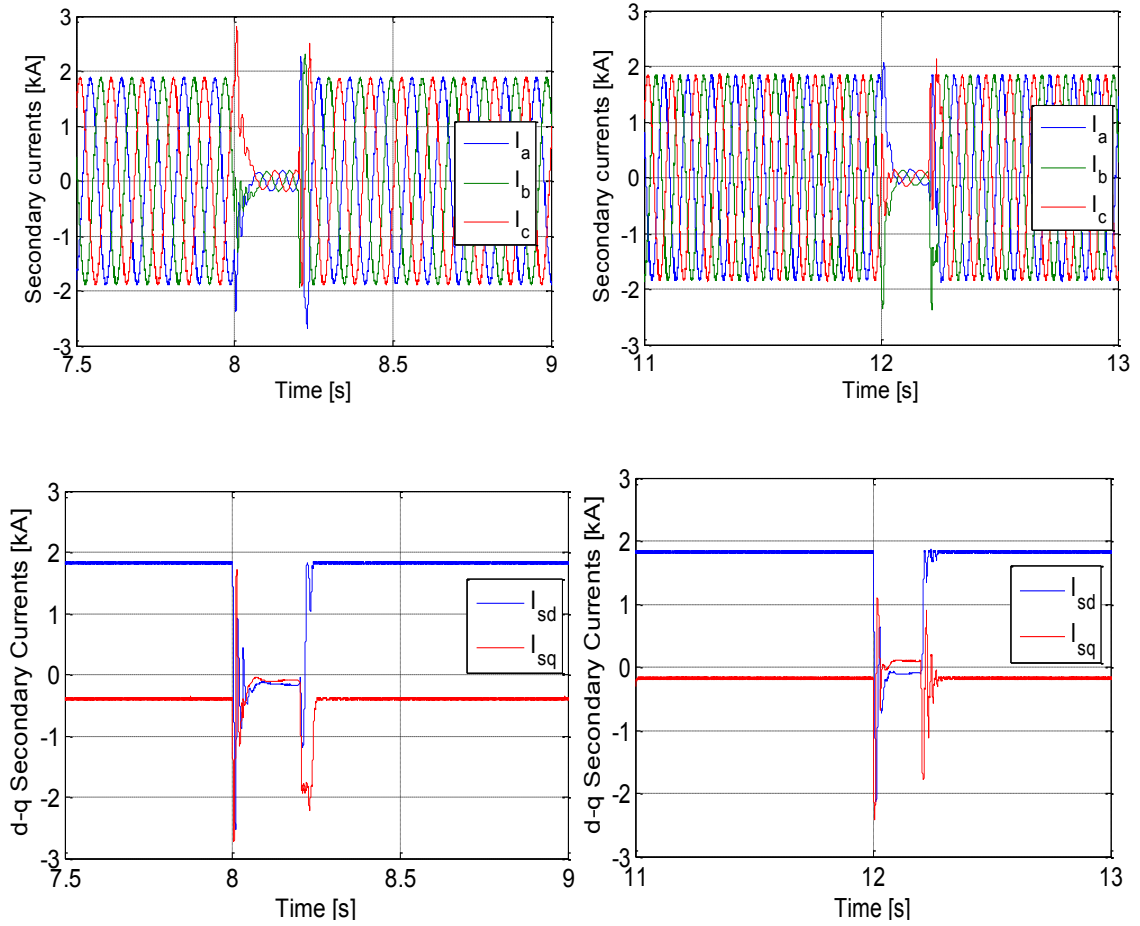
Figure 6.14: The secondary current magnitudes based failed save mode.

6.7   Conclusions

The result present three procedures without and with LVRTH requirements (case symmetrical fault) reflects the stability of the control method that adopted FOC strategy unity power factor in normal control condition when the Q= 0 and i_{sd} max. The BDFRG is reacting confidently to recover the Grid disturbance and promise protected future work in practical applications, as a machine which readily assents to control theories. Depending on the gained results from simulation models, there is an obtainable analysis for susceptibility of the machine to ride through symmetric fault can be presented according to the data variability through the fault duration.

- The first procedure (unsupported mode) reflect the behaviour of system under condition Q=0 and the rated voltage and i_{sd} current dropped to 15% its worst scenario can be achieved in fault period due lack compensating reactive power Fig.6. 7-6.9.

- The second procedure reflect low voltage ride through requirement which justify the supporting mode when the system inject reactive power through fault duration to enhance the correlation relationship between the machine and grid .In this case the $i_{sd}=i_{rated}$,$i_{sq}=0$ the system effectively inject marked negative reactive power to the grid shown in Figs. 6.10-6.12. The machine in this mode responded to LVRT requirements successfully without any extended devices like crowbar resistance comparing with DFIG under same fault condition. The transient speed is obviously lower than unsupported mode. The LVRT in this project reflect maximum injection reactive power supported to the grid and their ability to support lower reactive power according to fault nature. The

primary power even with full injection reactive power not exceeded over the rated current. All this advantages prove the capability the BDFRG of the control strategy based grid code requirement to ride through the fault.

- The brushless doubly feed reluctance machine BDFRM has already inherited save mode when the secondary winding short-circuited Fig. 6.13 to behave like conventional induction machines. The adopting save mode with BDFRG record advantage over DFIG when its action in fault duration not require crowbar resistance

Chapter 7 **Conclusions and Perspective**

This research work through the deferent stage has allowed accomplishing a number of primaries objectives in line with the project plane including:

Chapter 1 gave an overview of aims and contribution and The purpose of this project is to investigate, develop and compare scalar and vector control strategies for the BDFRM under healthy (considering both motoring and generating modes) and/or faulty (e.g. investigating fault-ride-through capabilities of the machine in generating regime) operating conditions. The target variable speed applications to be considered are large pump-alike drives and grid-connected wind turbines. The developed control algorithms will be first examined by computer simulation followed by experimental verification on the existing test rig based on a small-scale BDFRM prototype in the power.

Chapter 2 presents critical reviews of the key papers published on BDFRM with particular attention on the control related work and performance analysis. Aspects related to the machine construction, main properties (e.g. advantages and limitations), fundamental principles of operation and dynamic modelling, as well as space-vector steady-state equations have been co

Chapter 3 is concerned with the experimental work using dSPACE development platform for rapid control prototyping. The results for the BDFRM in motoring and generating operating modes under variable speed and/or loading conditions with scalar control real-time implementation of the MTPIA strategy have been presented and discussed.

Chapter 4 outlines a new simulation study approach for a custom-designed large-scale BDFRG for wind turbines with MPPT.

Chapter 5describes in detail a vector control (VC) algorithm for bi-directional power converter (e.g. machine-side and grid-side bridges) followed by extensive simulation studies.

Chapter 6addresses issues related to low-voltage fault ride through performance and development of a dedicated control scheme. This kind of work is novel and has not been published for this particular machine.

Conclusion

This research work has presented a high performance digital Scalar Control controller for a 1.5kW axially laminated BDFRM. The SC controller was implemented in Matlab/Simulink. dSPACE control board was used as the compiler and interface between PC and other hardware components. It was experimentally shown to be capable and fast speed control over a range that is above and below synchronous speed under variable loading conditions. The Experimental work about open-loop control verifies the simulation results for BDFRM/G on the existing laboratory test rig for target application which proves the capability and robustness of the scalar control based on RTI to have a competitive performance similar to other high performance strategies such as Vector Control and Field Oriented Control. It has been proven that the highest efficiency can be obtained under the MTPIA conditions which can be derived from the nameplate data of a machine without any need for parameter knowledge or off-line testing procedures. Such properties should make the developed low-cost controller very attractive for commercialisation and, given its versatility and inherent robustness, may lead to its potentially wider use for any doubly-fed machine, foremost a conventional doubly-fed slip ring induction machine (DFIM), in low to medium performance applications where only the steady-state operation, and not fast transient response, is of major concern.

Second trend was to evaluate the capability of large scale BDFRG to follow the sudden change in turbine side based scalar and FOC strategy on WECS. The obtained results were very promising, since they have shown a very high tracking performance on the two control strategies considered for the large scaled system under the influence of the WECS emulation.The research Value comes from large scale machine capacity to produce large renewable energy in variable speed condition and under non linearity of wind front velocity .the parameter of the large scale turbine and BDFRG developed under extent investigation of the theoretical and off-line data used in experimental work for small scale machine and finite-element design of 2MW BDFRG (Dr Dorel).Remarkable success in the control algorithms over these large scale generators would have a significant impact on the nature of future research, which is planning to design large plants, taking advantage of the competitive aspects provided by BDFRG.

Finally, a thorough investigation of LVFRT capabilities of the BDFRM and comparisons with DFIG for symmetrical faults have been detailed under the development of the respective field-oriented control approach (including dedicated converter configuration) and preliminary performance analysis of the entire system, using computer simulations in order to support the capability of the machine to ride through the voltage grid sag. The deep investigation which is already done in this thesis about the faulty side or response of the BDFRG in faulty condition will enhanced the machine performance and increase experimental work under this requirements satisfying from the positive reaction of machine in deferent fault condition especially in case LVRT capability when the machine is capable to support amount of reactive power to the grid along fault duration.

Future Work

- Assessment of the performance SC in grid healthy condition and different WECS practise scenarios especially in case of use open loop algorithms as boost system or back up protection control cooperating with for high performance control algorithms as VC or FOC.

- Study of the obtained results and production of proper comparison reports, focusing on the advantages can be achieved from each control strategy under variable speed condition. The cost and stiffest of the SC with the accuracy and high performance of VC Should integrated and take advantage to overcome negatives that occur in the BDFRM/G behaviours and control system as a while.

- The fault Conditions are the concerning challenges that arise from the up normal work of the grid, reduce the degree of machine performance. So the practical test for low voltage ride through capability and grid code circumstance for the BDFRG under the appropriate control can give impressive results can machine offered to network through the fault period. The Experimental Fault Rid through Capability evolution of BDFRG performance with emulation grid fault to evaluate the success obtained in simulation study (chapter 6) recommended as a superior advantage of doubly feed reluctance machine over DFIG and other CIM.

- Integration and test of crowbar and fault emulate with DFIG/BDFRG test rigs, can develop the performance and the cooperating work between the DFIG farms and BDFRG in case optimal grid code connection.

References

[1]   L. Haiyan, K. Yanli, F. Chuanglin, and L. Maoxun, "Wind energy resources exploitation and large-scale, non-grid-connection wind-powered industrial bases, construction in China Northwest Territories," in *World Non-Grid-Connected Wind Power and Energy Conference, 2009. WNWEC 2009*, 2009, pp. 1-5.

[2]   E. Lerch, "Storage of fluctuating wind energy," in *Power Electronics and Applications, 2007 European Conference on*, 2007, pp. 1-8.

[3]   S. White, "Germany scraps nucleare power after Fukushima disaster," in *Daily Mirror*, 2011.

[4]   H. Louie and K. Strunz, "Energy market-integrative wind plant modeling for wind plant integration economic analysis," in *Power and Energy Society General Meeting - Conversion and Delivery of Electrical Energy in the 21st Century, 2008 IEEE*, 2008, pp. 1-8.

[5]   J. C. Saenz-Diez Muro, J. M. Blanco Barrero, E. Jimenez Macias, J. Blanco Fernandez, and M. Perez de la Parte, "Optimization of power generation from small wind energy in buildings through modular wind collector for cornice© for capturing and amplification of the vertical wind component," in *Clean Electrical Power (ICCEP), 2011 International Conference on*, pp. 609-613.

[6]   L. Ming-Shun, C. Chung-Liang, L. Wei-Jen, and W. Li, "Combining the Wind Power Generation System with Energy Storage Equipments," in *Industry Applications Society Annual Meeting, 2008. IAS '08. IEEE*, 2008, pp. 1-6.

[7]   P. J. Musgrove, "Wind energy conversionÃ‚Â¿an introduction," *Physical Science, Measurement and Instrumentation, Management and Education - Reviews, IEE Proceedings A,* vol. 130, pp. 506-516, 1983.

[8]   J. P. da Costa, H. Pinheiro, T. Degner, and G. Arnold, "Robust Controller for DFIGs of Grid-Connected Wind Turbines," *Industrial Electronics, IEEE Transactions on,* vol. 58, pp. 4023-4038.

[9]   N. Arthur, J. Penman, A. McLean, and A. Parsons, "Induction machine condition monitoring with higher order spectra. II. Variable frequency operation and automated diagnosis," in *Industrial Electronics Society, 1998. IECON '98. Proceedings of the 24th Annual Conference of the IEEE*, 1998, pp. 1895-1900 vol.3.

[10]   Y. Li, K. J. Bradley, P. Sewell, and D. Gerada, "Cascaded doubly fed induction machine system modelling based on Dynamic Reluctance Mesh modelling method," in *Electrical Machines, 2008. ICEM 2008. 18th International Conference on*, 2008, pp. 1-5.

[11]   E. M. Schulz and R. E. Betz, "Use of Doubly Fed Reluctance Machines in Wind Power Generation," in *Power Electronics and Motion Control Conference, 2006. EPE-PEMC 2006. 12th International*, 2006, pp. 1901-1906.

[12]   D. G. Dorrell and M. Jovanovic, "On the Possibilities of Using a Brushless Doubly-Fed Reluctance Generator in a 2 MW Wind Turbine," in *Industry Applications Society Annual Meeting, 2008. IAS '08. IEEE*, 2008, pp. 1-8.

[13]   S. Ademi and M. Jovanovic, "High-efficiency control of brushless doubly-fed machines for wind turbines and pump drives," *Energy Conversion and Management,* vol. 81, pp. 120-132.

[14]   M. G. Jovanovic, J. Yu, and E. Levi, "A review of control methods for brushless doubly-fed reluctance machines," in *Power Electronics, Machines and Drives, 2002. International Conference on (Conf. Publ. No. 487)*, 2002, pp. 528-533.

[15]   M. Figueiredo, R. Santos-Tavares, E. Santin, J. Ferreira, G. Evans, and J. Goes, "A Two-Stage Fully Differential Inverter-Based Self-Biased CMOS Amplifier With High Efficiency," *Circuits and Systems I: Regular Papers, IEEE Transactions on,* vol. 58, pp. 1591-1603.

[16]   R. E. Betz and M. G. Jovanovic, "The brushless doubly fed reluctance machine and the synchronous reluctance machine-a comparison," *Industry Applications, IEEE Transactions on,* vol. 36, pp. 1103-1110, 2000.

[17]   W. Fengxiang, Z. Fengge, and X. Longya, "Parameter and performance comparison of doubly-fed brushless machine with cage and reluctance rotors," in *Industry Applications Conference, 2000. Conference Record of the 2000 IEEE*, 2000, pp. 539-544 vol.1.

[18]   M. G. Jovanovic, "Power factor and inverter rating. A compromise in doubly fed reluctance machine drives," in *Power Electronics and Variable Speed Drives, 2000. Eighth International Conference on (IEE Conf. Publ. No. 475)*, 2000, pp. 311-316.

[19]   F. Valenciaga, "Active and reactive power control of a brushless doubly fed reluctance machine using high order sliding modes," in *Electrical Machines, 2008. ICEM 2008. 18th International Conference on*, 2008, pp. 1-6.

[20]   M. G. Jovanovic, R. E. Betz, and Y. Jian, "The use of doubly fed reluctance machines for large pumps and wind turbines," in *Industry Applications Conference, 2001. Thirty-Sixth IAS Annual Meeting. Conference Record of the 2001 IEEE*, 2001, pp. 2318-2325 vol.4.

[21]   W. K. Song and D. G. Dorrell, "Improved Direct Torque Control method of brushless doubly-fed reluctance machines for wind turbine," in *Industrial Electronics (ISIE), 2013 IEEE International Symposium on*, pp. 1-5.

[22]   L. Ji and X. Yang, "Optimization design on salient pole rotor of BDFRM using the Taguchi method," in *Power Electronics Systems and Applications (PESA), 2011 4th International Conference on*, pp. 1-4.

[23]   M. Jovanovic and R. E. Betz, "Optimal performance of brushless doubly fed reluctance machines," in *Electrical Machines and Drives, 1999. Ninth International Conference on (Conf. Publ. No. 468)*, 1999, pp. 386-390.

[24]   H. Chaal and M. Jovanovic, "Direct Power Control of Brushless Doubly-Fed Reluctance Machines," in *Power Electronics, Machines and Drives (PEMD 2010), 5th IET International Conference on*, pp. 1-6.

[25]   M. G. Jovanovic, R. E. Betz, Y. Jian, and E. Levi, "Aspects of vector and scalar control of brushless doubly fed reluctance machines," in *Power Electronics and Drive Systems, 2001. Proceedings., 2001 4th IEEE International Conference on*, 2001, pp. 461-467 vol.2.

[26]   Z. Qian and L. Huijuan, "Comparative Study of Brushless Doubly Fed Machine with Different Rotor Structures Used in Wind Power Generation System," in *Power and Energy Engineering Conference (APPEEC), 2010 Asia-Pacific*, pp. 1-4.

[27]   F. Valenciaga and P. F. Puleston, "Variable Structure Control of a Wind Energy Conversion System Based on a Brushless Doubly Fed Reluctance Generator," *Energy Conversion, IEEE Transactions on,* vol. 22, pp. 499-506, 2007.

[28]   X. Longya and W. Fengxiang, "Comparative study of magnetic coupling for a doubly fed brushless machine with reluctance and cage rotors," in *Industry Applications Conference, 1997. Thirty-Second IAS Annual Meeting, IAS '97., Conference Record of the 1997 IEEE*, 1997, pp. 326-332 vol.1.

[29]   P. F. Wang, "Design and Performance of Wind Power Generators," 2011.

[30]   R. E. B. M.G.JOVANOVIC, "Introduction to space vector Modeling of the Brushless Doubly fed Reluctance machine," p. 25, 2003.

[31]   H. Chaal and M. Jovanovic, "Flux observer algorithms for direct torque control of Brushless Doubly-Fed Reluctance machines," in *Industrial Electronics, 2009. IECON '09. 35th Annual Conference of IEEE*, 2009, pp. 4440-4445.

[32] M. G. Jovanovic and D. G. Dorrell, "Sensorless Control of Brushless Doubly-Fed Reluctance Machines using an Angular Velocity Observer," in *Power Electronics and Drive Systems, 2007. PEDS '07. 7th International Conference on*, 2007, pp. 717-724.

[33] L. Shuhui and T. A. Haskew, "Analysis of Decoupled d-q Vector Control in DFIG Back-to-Back PWM Converter," in *Power Engineering Society General Meeting, 2007. IEEE*, 2007, pp. 1-7.

[34] D. d. atkinson, "Electrical Drive," n. university, Ed., 2010.

[35] M. G. Jovanovic, "Brushless doubly fed reluctance machines for low cost variable speed drives," in *Power Electronics and Motion Control Conference, 2000. Proceedings. IPEMC 2000. The Third International*, 2000, pp. 1236-1241 vol.3.

[36] E. Muljadi, C. P. Butterfield, J. Chacon, and H. Romanowitz, "Power quality aspects in a wind power plant," in *Power Engineering Society General Meeting, 2006. IEEE*, 2006, p. 8 pp.

[37] Z. Ying and L. Hongyan, "Evaluation on comprehensive benefit of wind power generation and utilization of wind energy," in *Software Engineering and Service Science (ICSESS), 2012 IEEE 3rd International Conference on*, pp. 635-638.

[38] G. Roy and G.-e. April, "Direct frequency changer operation under a new scalar control algorithm," *Power Electronics, IEEE Transactions on,* vol. 6, pp. 100-107, 1991.

[39] S. Ademi and M. Jovanovic, "Vector control strategies for brushless doubly-fed reluctance wind generators," in *Environment Friendly Energies and Applications (EFEA), 2012 2nd International Symposium on*, pp. 44-49.

[40] X. Longya, Z. Li, and K. Eel-Hwan, "Field-orientation control of a doubly excited brushless reluctance machine," *Industry Applications, IEEE Transactions on,* vol. 34, pp. 148-155, 1998.

[41] A. Nikolic and B. Jeftenic, "Direct torque control and virtual-flux based direct power control of current source converter in wind turbine application," in *Power Electronics and Applications (EPE 2011), Proceedings of the 2011-14th European Conference on*, pp. 1-10.

[42] H. Jiefeng, Z. Jianguo, Z. Yongchang, G. Platt, M. Qishuang, and D. G. Dorrell, "Predictive Direct Virtual Torque and Power Control of Doubly Fed Induction Generators for Fast and Smooth Grid Synchronization and Flexible Power Regulation," *Power Electronics, IEEE Transactions on,* vol. 28, pp. 3182-3194.

[43] L. Qian and K. Hameyer, "A direct torque and reactive power control approach for doubly fed induction generator in wind turbine applications," in *Electrical Machines (ICEM), 2012 XXth International Conference on*, pp. 804-809.

[44] G. Escobar, A. M. Stankovic, J. M. Carrasco, E. Galvan, and R. Ortega, "Analysis and design of direct power control (DPC) for a three phase synchronous rectifier via output regulation subspaces," *Power Electronics, IEEE Transactions on,* vol. 18, pp. 823-830, 2003.

[45] B. Beltran, T. Ahmed-Ali, and M. E. H. Benbouzid, "Sliding Mode Power Control of Variable-Speed Wind Energy Conversion Systems," *Energy Conversion, IEEE Transactions on,* vol. 23, pp. 551-558, 2008.

[46] H. Kamrani, A. Ebrahimnejad, and N. Kohan, "Time Hopping Multiple input-Multiple output (TH-MIMO) systems," in *Engineering and Industries (ICEI), 2011 International Conference on*, pp. 1-4.

[47] H. Ambrose and Z. Qu, "Model reference robust control for MIMO systems," in *American Control Conference, 1997. Proceedings of the 1997*, 1997, pp. 345-349 vol.1.

[48] R. E. Betz and M. G. Jovanovic, "Theoretical analysis of control properties for the brushless doubly fed reluctance machine," *Energy Conversion, IEEE Transactions on,* vol. 17, pp. 332-339, 2002.

[49] Z. Zhiheng, W. Yi, L. Heming, and S. Xiaoqing, "Comparison of inertia control methods for DFIG-based wind turbines," in *ECCE Asia Downunder (ECCE Asia), 2013 IEEE*, pp. 960-964.

[50] M. Jovanovic, "Sensored and sensorless speed control methods for brushless doubly fed reluctance motors," *Electric Power Applications, IET,* vol. 3, pp. 503-513, 2009.

[51] W. Chen, F. Yang Rong, Y. Yu, L. Wang Gao, and G. Xu Dian, "A novel stability improvement method for V/F controlled induction motor drive systems," in *Electrical Machines and Systems, 2008. ICEMS 2008. International Conference on*, 2008, pp. 1073-1076.

[52] Y. Rongfeng, C. Wei, Y. Yong, and X. Dianguo, "Stability improvement of V/F controlled induction motor driver systems based on reactive current compensation," in *Electrical Machines and Systems, 2008. ICEMS 2008. International Conference on*, 2008, pp. 88-90.

[53] K. Sandeep kumar and K. Pritam satsangi, "Micro-controller based closed loop control of induction motor using V/F method," in *Information and Communication Technology in Electrical Sciences (ICTES 2007), 2007. ICTES. IET-UK International Conference on*, 2007, pp. 340-342.

[54] Z. Fengge, T. Ningze, W. Huijun, L. Wenjun, and W. Fengxiang, "Modeling and simulation of variable speed constant frequency wind power generation system with doubly fed brushless machine," in *Power System Technology, 2004. PowerCon 2004. 2004 International Conference on*, 2004, pp. 801-805 Vol.1.

[55] A. K. Jain and V. T. Ranganathan, "Modeling and Field Oriented Control of Salient Pole Wound Field Synchronous Machine in Stator Flux Coordinates," *Industrial Electronics, IEEE Transactions on,* vol. 58, pp. 960-970.

[56] L. Hui, W. Qingyi, D. Xin, and W. Shuyun, "A Novel V/f Scalar Controlled Induction Motor Drives with Compensation Based on Decoupled Stator Current," in *Industrial Technology, 2006. ICIT 2006. IEEE International Conference on*, 2006, pp. 1989-1994.

[57] J. M. Lazi, Z. Ibrahim, S. N. M. Isa, A. Anugerah, F. A. Patakor, and R. Mustafa, "Sensorless speed control of PMSM drives using dSPACE DS1103 board," in *Power and Energy (PECon), 2012 IEEE International Conference on*, pp. 922-927.

[58] R. Mohideen, "The implications of clean and renewable energy development for gender equality in poor communities in South Asia," in *Technology and Society in Asia (T&SA), 2012 IEEE Conference on*, pp. 1-6.

[59] H. Li and Z. Chen, "Overview of different wind generator systems and their comparisons," *Renewable Power Generation, IET,* vol. 2, pp. 123-138, 2008.

[60] J. W. Smith, J. A. Taylor, D. L. Brooks, and R. C. Dugan, "Interconnection studies for wind generation," in *Rural Electric Power Conference, 2004*, 2004, pp. C3-1-8.

[61] Y. Errami, M. Maaroufi, and M. Ouassaid, "Modelling and control strategy of PMSG based variable speed wind energy conversion system," in *Multimedia Computing and Systems (ICMCS), 2011 International Conference on*, pp. 1-6.

[62] Z. Han, Y. Cao, H. Jia, J. Wang, and l. Lu, "Analysis on and precautions against large-scale wind turbines off-grid," in *Advanced Power System Automation and Protection (APAP), 2011 International Conference on*, pp. 1974-1980.

[63] J. Zhenhua and Y. Xunwei, "Modeling and control of an integrated wind power generation and energy storage system," in *Power & Energy Society General Meeting, 2009. PES '09. IEEE*, 2009, pp. 1-8.

[64] M. H. Zamani, G. H. Riahy, and R. Z. Foroushani, "Introduction of a new index for evaluating the effect of wind dynamics on the power of variable speed wind turbines," in *Transmission and Distribution Conference and Exposition, 2008. T&D. IEEE/PES*, 2008, pp. 1-6.

[65] L. Chae-Wook, "A basic study on a nonlinear parameter of aerodynamic torque and a torque control method of wind turbine," in *Control, Automation and Systems (ICCAS), 2011 11th International Conference on*, pp. 979-980.

[66] N. Budisan, V. Groza, O. Prostean, I. Filip, M. Biriescu, I. Szeidert, and M. Stern, "Rotation Speed and Wind Speed Indirect Measurement Methods for the Control of Windmills with Fixed Blades Turbine," in *Instrumentation and Measurement Technology Conference Proceedings, 2008. IMTC 2008. IEEE*, 2008, pp. 912-916.

[67] M. B. C. Salles, K. Hameyer, J. R. Cardoso, and W. Freitas, "Dynamic analysis of wind turbines considering new grid code requirements," in *Electrical Machines, 2008. ICEM 2008. 18th International Conference on*, 2008, pp. 1-6.

[68] L. F. M. Gevaert, J. D. M. De Kooning, T. L. Vandoorn, J. Van de Vyver, and L. Vandevelde, "Evaluation of the MPPT performance in small wind turbines by estimating the tip-speed ratio," in *Power Engineering Conference (UPEC), 2013 48th International Universities'*, pp. 1-5.

[69] D. G. Dorrell, I. Scian, E. M. Schulz, R. B. Betz, and M. Jovanovic, "Electromagnetic Considerations in the Design of Doubly-Fed Reluctance Generators for use in Wind Turbines," in *IEEE Industrial Electronics, IECON 2006 - 32nd Annual Conference on*, 2006, pp. 4272-4277.

[70] A. J. Sguarezi Filho and E. Ruppert, "The complex controller applied to the induciton motor stator flux orientation control," in *Power Electronics Conference, 2009. COBEP '09. Brazilian*, 2009, pp. 130-137.

[71] R. E. Betz, R. Lagerquist, M. Jovanovic, T. J. E. Miller, and R. H. Middleton, "Control of synchronous reluctance machines," *Industry Applications, IEEE Transactions on,* vol. 29, pp. 1110-1122, 1993.

[72] E. Levi, "Improvements in operation of vector controlled induction machines by application of modified machine models," in *Advances in Control Systems for Electric Drives, IEE Colloquium on*, 1995, pp. 3/1-3/8.

[73] S. Wade, M. W. Dunnigan, and B. W. Williams, "Improving the accuracy of the rotor resistance estimate for vector-controlled induction machines," *Electric Power Applications, IEE Proceedings -,* vol. 144, pp. 285-294, 1997.

[74] D. Forchetti, G. Garcia, and M. I. Valla, "Vector control strategy for a doubly-fed stand-alone induction generator," in *IECON 02 [Industrial Electronics Society, IEEE 2002 28th Annual Conference of the]*, 2002, pp. 991-995 vol.2.

[75] X. Lie and W. Yi, "Dynamic Modeling and Control of DFIG-Based Wind Turbines Under Unbalanced Network Conditions," *Power Systems, IEEE Transactions on,* vol. 22, pp. 314-323, 2007.

[76] S. Shiyi, E. Abdi, F. Barati, and R. McMahon, "Stator-Flux-Oriented Vector Control for Brushless Doubly Fed Induction Generator," *Industrial Electronics, IEEE Transactions on,* vol. 56, pp. 4220-4228, 2009.

[77] C. B. Jacobina, E. R. C. Da Silva, A. M. N. Lima, and R. L. A. Ribeiro, "Vector and scalar control of a four switch three phase inverter," in *Industry Applications Conference, 1995. Thirtieth IAS Annual Meeting, IAS '95., Conference Record of the 1995 IEEE*, 1995, pp. 2422-2429 vol.3.

[78] Y. Deng-ke, X. Guo-Qing, H. Bo, X. An, and K. Jin-song, "Research on a novel SVPWM for three-phase VSI," in *Vehicle Power and Propulsion Conference, 2008. VPPC '08. IEEE*, 2008, pp. 1-5.

[79] R. Pena, J. C. Clare, and G. M. Asher, "Doubly fed induction generator using back-to-back PWM converters and its application to variable-speed wind-energy generation," *Electric Power Applications, IEE Proceedings -,* vol. 143, pp. 231-241, 1996.

[80] L. Chi-Seng, C. Wai-Hei, W. Man-Chung, and H. Ying-Duo, "Adaptive DC-Link Voltage-Controlled Hybrid Active Power Filters for Reactive Power Compensation," *Power Electronics, IEEE Transactions on,* vol. 27, pp. 1758-1772.

[81] L. Malesani, L. Rossetto, P. Tenti, and P. Tomasin, "AC/DC/AC PWM converter with reduced energy storage in the DC link," *Industry Applications, IEEE Transactions on,* vol. 31, pp. 287-292, 1995.

[82] J. S. Kim and S. K. Sul, "New control scheme for AC-DC-AC converter without DC link electrolytic capacitor," in *Power Electronics Specialists Conference, 1993. PESC '93 Record., 24th Annual IEEE*, 1993, pp. 300-306.

[83] T. Pana, "Model based speed and rotor resistance estimation for sensorless vector-controlled induction motor drives using floating point DSP," in *Advanced Motion Control, 1996. AMC '96-MIE. Proceedings., 1996 4th International Workshop on*, 1996, pp. 168-173 vol.1.

[84] F. W. Fuchs and A. Kloenne, "DC link and dynamic performance features of PWM IGBT current source converter induction machine drives with respect to industrial requirements," in *Power Electronics and Motion Control Conference, 2004. IPEMC 2004. The 4th International*, 2004, pp. 1393-1398 Vol.3.

[85] K. Gi-Taek and T. A. Lipo, "VSI-PWM rectifier/inverter system with a reduced switch count," *Industry Applications, IEEE Transactions on,* vol. 32, pp. 1331-1337, 1996.

[86] M. P. Kazmierkowski, M. A. Dzieniakowski, A. Kasprowicz, and S. Kanoza, "Control of DC link resonant inverter-fed induction motor drive without speed sensor," in *Industrial Electronics, 1995. ISIE '95., Proceedings of the IEEE International Symposium on*, 1995, pp. 628-632 vol.2.

[87] S. Hojoon, J. Hyun-Sam, and S. Seung-Ki, "Low Voltage Ride Through(LVRT) control strategy of grid-connected variable speed Wind Turbine Generator System," in *Power Electronics and ECCE Asia (ICPE & ECCE), 2011 IEEE 8th International Conference on*, pp. 96-101.

[88] W. A. Qureshi and N. C. Nair, "Systematic development of Low Voltage Ride-Through (LVRT) envelope for grids," in *TENCON 2010 - 2010 IEEE Region 10 Conference*, pp. 574-579.

[89] M. Mohseni, M. A. S. Masoum, and S. M. Islam, "Low voltage ride-through of DFIG wind turbines complying with Western-Power grid code in Australia," in *Power and Energy Society General Meeting, 2011 IEEE*, pp. 1-8.

[90] V. F. Mendes, C. V. de Sousa, S. R. Silva, B. Cezar Rabelo, and W. Hofmann, "Modeling and Ride-Through Control of Doubly Fed Induction Generators During Symmetrical Voltage Sags," *Energy Conversion, IEEE Transactions on,* vol. 26, pp. 1161-1171.

[91] I. Erlich, F. Shewarega, S. Engelhardt, J. Kretschmann, J. Fortmann, and F. Koch, "Effect of wind turbine output current during faults on grid voltage and the transient stability of wind parks," in *Power & Energy Society General Meeting, 2009. PES '09. IEEE*, 2009, pp. 1-8.

[92] Y. Lei, R. M. Tumilty, G. M. Burt, and J. R. McDonald, "Performance of Induction Generator Protection During Distribution Network Disturbances," in *Developments in Power System Protection, 2008. DPSP 2008. IET 9th International Conference on*, 2008, pp. 529-534.

[93] H. Che-Wei, L. Chia-Tse, and C. Po-Tai, "A low voltage ride-through technique for grid-connected converters of distributed energy resources," in *Energy Conversion Congress and Exposition (ECCE), 2010 IEEE*, pp. 3388-3395.

[94] A. C. Lopes, A. C. Nascimento, J. P. A. Vieira, M. V. A. Nunes, and U. H. Bezerra, "Reactive power control of direct drive synchronous wind generators to enhance the Low Voltage Ride-Through capability," in *Bulk Power System Dynamics and Control (iREP) - VIII (iREP), 2010 iREP Symposium*, pp. 1-6.

[95] J. M. Ordagci, H. C. T. Santos, S. R. Morand, R. Cespedes, R. Mano, and D. Caceres, "ONS - Brasil new control center architecture conceptual design," in *Transmission and Distribution Conference and Exposition: Latin America, 2008 IEEE/PES*, 2008, pp. 1-7.

[96] N. R. Ullah, T. Thiringer, and D. Karlsson, "Voltage and Transient Stability Support by Wind Farms Complying With the E.ON Netz Grid Code," *Power Systems, IEEE Transactions on,* vol. 22, pp. 1647-1656, 2007.

[97] H. Yang, "Reactive power capabilities of DFIG-based wind park for low-voltage ride-through (LVRT) performance," in *Quality, Reliability, Risk, Maintenance, and Safety Engineering (QR2MSE), 2013 International Conference on*, pp. 1992-1996.

[98] S. Tohidi, H. Oraee, M. R. Zolghadri, S. Shiyi, and P. Tavner, "Analysis and Enhancement of Low-Voltage Ride-Through Capability of Brushless Doubly Fed Induction Generator," *Industrial Electronics, IEEE Transactions on,* vol. 60, pp. 1146-1155.

[99]   C. Shih-Feng, L. Chia-Tse, C. Po-Tai, and F. Blaabjerg, "A reactive current injection technique for renewable energy converters in low voltage ride-through operations," in *Power and Energy Society General Meeting, 2011 IEEE*, pp. 1-7.

[100]   S. Foster, L. Xu, and B. Fox, "Coordinated reactive power control for facilitating fault ride through of doubly fed induction generator- and fixed speed induction generator-based wind farms," *Renewable Power Generation, IET,* vol. 4, pp. 128-138.

[101]   C. Wei, M. Han, S. Lin, and X. Li, "Low voltage ride-through control strategy of a large capacity DFIG with grid-side thyristor controlled voltage regulator," in *Renewable Power Generation (RPG 2011), IET Conference on*, pp. 1-6.

[102]   C. Wessels and F. W. Fuchs, "Fault ride through of DFIG wind turbines during symmetrical voltage dip with crowbar or stator current feedback solution," in *Energy Conversion Congress and Exposition (ECCE), 2010 IEEE*, pp. 2771-2777.

[103]   C. Peng and N. Heng, "An improved control strategy for DFIG system and dynamic voltage restorer under grid voltage dip," in *Industrial Electronics (ISIE), 2012 IEEE International Symposium on*, pp. 1868-1873.

[104]   L. Teng, S. Shiyi, P. Malliband, E. Abdi, and R. A. McMahon, "Crowbarless Fault Ride-Through of the Brushless Doubly Fed Induction Generator in a Wind Turbine Under Symmetrical Voltage Dips," *Industrial Electronics, IEEE Transactions on,* vol. 60, pp. 2833-2841.

[105]   S. Shiyi, L. Teng, E. Abdi, R. McMahon, and W. Yunxiang, "Symmetrical Low Voltage Ride-Through of the Brushless Doubly-Fed Induction Generator," in *IECON 2011 - 37th Annual Conference on IEEE Industrial Electronics Society*, pp. 3209-3214.

[106]   T. Long, S. Shao, E. Abdi, P. Malliband, M. E. Mathekga, R. A. McMahon, and P. J. Tavner, "Symmetrical low voltage ride-through of a 250 kW brushless DFIG," in *Power Electronics, Machines and Drives (PEMD 2012), 6th IET International Conference on*, pp. 1-6.

[107]   D. Gray, Z. Szekely, and C. Apostoaia, "Real-time observer for the vector control of an induction motor drive," in *Electro/Information Technology, 2009. eit '09. IEEE International Conference on*, 2009, pp. 411-416.

[108]   Y. Shijie, Z. Qun, and D. Heng, "A simplified SVPWM control strategy for PV inverter," in *Control and Decision Conference (CCDC), 2012 24th Chinese*, pp. 225-229.

[109]   R. Boopathi, P. Muthukumar, P. Melba Mary, and S. Jeevananthan, "Investigations on harmonic spreading effects of SVPWM switching patterns in VSI fed AC drives," in *Advances in Engineering, Science and Management (ICAESM), 2012 International Conference on*, pp. 651-656.

A   Appendix A

A.1   1.5kW BDFRM test rigs

The comprehensive simulation is necessary in that it will not only test the concepts but also serve as the basis for the real time experiment. The program is essentially designed to satisfy three main criteria:

- Good correspondence with the reality

- Good interface with the practical experiment, in this case, compatible with dSPACE system

- Friendly user interface

The simulation is achieved in the Matlab which can be programmed by C and compile in C environment. However, the programme at this stage is intended to use blocks available from Simulink library. The advantage of using Simulink in-library blocks to develop the controller is that dSPACE, the software used to develop hardware experiment, is deliberately created to pick up Simulink programme. There is even no need to change the function.In this study, the machine model that ignores the effect of saturation and core losses is made along with other function blocks in simulation. Some of the function blocks will be combined into a 'controller' that will be used in real time experiment in the later stage of the project. Others are developed just for the purpose of a completed simulation, such as the inverter and machine model. In the following sections, each function block will be explained in detail. The simulation is running in sensor-less condition. In sensor condition, the simulation uses the information from the feedback of rotor speed directly. In the sensor-less programme, an estimator is built to get the predicted

value of rotor speed. The plots of the simulation are presented. From these plots, it can be concluded that the Direct Torque Control is successfully applied on Brush-less Doubly Fed Reluctance Machine.
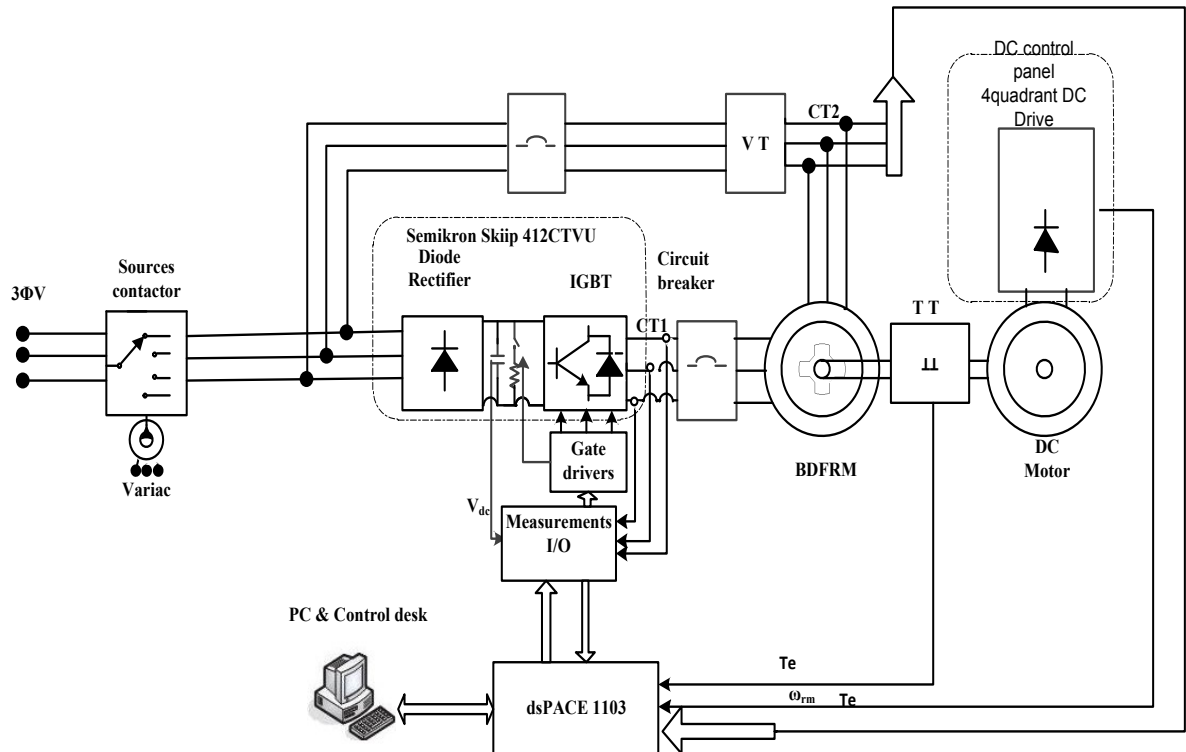

Figure A.1: The basic configuration of 1.5 KW BDFRM test rigs

- Variac: alternative and controllable voltage source

- Source contactors: with three positioning state of-3Ph Voltage-Variac

- Semipro Skip 421CTVU: including the power electronics devices as DC voltage rectifier, storage capacitance, Break chopper resistance and IGBT.

- Circuit breaker: provide save connection between the machine - inverter and achieve the start machine mode as induction machine.

- 1.5KW BDFRM.

- DC MOTOR.

- DC Control panel 4 quadrant DC drive.

- TT Torque transducer.

- VT Voltage Transducer.

- CT Current Transducer.

- Measurement I/O: are vital for applications that, involve numerous actuators and sensors. Used to Real-Time Interface (RTI).

- dSPACE 1103.

A.2 DC Drive

The DC Drive, Fig.A.2 is commercial four quadrant thyristor controlled 514C/16 from Eurotherm Drive Ltd (parker SSD).the feedback loops allow for Torque/speed control providing good performance for wind turbine emulation purposes. The drive has been installed including EMC filter, contactors and External fusses production (Fig. A.3)

Figure A.2: DC Drive unite
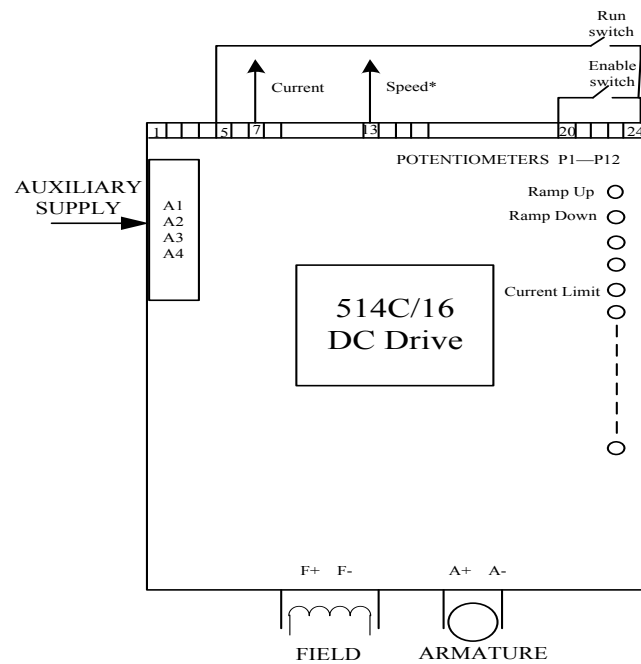
Figure A.3: DC Drive Connection

Satisfying from the machine data (secondary flux and armature currents] the 4 quadrature DC drives offers the control system suitable reference speed and applied torque (form i_{rq} Currents) in the deferent control processes motoring or generating modes. The limitation of the currents can be achieved by the DC Drive one of the benefits used to calibrate theload torque through the control process.

A.3 Key Benefit

The DS1103 is an all-rounder in rapid control prototyping. Its processing power and fast I/O are vital for applications that involve numerous actuators and sensors. Used with Real-Time Interface (RTI), the controller board is fully programmable from the Simulink block diagram environment. You can configure all I/O graphically by using RTI. This is a quick and easy way to implement your control functions on the board.

Figure A.4: Test Rigs 1.5 kW BDFRM.
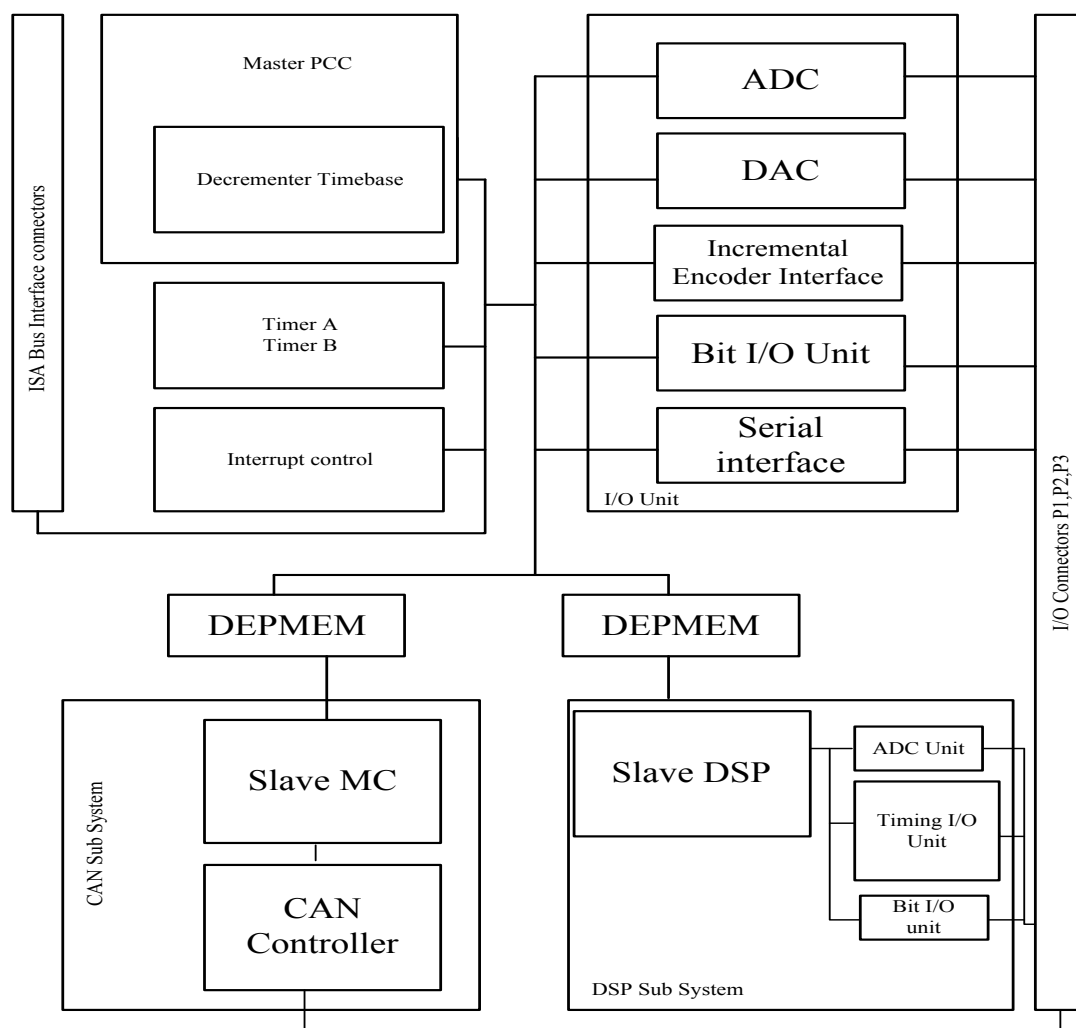
ADC	Analogy Digital Converters
MC	CAN Microcontroller 80C164
CAP	Capture
DAC	Digital/Analogy Converters
DPMEM	Dual-Port Memory
DSP	Digital Signal Processor TMs320F240
PPC	Power PC 604e Processor
PWM	Pulse Width Modulation

Figure A.5:DS 1103 PPC System construction

The **DS1103 PPC** is very flexible and powerful system featuring both high computational capability and comprehensive I/O periphery. Additionally, it features software Simulink interface that allows all application to be developed in Matlab /Simulink friendly environment. All complaining in down loading processes are cared out automatically in background.

Experimental software called control desk, allows real time management of running process by providing a virtual control panel with instruments and scopes Fig.A.5.

- **I/O Units**

They include analogy –digital converters, and digital-analogy converters, digital I/O ports (Bit I/O), and a serial interface .the PPC can also control up to six incremental encoders, which allow the development of advanced controller for robots.

- **DSP Subsystem**

The DSP subsystem based Texas Instrument DSP fixed-point processor, is especially designed for the control of electrical drives .among other I/O capabilities ,the DSP provides T1,T2 SVPWM satisfying from the advantages of SVPWM over sine wave PWM generations .

- **CAN Subsystem**

A further subsystem, based on Siemens 80C164 microcontroller (MC) .is used for connection to CAN bus.

- **Master PPC slave DSP slave MC**

The PPC has access to both DSP and the CAN Subsystem .Spoken in the terms of inter-processor communication, the PPC is the master, whereas the DSP and the CAN MC are Slave.

A.4 Time Vectors

In order to evaluate the performance of the scalar control method, which results in simulations showed remarkable success based open loop algorithm. The evaluation results in the laboratory namely prove this success, and asserted the software simulation behaviours by a real time implementation (RTI) which makes s the results more realistic. The development of software simulation to the RTI requires the high familiarity with the (Voltage /Time) conversion vectors, that's require revising for essential method can be   solved this challenge problems especially when we dealing with SVPWM which require vector time T1,T2 to properly operate [107].So there is an urgent need to build a suitable program for conversion simulations parameter as voltage vectors to operate as time vector, accepted by testing system hardware dSPACE. The time vector can gained with presence of rated voltage V_r, secondary angle θ_s, and rotating sectors sequence S which can gained by developing the 3 phase voltage to 6 sectors according to these equations:

$$\begin{bmatrix} V_d \\ V_q \end{bmatrix} = \frac{2}{3} \begin{bmatrix} 1 & -1/2 & -1/2 \\ 0 & \sqrt{3}/2 & -\sqrt{3}/2 \end{bmatrix} \begin{bmatrix} v_a \\ v_b \\ v_c \end{bmatrix} \tag{1}$$

$$\left| v_{ref} \right| = \sqrt{v_q^2 + v_d^2} \tag{2}$$

Then the secondary frame angle can be extracted as:

$$\theta = \tan^{-1}\left(\frac{v_q}{v_d}\right) = \omega t = 2\pi f t \tag{3}$$
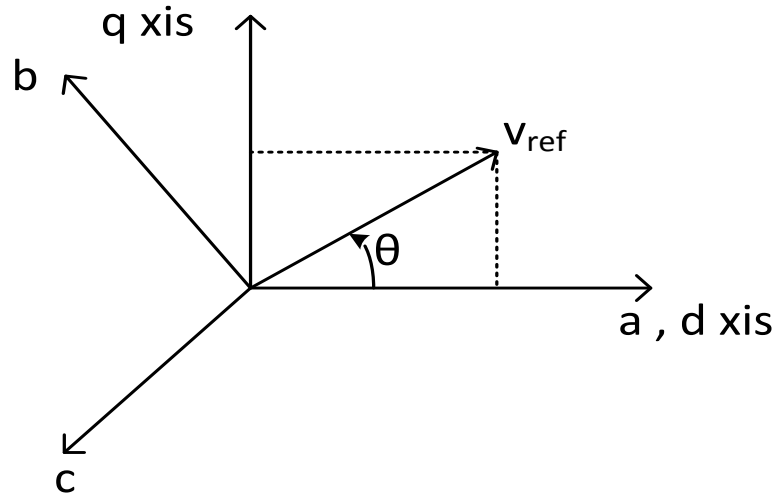
Figure A.6: Voltage Space vector and its component in d-q domain

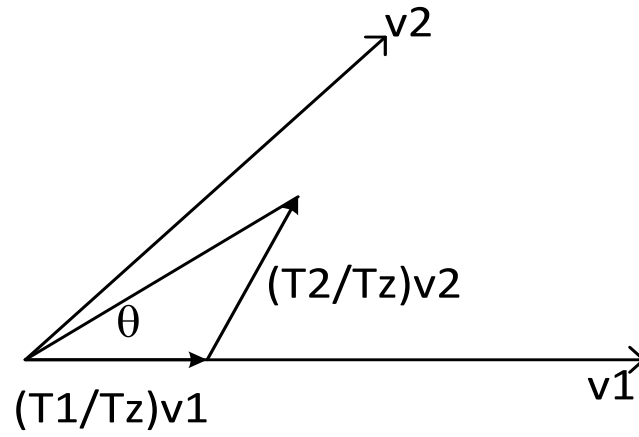Developing this voltage coordinate in time domain can be presented in following figure.
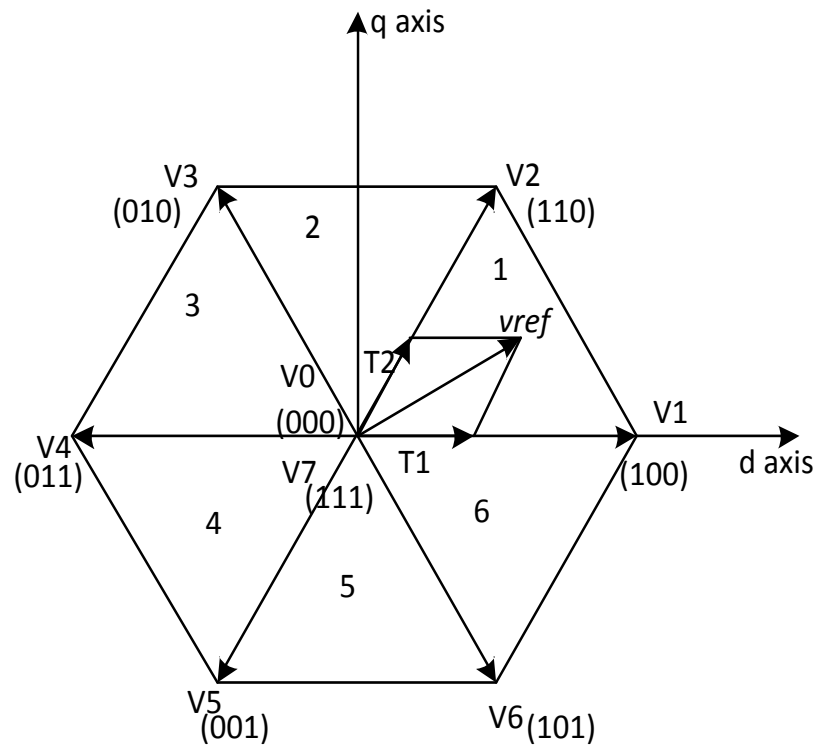
Figure A.7: Switching Duration during sector 1.

Figure A.8: Distribution sector over time domain.

The switching time can be calculated by the following equations:

$$T1 = T_z . a. \left(\frac{\sin(\frac{\pi}{3} - \theta)}{\sin(\frac{\pi}{3})} \right) \tag{4}$$

$$T2 = T_z . a. \left(\frac{\sin(\theta)}{\sin(\frac{\pi}{3})} \right) \tag{5}$$

$$a = \frac{|v_{ref}|}{\frac{2}{3} v_{dc}} \tag{6}$$

Where "**a"** presented as modulation index $0 \le a \le 1$ and the sector angle $0 \le \theta \le 60$
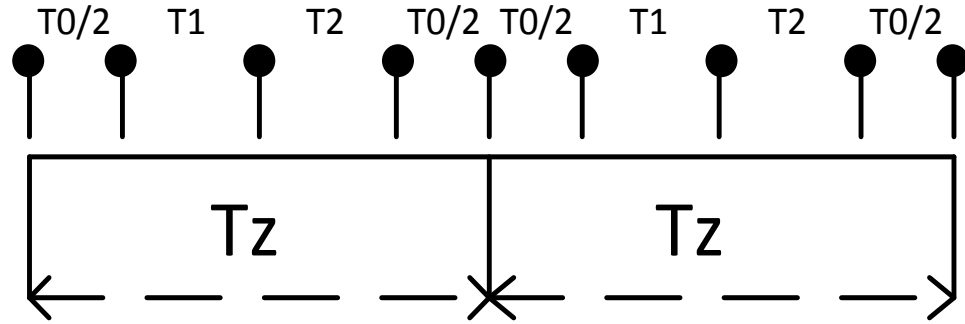
Figure A.9: vector time Distribution along switching Time.

$$T0 = T_z - (T1 + T2) \tag{7}$$
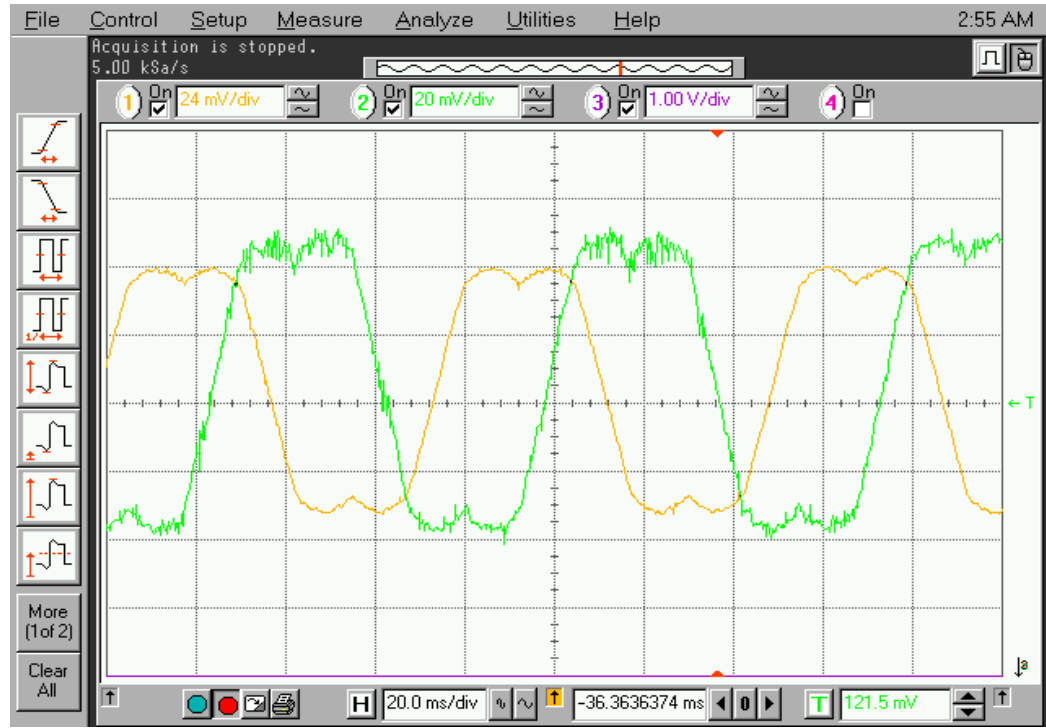
Figure A.10: The time vector T1, T2 as appear in Oscilloscope.

Table A.1: Time Sector.

Sector	Upper switches(S1,S3,S5)	Lower switches (S4,S6,S2)
1	S1=T1+T2+T0/2 S3=T2+T0/2 S5=T0/2	S4=T0/2 S6=T1+T0/2 S2=T1+T2+T0/2
2	S1=T1+T0/2 S3=T1+T2+T0/2 S5=T0/2	S4=T2+T0/2 S6=T0/2 S2=T1+T2+T0/2
3	S1=T0/2 S3=T1+T2+T0/2 S5=T2+T0/2	S4=T1+T2+T0/2 S6=T0/2 S2= T1+T0/2
4	S1=T0/2 S3=T1+T0/2 S5=T1+T2+T0/2	S4=T1+T2+T0/2 S6= T2+T0/2 S2=T0/2
5	S1=T2+T0/2 S3=T0/2 S5=T1+T2+T0/2	S4=T1+T0/2 S6=T1+T2+T0/2 S2=T2+T0/2
6	S1=T1+T2+T0/2 S3=T0/2 S5=T1+T0/2	S4=T0/2 S6=T1+T2+T0/2 S2=T2+T0/2

After close understanding how the sectors and T1and T2 established from this equation the new

Simulink software ready to take a role in the next analysing between the outgoing control data

and required time data of the SVPWM in term ($t_a = T_1/T_z$)and $t_b = T_2/T_z$) to build equivalent time

potential in real time implementation RTI, Fig A.11.
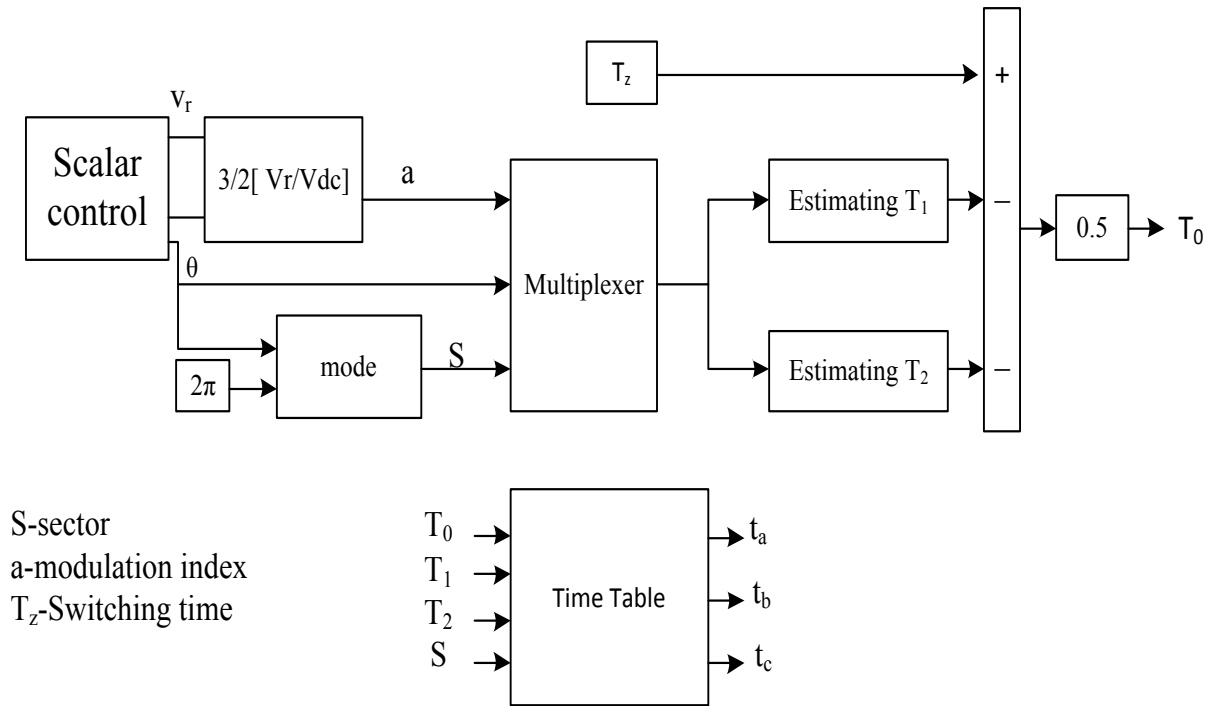
Figure A.11: conversion unit (coupling software).

The other concern spent to solve this question (if the time vectors reflect the equivalent

behaviour of the voltage vectors in RTI and that's need further attempt to prove that and

calibrate the voltages parameters with real parameters to get actual machine performance

responded to the control algorithm.

A.5 Calibrating output and input coupling data

The term of the test which we need to validate need to convert voltage conversation to the time vectors which is required as input data to the SVPWM. According to [78, 108, 109] the coupling software depending on rated voltage, DC voltage (build modulation factor a), sector and secondary rotating angle θ_s (build repeating sequence to the time vector correlated with control side machine) as shown in the Fig. A.12 .The time vector amplitude not more the 1 and t_a, t_b should keep $0 < t_a, t_b < 1$.
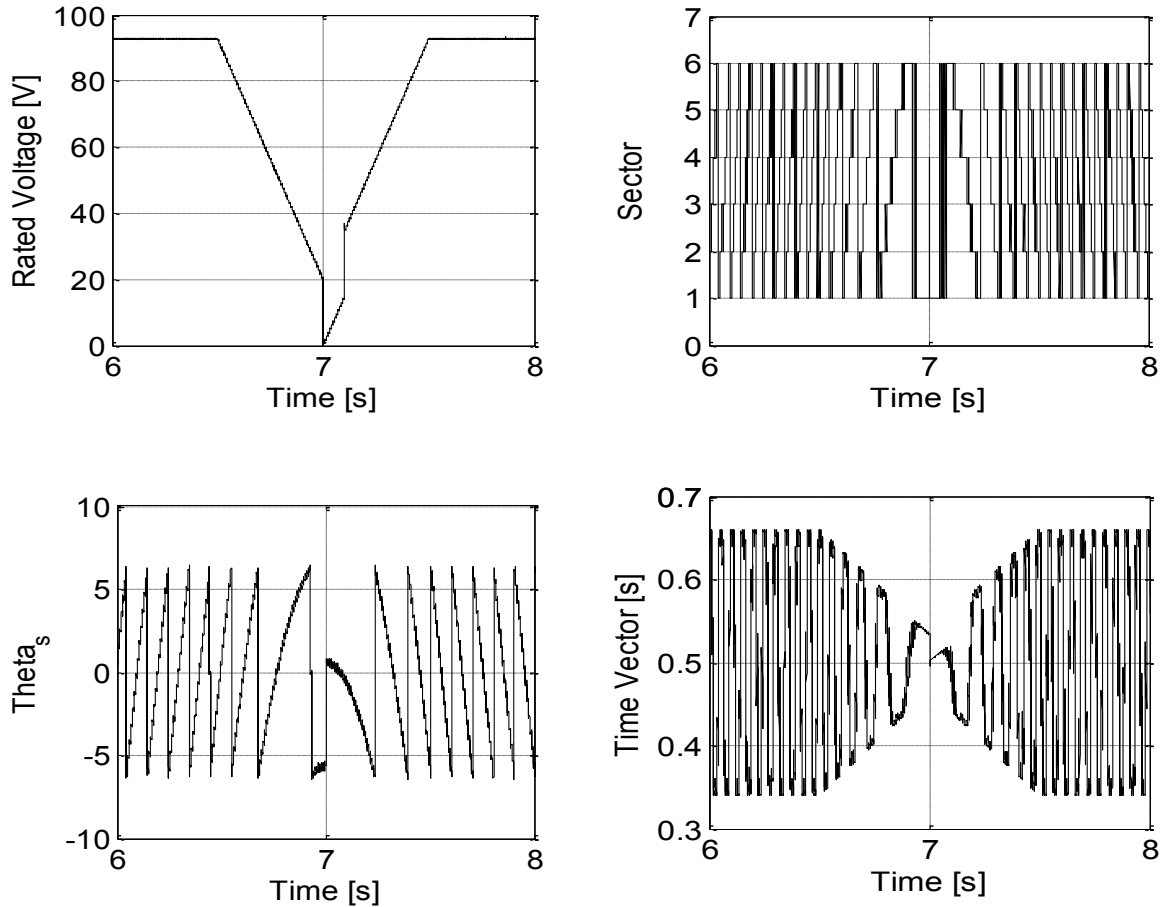
Figure A.12: The input &output data related to the coupling block.

Other concerning target is to use the Equivalent RTI units from DS1103 library control disc with associated hardware units linked to the 1.5 BDRM. The analogy, data extracted from the machine as Voltage, current Rotation speed and angle Positing can achieved by using a specific unit called an analogy-digital conversion (ADC) or Multi analogy-digital conversion (MADC) for multi inputs information linked to step down Gain to normalize with other simulation softer data otherwise the data which need to read on the control disk display regarding control algorithms can use the digital analogy converter (DAC) block to transfer the actual data suitable to extract from the computers or oscilloscopes or other display unit. The DAC should link to step up gain to display suitable measurement for different supported devices. The goal is to relate to other units use RTI criticism from the library with the DS1103, Fig. A.13.
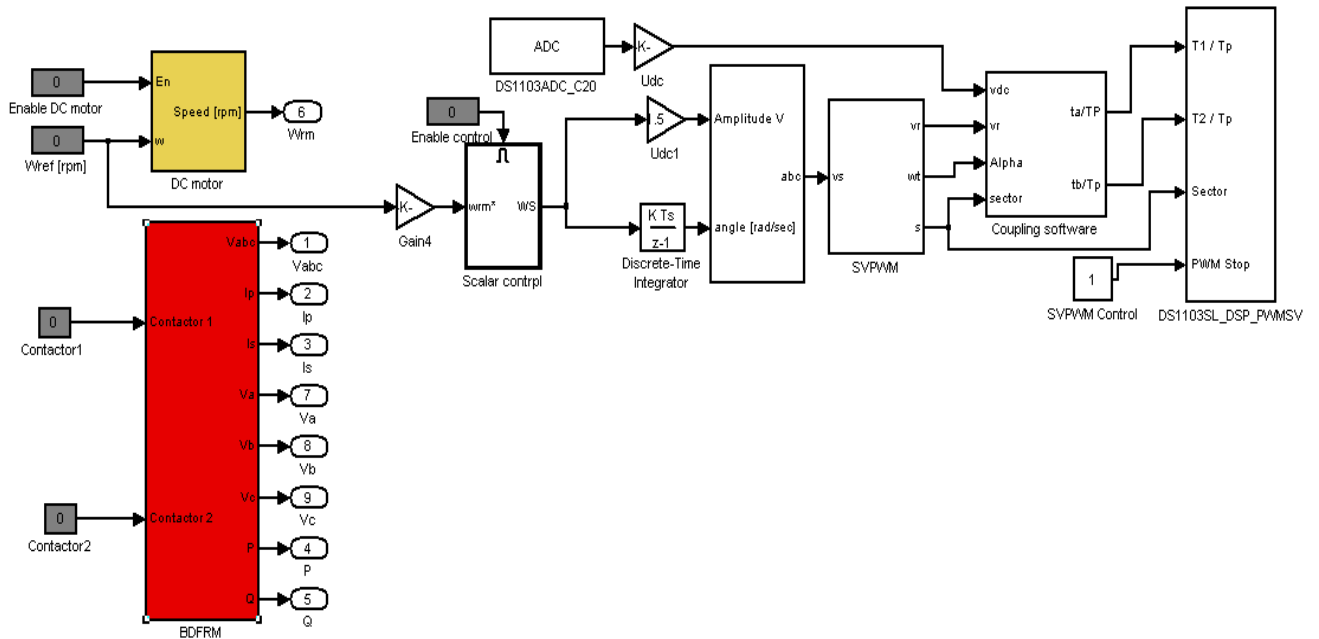
Figure A.13: The test rig configuration in PC hoisted control desk.
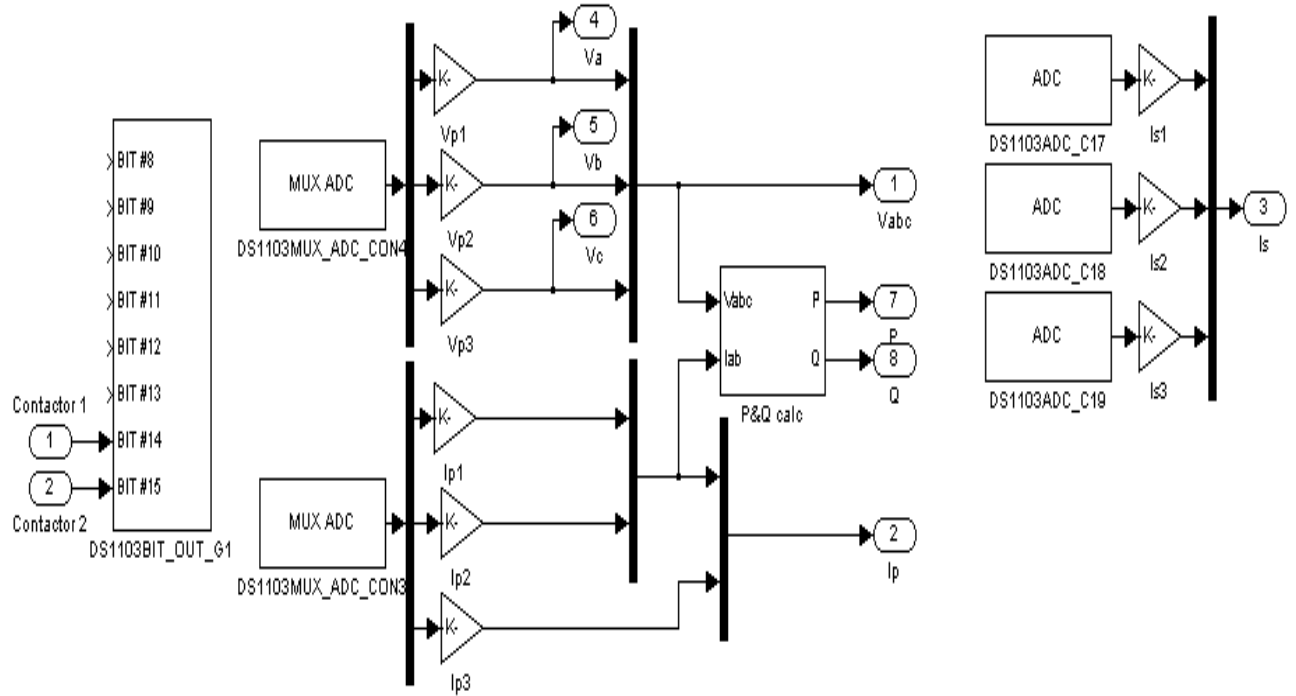
Figure A.14: BDFRM in term dSPACE unit configuration.

BDFRM (Fig .A.14) has built depending on data achievement, from the machine hardware side as 3ph (secondary & primary) Currents, Primary voltage, switching contacts and positioning angle from the machine encoder .the development in speed and torque is appear in the Fig.A.15 depending on the incremental information data from the encoder satisfying from four quadrant DC drive as reference source of the speed and by enabling switch in the PC – control desk can convert the positive and negative load torque to reflect the motoring and generating mode work

.
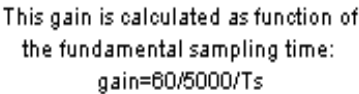
Figure A.15: DC motor configuration.

A.6 Configuration Control desk

Control desk is installed on the host PC during software installation .There is important feature based using dSPACE application that is the ability to upload the simulation software automatically to C code then the machine can be driven under RTI. Uploading scalar control software in c code consider the first step of real time Implementation and then configuration control desk coming as a next step to identify the desired variable ,the root action and selected instrument for each test which is retained already in capture unit as new experimental test in RT domain. Implementation software and Control Desk have considered the experiment software. The several steps required to implement a control system on the DS1103 Controller Board is described below. The first step consists in modelling the control system with Simulink and configuring the I/O connections of the Connector Panel thanks to the RTI toolbox. After that, the Real-Time Workshop (RTW) toolbox, using RTI, automatically generates the C-code for the board. Once the execution code has been generated, then dSPACE hardware can perform a real-

time experiment which can be controlled from a PC with Control Desk. After providing all appropriate conditions for the experiment work, the last challenge is the BDFRM respond to the reference speed Fig .A.16.
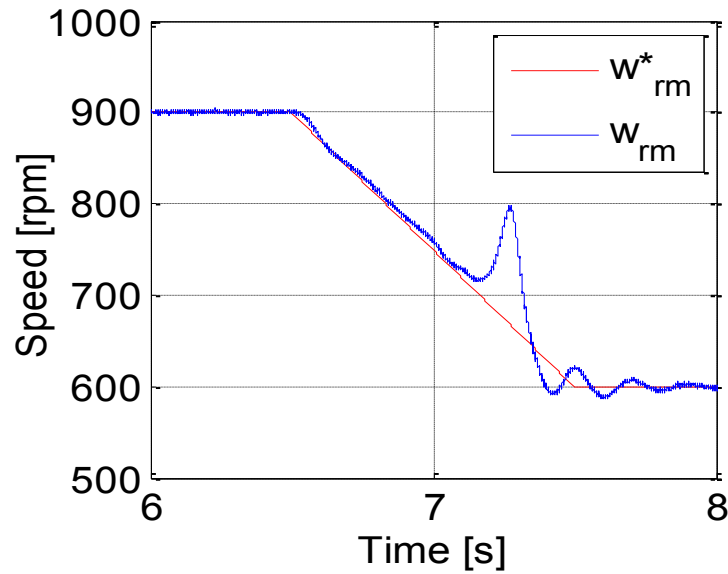

Figure A.16: Reference and actual speed verify the step precision of test rigs practise performance.

The Simulink program is adapted for real time software implementation using the dSPACE® system. The functional description of the control code developed and the experimental results generated on an axially laminated DBFRM prototype are given in Chapter 3. The controlled machine is shown to be capable of quality speed control, both below, at and beyond synchronous speed.
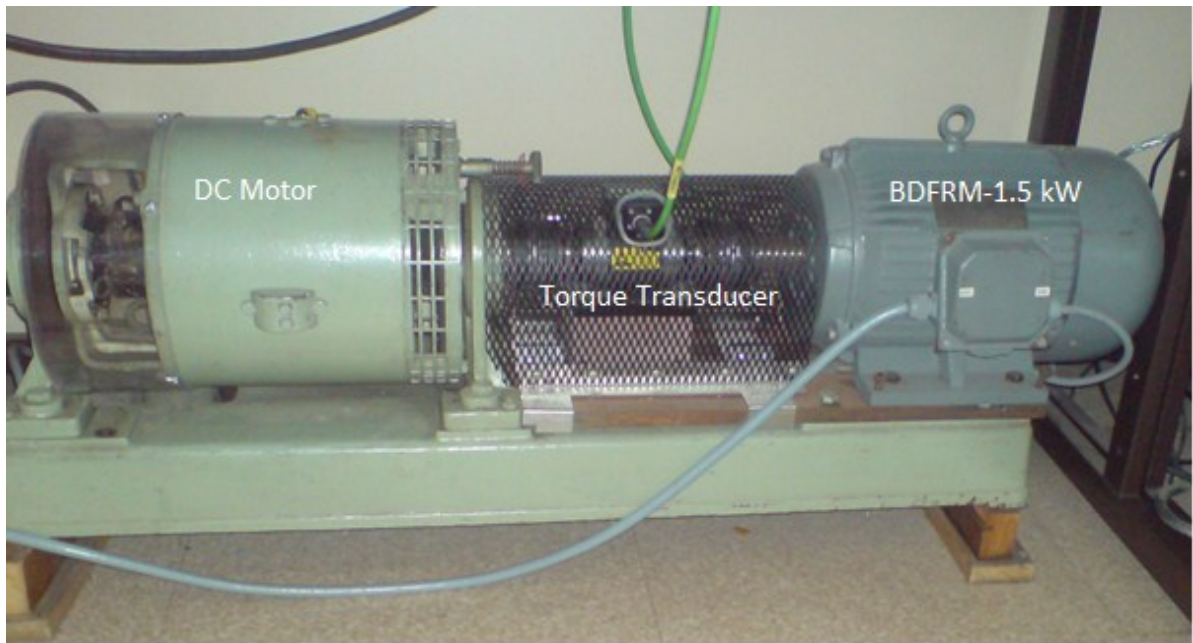
Figure A.17: 1.5 KW BDFRM (Torque transducer) supplied to I/O unit by green wire.
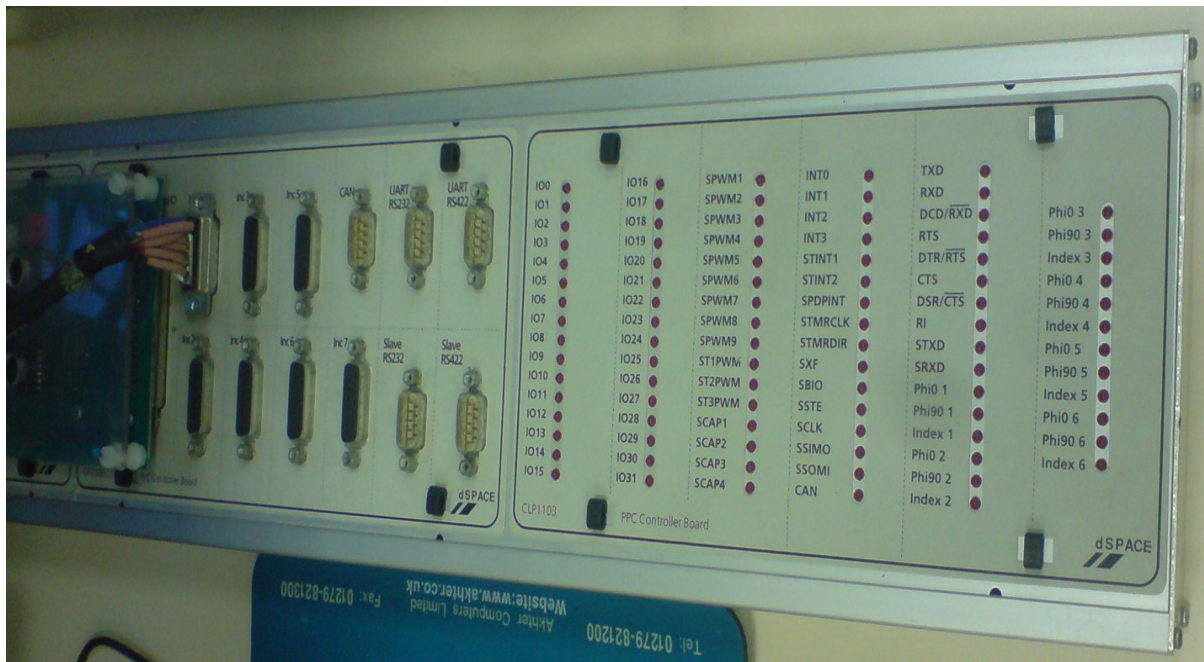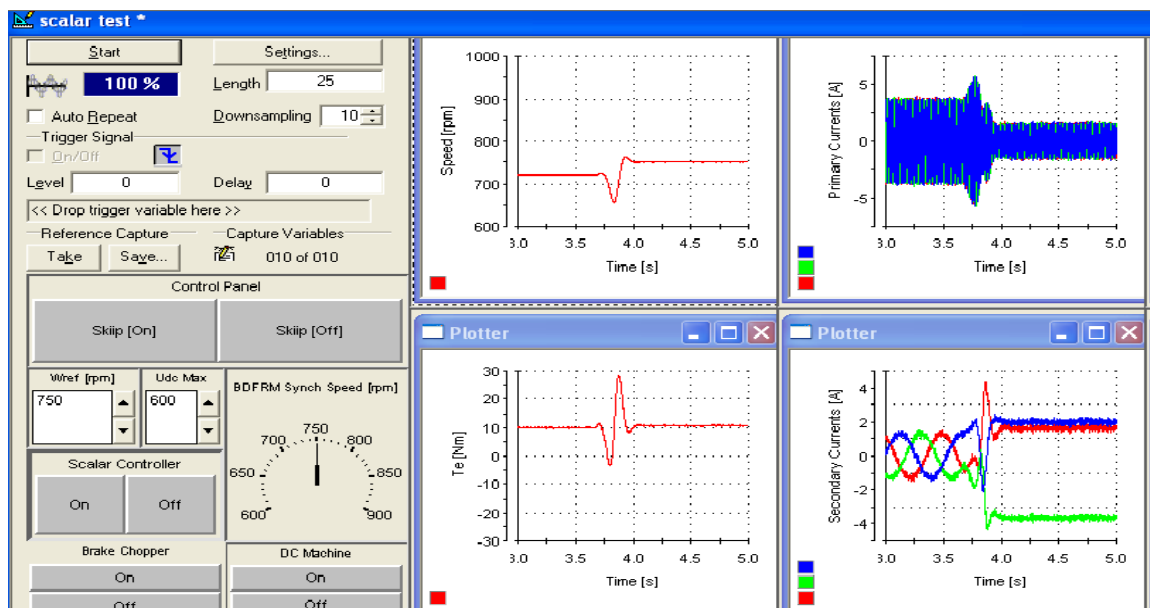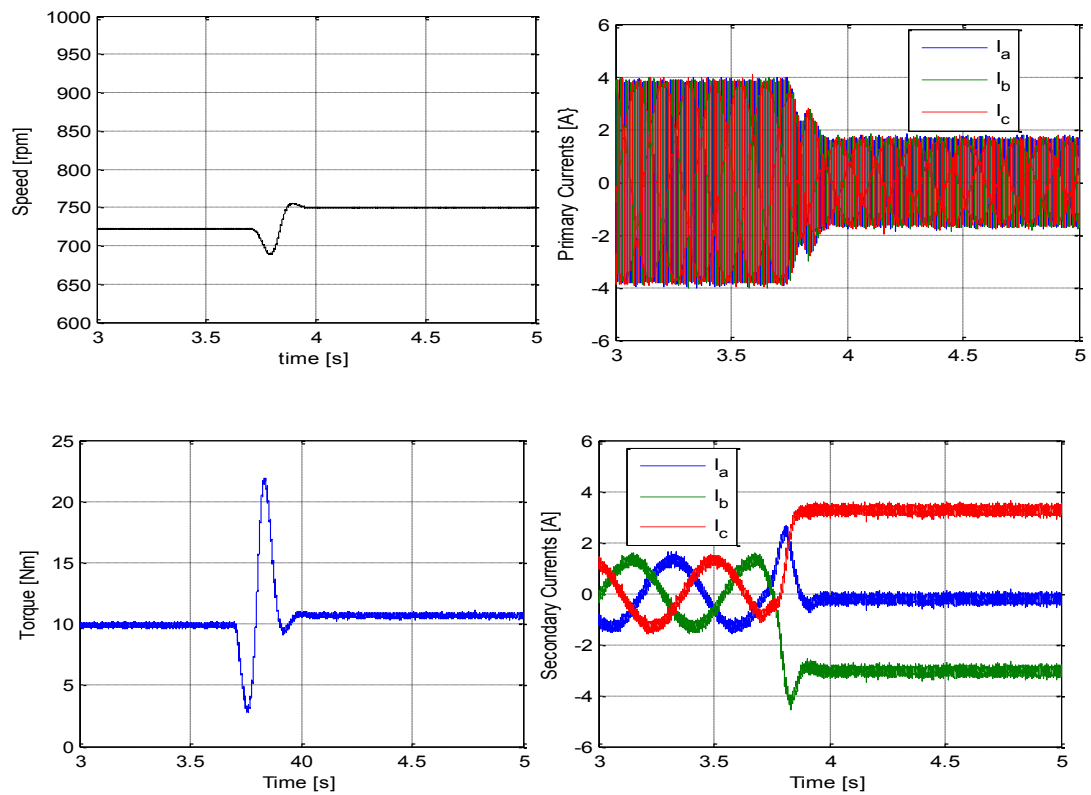

Figure A.18: Input and Output Data I/O unit.

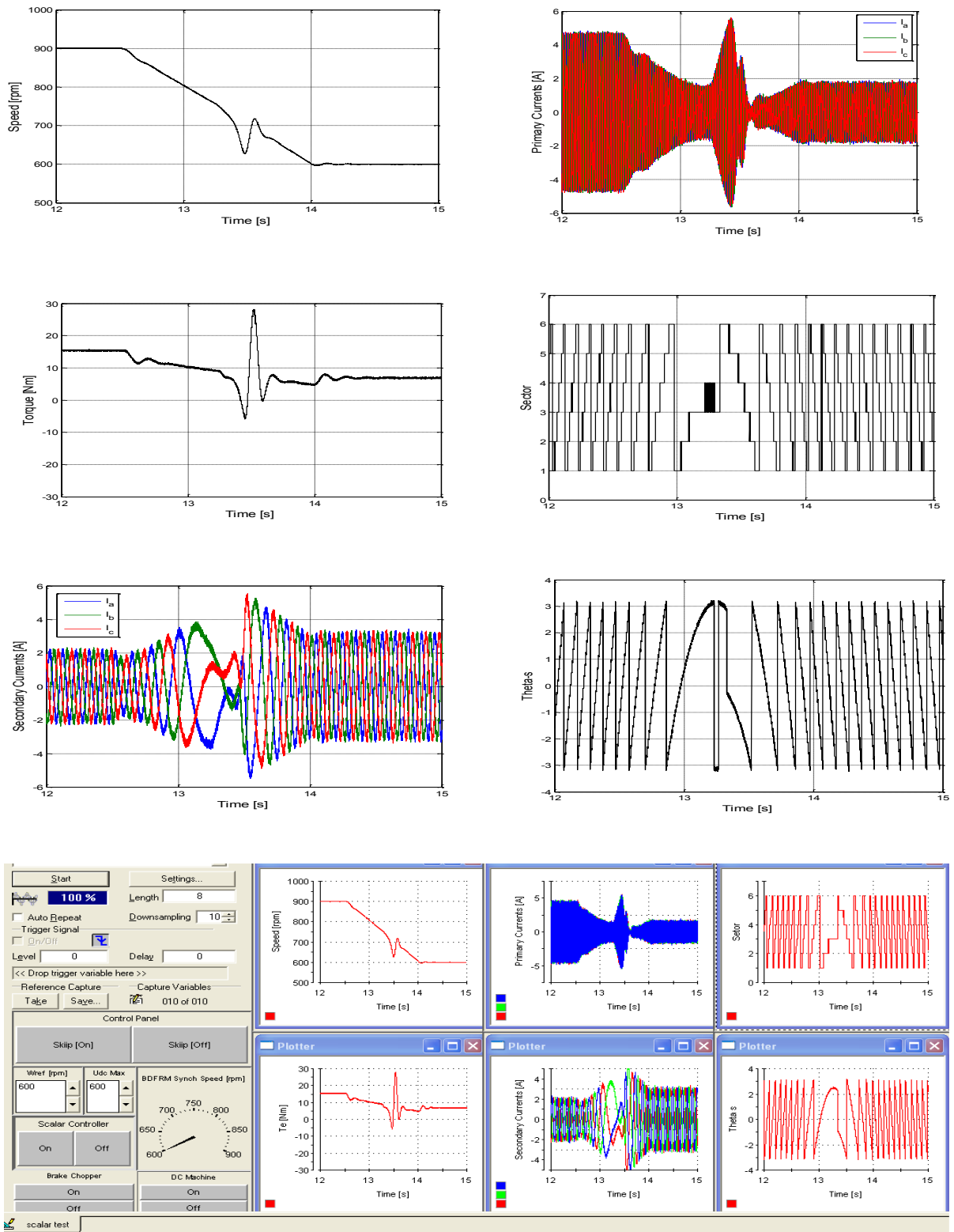Figure A.19: Simulation and real time Results (Induction to synchronous Mode).

Figure A.20: Simulation and real time Results (super to sub synchronous Mode).

B Appendix B

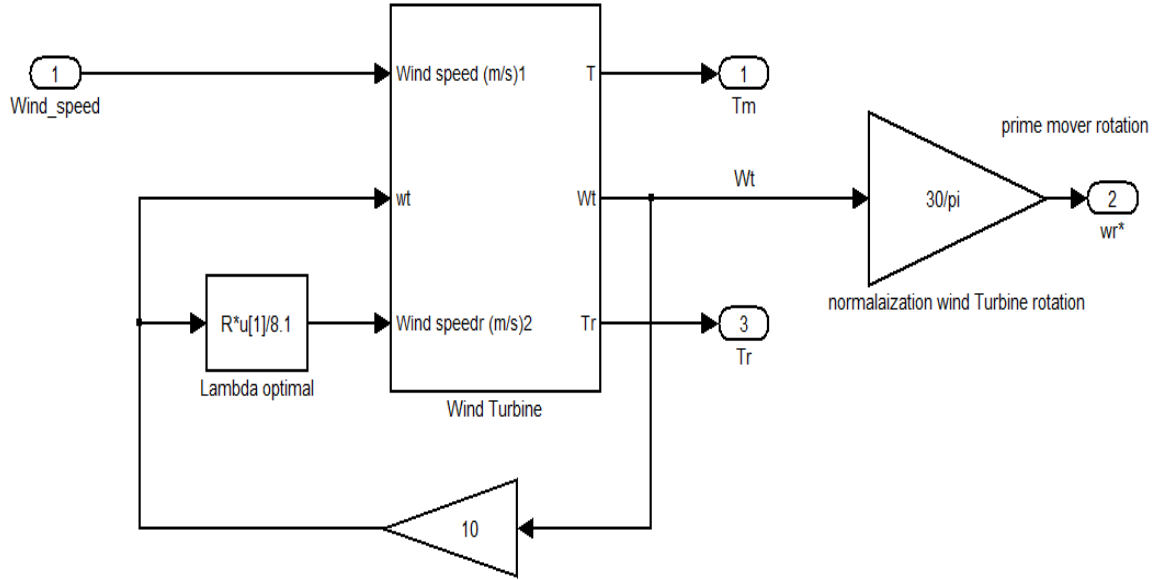## B.1 Code of the turbine side for Maximum Power Point Tracking

Figure B.1: the methodical approach for Control turbine side Machine.

Most of the designs for the system simulations that describe the process of generating energy through wind turbine applications, based on the closed-loop system, which utilize information from the rotation shaft (generator), electromagnetic torque and the production currents, to correct errors resulting from transaction with nonlinear waves wind.

Sensor less control is considered a scientific revolution in the control system technology for easy handling generators without the need to know the characteristics or parameters have.

Scalar control one of promising control algorithm has promising success over BDFRM/G machine (chapter 3) so that need as well the independent control turbine adopted sensor less control approach.
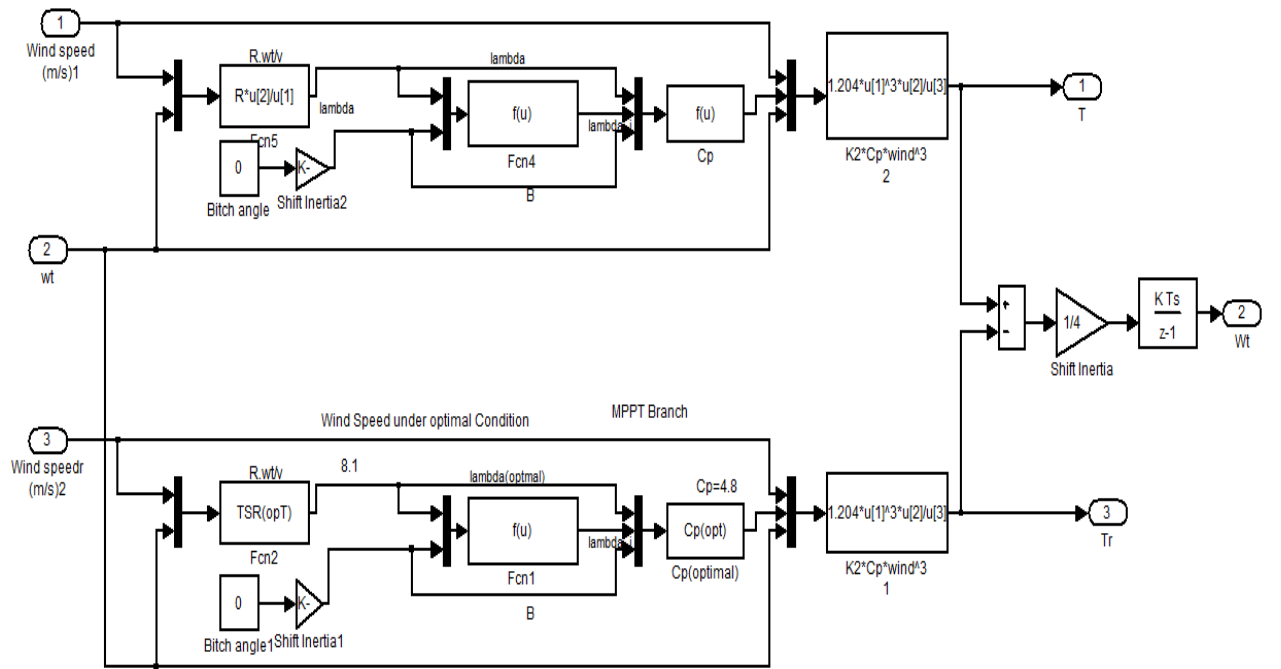

Figure B.2 :Wind Turbine code and development kinetic energy through TSR control.

Our approach TSR control design can offer this specification, adopting the peak of maximum power point tracking curve to get optimum values to extract maximum power tip speed ratio TSR ($_{opt}$) characteristics vs coefficient power $C_p(_{opt})$. Comprehensive simulation between the optimal branch and actual branch(deal proportional with variable wind speed) will produce the appropriate wind turbine rotating can be used as reference speed to the scalar control or field

oriented control as well. The wind turbine simulated in Fig. B.2 developing the torque (T_r, T_m) from the both branches to the turbine rotating Eq(4.8) and then to the shaft speed satisfying from the N gear box and synchronous speed ratio ($60/2\pi$) to reference speed appropriate to use with synchronous generators Eq.(4.10).

The generator can extract two valued information from the TSR control they are reference speed ωr^*, and negative torque (T) as generating mode.

B.2 Code for the Generator Side

Scalar control as the senseless control strategy satisfied from the data out come from the turbine side as reference speed and the speed trajectory depending on the wind speed variation the same approach will done in FOC when the reference speed developed in certain torque and through PI controller can be presented as I_{sq}^* current in case to control the Generator depending on FOC Strategy.
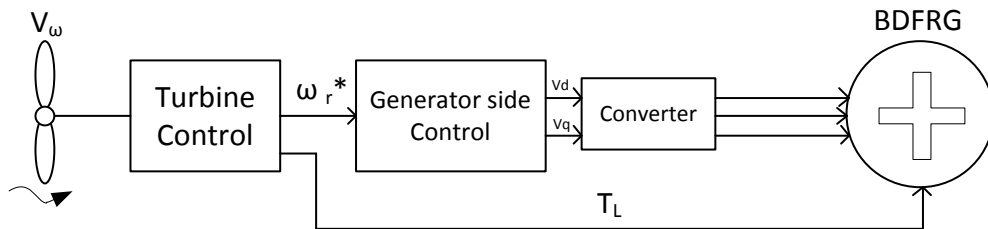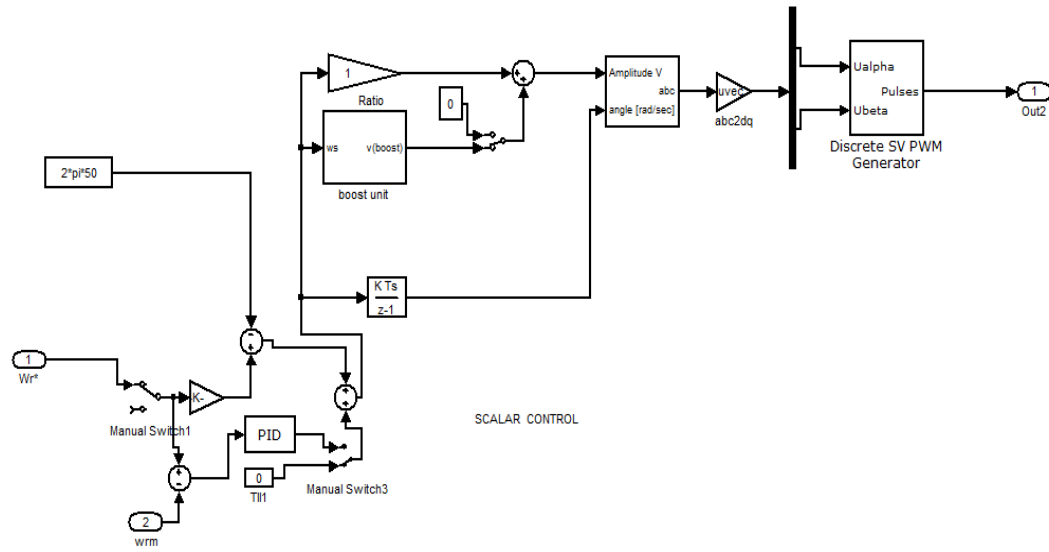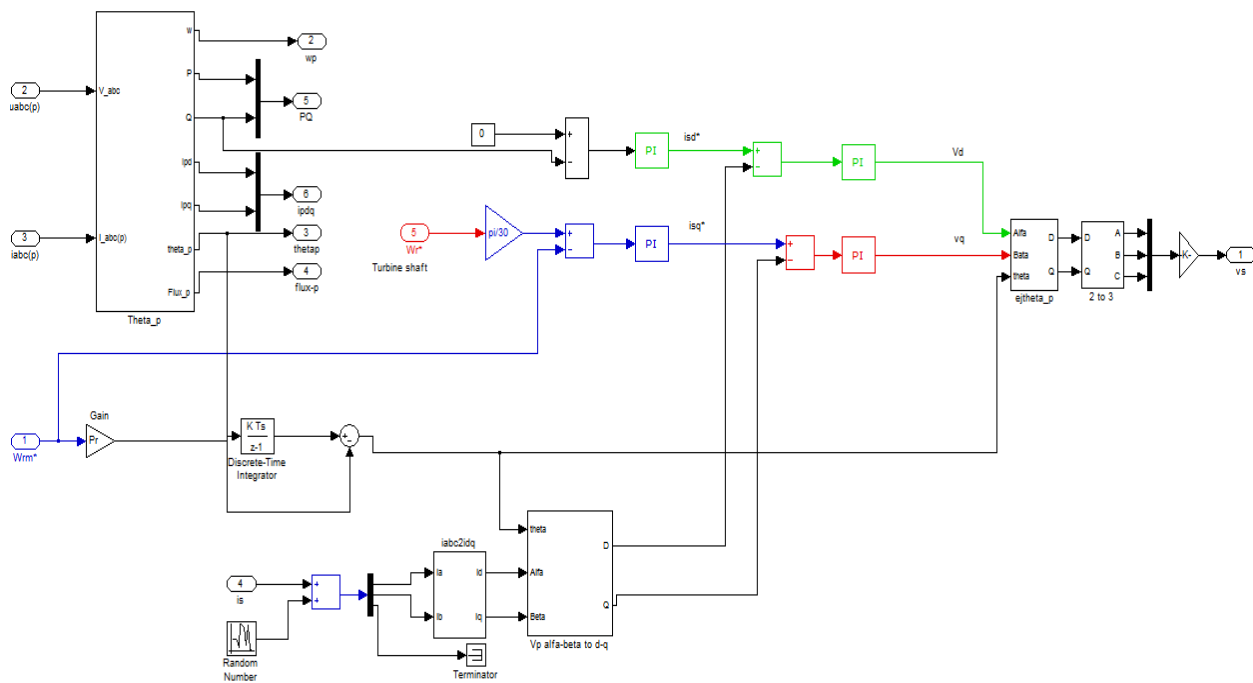

Figure B.3: Generator side control.

(a)

(b)

Figure B.4: (a) scalar control, (b) FOC adopted in MPPT application.

C Scholarly Outcomes

1. M. Hassan and M. Jovanovic, "Improved scalar control using flexible DC-Link voltage in Brushless Doubly-Fed Reluctance Machines for wind applications," in Environment Friendly Energies and Applications (EFEA), 2012 2nd International Symposium on, pp. 482-487.

2. M. Hassan, M. Jovanovic and S. Ademi "Control of Brushless Doubly–Fed Reluctance Generator for Wind Energy Conversion System" to appear in IEEE Transactions on Energy Conversion 2014.